Exploring the Photophysics of Engineered and Intrinsic Charge-Carrier Trapping Processes in Semiconductor Nanocrystals

Kira Elizabeth Hughes

A dissertation

submitted in partial fulfillment of the

requirements for the degree of

Doctor of Philosophy

University of Washington

2019

Reading Committee:

Daniel R. Gamelin, Chair

Brandi M. Cossairt

Cody W. Schlenker

Program authorized to offer degree:

Chemistry

University of Washington

Abstract

Exploring the Photophysics of Engineered and Intrinsic Charge-Carrier Trapping Processes in Semiconductor Nanocrystals

Kira Elizabeth Hughes

Chair of the Supervisory Committee:

Daniel R. Gamelin

Department of Chemistry

Colloidal semiconductor nanocrystals (NCs) have been a topic of extensive research over the past few decades, as the materials' photoluminescence (PL) properties are particularly interesting for a variety of applications. Emissive materials are only of interest, however, if the highest PL efficiencies can be attained—something that has yet to be achieved for a variety of NCs. Low PL efficiencies can often be blamed on unwanted charge-carrier trapping processes that limit band edge recombination. This thesis describes methods of addressing charge-carrier trapping, including incorporating an efficient "engineered" trap to control charge-carrier movement as well as targeted synthetic and spectroscopic studies to eliminate surface trapping in semiconductor NCs. Chapter 1 provides a general overview of these topics accompanied by relevant literature studies on both engineered traps and surface trapping in semiconductor NCs.

Chapter 2 presents ultrafast spectroscopic data for Cu^{+}:CdSe/CdS NCs, a system in which copper serves as an efficient hole trap. The data include time-resolved photoluminescence (TRPL) spectroscopy to study hole localization at copper after photoexcitation and transient absorption (TA) spectroscopy to observe transitions involving excited-state Cu^{2+}. Chapter 3 details the synthesis and spectroscopic results for a series of $Ag_{1-x}Cu_xInS_2$ NCs, a material of interest due to the spectroscopic similarities of $CuInS_2$ NCs to the copper-doped materials. Through creating a synthetic bridge from $AgInS_2$ to $CuInS_2$ NCs, we can monitor the PL energy as a function of increasing copper content. This aims to help support previous assignments that the PL in $CuInS_2$ NCs arises due to a self-trapped exciton. Chapter 4 discusses the importance of electron and hole trapping in determining the PLQY of InP NCs, a material with inherently low PL efficiencies. Studying a sample series of InP NCs with five different surface chemistries using both TRPL and TA allows us to investigate how different surface treatments affect charge-carrier trapping processes. Together, these studies help elucidate the role charge-carrier trapping plays in determining the PL efficiencies of colloidal semiconductor nanocrystals and will help us design targeted synthetic strategies for obtaining materials with 100% PL efficiencies.

Acknowledgments

I want to begin by thanking Professor Daniel Gamelin for allowing me to further my growth as a scientist in his research group for the past five years. Starting at UW, I had no idea how much I would learn and grow during my time as a graduate student. When I first joined your group, I had never heard the words "semiconductor nanocrystal," but I knew your science was fascinating and that I wanted to be a part of it. Five years later, and I managed to compile a whole doctoral thesis on the topic; I attribute that to your guidance and mentorship. Thank you for the times spent talking science, explaining projects, and brainstorming ideas. You always inspire me with your knowledge, and I will forever continue to aspire to be the type of scientist you are.

To Professor Brandi Cossairt—thank you for welcoming me into your group as a fifth-year graduate student and giving me the opportunity to expand the scope of my research. The experience I've had becoming a member of a second research group so far into my graduate career has been unlike any other. You welcomed and sought my ideas and provided me with the space to collaborate and grow my passion for using spectroscopy to study your NCs. This really helped me grow even more as a scientist. Being a member of your group has been one of my favorite things from the past year, and your mentorship has meant so much.

To the rest of my committee members, Prof. Cody Schlenker, Prof. Mike Heinekey, and Prof. Peter Pauzauskie. Thank you for the hours spent listening to and reading my science. I appreciate your commitment to helping further scientific knowledge.

My five years as a graduate student would not have been the same without my fellow Gamelin group members. Fellow Team Copper, thank you for welcoming me into your group and teaching me your ways. Prof. Katie Knowles, I credit you for helping kickstart my research journey in the group. Thank you for always being there to answer my questions but also knowing, much better than me, when to step away and make sure that I could fly on my own. You were one of my favorite parts of being a young student in the group, and I strive to be a mentor like you. Thank you to Dr. Arianna Marchioro for instilling in me a love of transient absorption. Without your guidance, I would not have learned how much I love being a spectroscopist. To all the other members of the Gamelin group: thank you for fostering a welcoming scientific community, allowing me to ask even the "stupid questions" that helped me to grow, and providing great camaraderie that made the lab a place I wanted to be. Dr. Alina Schimpf, thank you for leaving a lasting legacy in the lab. I will always remember what you told me before you left in regard to my bright research future, and I strove to live up to that every day. Dr. Liam Bradshaw, we didn't overlap in the group for long, but I'm thankful I got to know you through the Molecular Analysis Facility. Thank you for helping train me in yet another TA setup. Dr. Charlie Barrows, thank you for the lab-life wisdom. I knew I could always count on you to give it to me straight, but also for dragging me along to ultimate frisbee that first time, and for your continued friendship. Dr. Patrick Whitham for your patience in the laser lab and willingness to walk/help me through my experiments. Dr. Heidi Nelson thank you for the beautiful calculations that helped me understand my research that much better. To Professors Sidney Creutz, Carl Brozek, Emily Tsui and Dr. Rachel Fainblat, thank you for your leadership, guidance, and support of myself and the rest of the group. Dr. Mike Carroll, thank you for sharing your MolES space and teaching me how to make thin films. Also thanks for sharing your wicked snowboarding moves on the mountain during our group ski trip. Dr. Dan Kroupa, thank you for sharing your spectroscopic knowledge, your help interpreting data, and your guidance getting started on the InP project. Dr. Matt Crane, thank you for taking the time to re-align the pulse picker more than should ever be required. Your patience

is admirable. Dr. Matt Smith, thank you for letting me know I always have someone in lab with whom I can discuss the previous night's episode of the Bachelorette. Michael de Siena for the coffee trips even when you pretended to dislike me. It only took five years, but I think I wore you down, and I'm thankful to say we're friends now. Jose Araujo, thank you for always saying good morning and the willingness to listen to me ramble. Christian Erickson for never backing down from a science argument, and you both for sticking it out these five years with me, even if it did occasionally result in merciless teasing. I will miss sharing an office with you. Sarah Ostheller, thank you for allowing me to be your mentor and for being patient with me as I continued to learn alongside you. You were a joy to work with, teach, and mentor, and you have such a bright future ahead of you. Ted and Tyler, thank you for greeting me with a smile, saying hi in the hallway, and keeping us young with your jokes. TK and Anna, thank you for always asking questions, because they also help everyone else think critically about our science. Diana, your ability to speak your mind inspires me, and your desire to learn and further your scientific knowledge is incredible. Kelly, thank you for the basement talks during data collection and for always being enthusiastic. Your smile and determination help make my days. Laura, thank you for your encouragement and words of excitement, especially when I needed it the most. Atch, I will never forget that cowboy hat you bought when you came as an exchange student. I'm glad to have been able to do research alongside you again this past year. Prof. Victor Polinger, thank you for always asking me the tough questions during my Group Meetings. You made me think outside the box and helped me to analyze my research even more critically. And finally, Dr. Kimberly Hartstein. You made coming to work everyday something I looked forward to. Thank you for your mentorship, scientific guidance, but most of all your friendship. I will always cherish our walks around the fountain, trips to the library just so we could chat, and a relationship I know will span so much more than just five years of graduate school. Only a true friend would record you doing your happy dance after a successful day in lab just to save it for ~3 years so your advisor could show it before your defense.

To the Cossairt group, thank you for welcoming me with open arms. You answered my questions, listened to my thoughts, and welcomed my suggestions. It was a pleasure being a part of your group over the past year and learning about your incredible science. Dr. Jenny Stein, thank you for sharing your beautiful samples with me and always being open to my ideas. Dr. Max Friedfeld, thank you for the (also beautiful) samples and always being up for running that one extra experiment. Thank you also for seeking my opinion on projects; it means so much. To Beth Mundy, my honorary Team Copper mate. I'm so excited to see you to continue the Team Copper legacy, and I know you will do great things with your career. Nayon, you are such a capable scientist, an even sweeter person, and it was a pleasure to spend the past year collaborating with you. Forrest, fellow ABQ friend! Thank you for spending those hours in the dark basement laser lab, even when you didn't need to. It really showcased your desire to learn TRPL. Your enthusiasm helped fuel my sometimes-waning excitement. I know you will be a fantastic spectroscopist.

Before I joined the Gamelin group, my UW family was my first-year cohort. Specifically, Katie Corp, James Gaynor, Lucas Flagg, Nick Montoni, and Caitlin Cornell. Classes were some of the most challenging I had ever encountered, but I got through it because of you. From your patience while I was learning to code *p*-orbitals or do quantum homework to the nights out in Cap Hill; you all are incredible scientists, even better people, and I'm lucky to have your camaraderie. Katie Corp: my first real friend in Seattle. I will always remember our study dates, Bachelor Mondays, and evenings spent chatting about science, life, and your new kitties. I'm so thankful for your friendship.

To all the Chemistry department front office staff, especially Diana Knight and Kimberly Quigley. Thank you for helping make the logistics of being a grad student run more smoothly than I ever could have imagined. You two are terrific, and the department is all the better because of your presence.

To my friends beyond the walls of the Chemistry Building. Jenny Taylor, thank you for being so warm and welcoming in a city where it's not always easy to make friends. Thank you for the baked goods, hot meals, late-night chats, opening your home when I needed an escape, and you and Nick Weber introducing me to the Newman Center. I have you both to thank for my integration into an amazing and loving community, something for which I will always be grateful. To the "Elite 8." From our High Hut trips to the weekend hangouts, the past couple of years have been so much fun, and I'm thankful to have had an incredible group of friends with which to share it. Even though this year brings lots of change and big moves, I know that our friendships will remain strong as we continue to support each other and share our journeys.

To Nancy Cogan, my first science teacher. Thank you for instilling in me a love of science and creating a space where I could figure out how much I loved learning about the small building blocks of our universe. When I think back about my scientific journey, it always starts with you. You made learning science fun, and that has helped propel me to where I am now.

Encouragement along the way doesn't hurt, though, and I'm incredibly thankful to Prof. Rick Kemp for helping me keep on the scientific path. Despite a brief desire to veer towards medicine, you saw the potential I had to contribute to the scientific community and let me know it. I truly believe that had I not taken your class and asked you for a letter of recommendation, that I would not be where I am now. I applied to University of Washington because of you, and attending here was one of the best decisions I've ever made. Thank you again, for telling me how much science needed my brains, introducing me to graduate-level research, and supporting me through this whole process.

To the Lunds and your whole Chehalis community. Thank you for welcoming me into your community with open arms, inviting me on trips to experience the PNW, and asking me about my research enough times that it actually helped me learn how to talk about my work outside the walls of my lab. I can't wait to officially join your family next month.

To my life-long family. Mom, Dad, Don, and Torrie. Anything I write here would feel insufficient to express my gratitude towards you for helping me through the past five years. Through it all you've been there to support me, encourage me, stress with me, and celebrate with me. New Mexico is far, but I knew you would always be at the other end of the phone if I needed to call, even if it was just for emotional support. You sent me care packages, bought me food, and sent Starbucks gift cards to help fuel the late nights reading, studying, and collecting data. I love you all so much, and I could not have done this without you. You believed in me all along, even when I doubted myself, and I'm so excited to share in the excitement with you as I close this chapter and move to the next. Again, thank you from the bottom of my heart.

Speaking of next chapters. Mitch. I'm so incredibly thankful you came into my life two and a half years ago. You were a constant amid the ups and downs of grad school. Thank you for asking me questions about my research, being excited when I got excited, reassuring me when I freaked out, and feeding me when I got hangry and forgot to eat because I was too busy writing or working up data. But most of all, thank you for being by my side and loving me every day through it all. I can't wait to marry you next month and to continue to be by your side every day after. I love you.

Table of Contents

List of Figures and Schemes

List of Tables

Abbreviations and Symbols

A/A_0	Normalized absorbance
Ag	Silver
$Ag_{1-x}Cu_xInS_2$	Silver copper indium sulfide with varying concentrations of silver and copper
$Ag_{1-x}Cu_xInSe_2$	Silver copper indium selenide with varying concentrations of silver and copper
$AgInS_2$	Silver indium sulfide
Al	Aluminum
As	Arsenic
B-D	Bright-dark (excitonic splitting)
CaH_2	Calcium hydride
CB	Conduction band
Cd	Cadmium sulfide
CdO	Cadmium oxide
CdSe	Cadmium selenide
$Cd_{1-x}Zn_xSe$	Cadmium zinc selenide with varying concentrations of cadmium and zinc
Cu	Copper
Cu^+:CdSe	Copper-doped cadmium selenide
Cu^+:CdSe/CdS	Copper-doped cadmium selenide with a cadmium sulfide shell
CuI	Copper iodide
Cu^+:InP	Copper-doped indium phosphide
$CuInS_2$	Copper indium sulfide
$CuSe_4$	Copper selenide
CW	Continuous-wave
Δ	Change (in)
d	Diameter
DAP	Donor-acceptor pair
DDT	Dodecanethiol
DFT	Density functional theory
ε	Extinction coefficient
E	General abbreviation for a chalcogenide element
eV	Electronvolt
F	Fluorine
fs	Femtosecond
GaP	Gallium phosphide
HDA	Hexadecylamine
HF	Hydrofluoric acid
HOMO	Highest-occupied molecular orbital
hmim BF_4	1-hexyl-3-methylimidazolium tetrafluoroborate
Hz	Hertz
ICP-AES	Inductively-coupled plasma atomic emission spectrometry
ICP-OES	Inductively-coupled plasma optical emission spectrometry
I/I_0	Normalized PL Intensity
IL	Ionic liquid

In	Indium
InAs	Indium arsenide
InP	Indium phosphide
InP/Cd	Indium phosphide with a cadmium-rich surface
InP/F	Indium phosphide with with surface indium-fluoride bonds
InP/Zn	Indium phosphide with a zinc-rich surface
InP/ZnS	Indium phosphide with a zinc sulfide shell
InP/ZnSe	Indium phosphide with a zinc selenide shell
InP/ZnSeS	Indium phosphide with a zinc sulfide-selenide shell
IR	Infrared
IRF	Instrument response function
K	Kelvin
kHz	Kilohertz
kV	Kilovolt
LED	Light emitting diode
Li[Et_3BH]	Lithium triethylborohydride
LMCT	Ligand-to-metal charge transfer
LSC	Luminescent solar concentrator
LUMO	Lowest-unoccupied molecular orbital
M	Molar
meV	Millielectronvolt
MLCT	Metal-to-ligand charge transfer
mmol	Millimole
Mn	Manganese
MO	Molecular-orbital
mW	Milliwatt
$\langle n \rangle$	Average number of excess conduction band electrons per nanocrystal
NC	Nanocrystal
Nd:YAG	Neodymium-doped yttrium aluminum garnet
NIR	Near infrared
nm	Nanometer
ns	Nanosecond
OA	Oleic acid
$^{-}O_2CR$	Carboxlyate
OD	Optical density
ODE	Octadecene
ODMR	Optically detected magnetic resonance spectroscopy
OPA	Optical parametric amplifier
P	Power/Phosphorus (context dependent)
Pb	Lead
PL	Photoluminescence
PLQY	Photoluminescence quantum yield
ps	Picosecond
PTFE	Polytetrafluoroethylene
PV	Photovoltaic
QD	Quantum dot

S	Sulfur
Se	Selenium
τ	Lifetime/time constant
TA	Transient absorption spectroscopy
TEM	Transmission electron microscopy
Ti	Titanium
TOPO	Trioctylphosphine oxide
TOP	Trioctylphosphine
TRPL	Time-resolved photoluminescence spectroscopy
µJ	Microjoule
µm	Micrometer
µs	Microsecond
UV	Ultraviolet
VB	Valence band
VT	Variable temperature
XAS	X-ray absorption spectroscopy
Xe	Xenon
Zn	Zinc
$Zn_{2(1-x)}(Cu,In)_xS_2$	Zinc cadmium indium sulfide with varying concentrations of zinc, copper, and indium
ZnS	Zinc sulfide
ZnSeS	Zinc selenide sulfide

Chapter 1: Introduction

1.1 Overview

Semiconductor photoluminescence (PL), the radiative recombination of a photoexcited electron and hole,[1] is a fundamental process sought for a wide range of applications.[2] Early luminescent materials such as copper-containing semiconductors were utilized in oscilloscope displays for their green color emission.[3] Imaging applications utilize PL to help track biological indicators.[4] Absorption of high energy light by semiconductors can result in low energy emission that can be paired with traditional silicon photovoltaics (PV) to increase device efficiencies.[5-6] And recently, semiconductors with varying emission energies have been combined with light emitting diodes (LEDs)[7] to create vivid, color-pure TV displays.[8] These applications all rely on the behavior and movement of photoexcited charge carriers and specifically require the highest probability that the charge-carriers will recombine and emit a photon. High PL efficiency, or PL quantum yield (PLQY), is attained when factors that inhibit this radiative recombination are limited.

In recent years, luminescence properties have been studied extensively in colloidal semiconductor nanocrystals (NCs)[9-10]—nanometer-scale semiconductors, the size of which can be manipulated to influence the material's optical properties.[1,10] When the NC size is reduced to that of the material's exciton Bohr radius, or the radial extent of an electron-hole pair, the NC experiences quantum confinement such that the bandgap energy can be tuned by changing the NC size.[1,11] In this way, a material can be synthesized to absorb and emit throughout the UV, visible, or NIR. Solution-processability, optical tunability, composition control, ease of synthesis, and the wide variety of potential applications have helped colloidal NCs gain momentum in the research community.

1.2 Trapping in Semiconductor Nanocrystals

Upon photoexcitation in semiconductor NCs, an electron is promoted from the NC valence band (VB) across the bandgap to the conduction band (CB), leaving behind a hole (Scheme 1.1).[1,12] At the CB minimum and VB maximum, these charge carriers are susceptible to trapping—localization to orbitals, or trap sites, within the bandgap that are energetically more favorable than the band edges. Trap sites vary across materials and can be detrimental to the PLQY. Determining how to identify and eliminate unwanted trap sites and increase PLQYs towards 100%, or unity, is an area of intense investigation in the colloidal semiconductor NC field.

Scheme 1.1. Photoluminescence in semiconductor NCs.

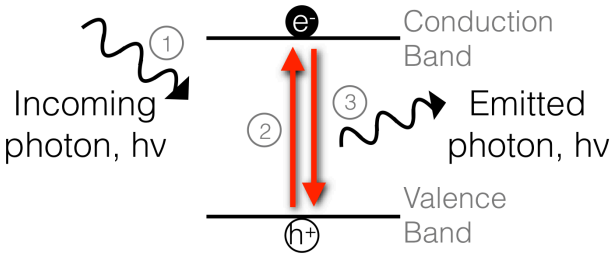

When an electron or hole traps, the likelihood of non-radiative recombination increases. Non-radiative recombination is a phonon-assisted pathway that allows for relaxation of the charge-carriers back to the ground state without emitting a photon.[12] These charge-carrier traps may be present at the surface or in the core of the NC. Surface traps arise when atoms at the NC surface are not fully coordinated to capping ligands or otherwise experience extreme localized distortions due to their chemical environment. Core traps are usually lattice defects, such as vacancies or interstitial ions. Not all trapping processes lead to non-radiative recombination of the charge-carriers, however. Trapped carriers that recombine radiatively exhibit "trap PL," typically a broad PL feature lower in energy than the excitonic PL. The origin of trap PL varies, but regardless of

the chemical nature of trap sites, unwanted carrier trapping can be detrimental to the efficiency of the desired luminescent transition.

1.3 Engineered Traps in Semiconductor Nanocrystals

1.3.1. Copper Dopant Ions as Traps in Semiconductor Nanocrystals. Rather than leaving trap site formation to chance, it can be beneficial to "engineer" a trap site to gain control over the luminescence properties. Engineered traps impart characteristic photophysical changes, some of which are sought for specific applications. Copper(I) has been heavily researched as an "engineered" trap site, as it is an efficient hole trap when incorporated as a dopant and also as a stoichiometric component in a variety of NC lattices.[13] Copper incorporation pre-dates the advent of NCs, as a synthesis of copper-doped zinc sulfide (ZnS) was discovered in the late-1800s.[14] Copper and aluminum co-doped ZnS (Cu^+,Al^{3+}:ZnS) phosphors utilize the copper and aluminum dopant ions as localization centers for charge-carriers that then recombine to give characteristic "green-Cu" luminescence,[15-16] named such for the color of the emission. Easy extension of doping to NC materials has opened the door to investigations of the unique photophysical mechanisms that arise upon incorporation of an "impurity" center into the NC lattice and has allowed for exploration into a wide variety of applications. One such application that utilizes copper's unique PL signature, which will be discussed shortly, is a luminescent solar concentrator (LSC). LSCs rely on little-to-no overlap of phosphor absorption and emission (*i.e.* a large-effective Stokes shift), and emission energy positioned in an ideal range for pairing with traditional silicon-based PV devices.[5-6,17]

In NC lattices like cadmium selenide (CdSe), cadmium sulfide (CdS), indium phosphide (InP), ZnS, and copper indium sulfide ($CuInS_2$), copper exists as Cu^+ with a full 3*d* shell containing

10 electrons.[18] The atomic *d* orbitals of Cu^{+}-doped materials lie within the bandgap at a fixed energy level above the VB edge, allowing for tunability of the copper PL energy when the NC bandgap is changed.[19] Upon photoexcitation, the VB hole rapidly localizes at Cu^{+}; copper is oxidized to Cu^{2+}, a d^9 atom, and the "$ML_{CB}CT$" excited state is formed (where the metal is copper, and the "ligand" is the CB).[18] This excited state undergoes a symmetry-breaking Jahn-Teller distortion accompanied by strong electron-phonon coupling, giving rise to broad PL linewidths averaging several hundred meV.[18,20] As a result, the characteristic PL of copper-doped and copper-based NCs then, is broad and red-shifted from the absorption onset. It occurs as the radiative recombination of the delocalized CB electron with the Cu^{2+}-localized hole, a transition referred to as a metal-to-ligand charge transfer ($ML_{CB}CT$) transition.[18] Figure 1.1A shows a representative absorption and PL spectrum for un-doped CdSe NCs along with a scheme depicting the corresponding excitonic processes. The excitonic PL is narrow and minimally Stokes-shifted from the absorption, typical of band-edge PL with little vibronic contribution. Figure 1.1B shows an average absorption and PL spectrum of Cu^{+}:CdSe NCs with a scheme depicting the corresponding processes with copper incorporated into the lattice. The PL spectrum demonstrates the Stokes-shift and broad linewidths characteristic of the $ML_{CB}CT$ PL in these NCs.

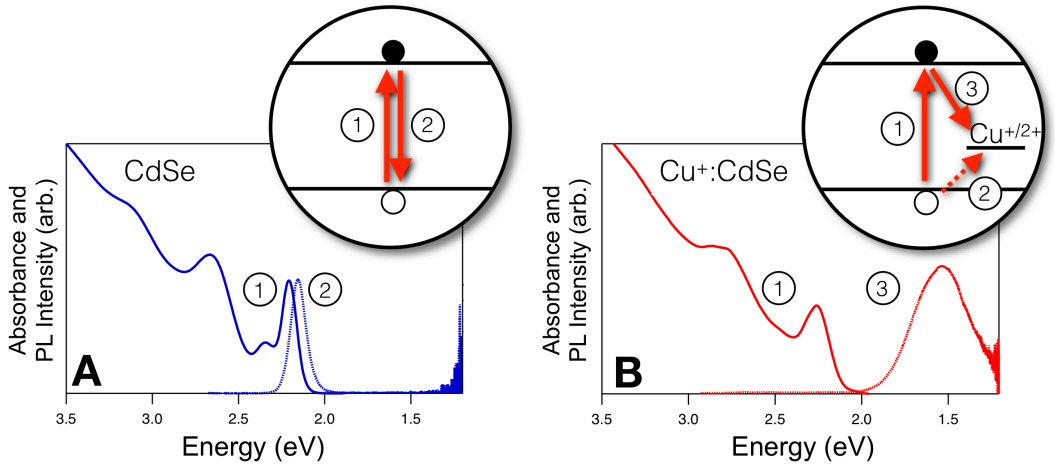

Figure 1.1. Absorption (solid line, left) and PL (dotted line, right) spectra of CdSe (**A**) and Cu^+:CdSe (**B**) NCs with corresponding schematics detailing the absorption and emission processes for each sample. The transitions numbered in the spectra correlate with the numbered transitions in the schematics.

In the absorption spectrum of Cu^+:CdSe NCs, a low-intensity absorption feature can be seen below the onset of the first excitonic transition. This corresponds to the below-bandgap absorption from the Cu^+ *d*-orbitals to the CB edge, or the $ML_{CB}CT$ transition, and is also referred to as the copper "foot."

1.3.2. Formation and Exploration of the $ML_{CB}CT$ Excited State. Until recently, hole localization at copper was understood to be "fast," but the literature lacked a specific time associated with the trapping process. In fact, one literature report even claimed the presence of "permanent" holes on copper, meaning copper was present as d^9 Cu^{2+} in the ground state of the NC prior to photoexcitation.[21] This conclusion was drawn based on the observed increase in copper PL intensity upon addition of a hole acceptor. In the proposed mechanism, the hole acceptor extracts the photogenerated VB hole allowing for recombination of the CB electron with the permanent hole on copper. Additionally, previous attempts at observing hole localization using time-resolved photoluminescence (TRPL) spectroscopy were complicated by rapid PL losses from

surface trapping. Despite a 2016 report detailing a synthesis to obtain Cu^+:CdSe NCs with a PLQY of ~35%,[22] fast trapping was still present, making it nearly impossible to deconvolute the dynamics and distinguish the various decay components on a sub-ns time-scale. In order to eliminate surface trapping, shells are typically grown around the cores of NCs to passivate under-coordinated surface ions. However, copper is a highly mobile cation, and any post-synthetic shelling attempt drives copper out of the NC lattice.[22] Reports of copper-doped NCs that are shelled after doping show excitonic PL,[21] indicating the presence of a subset of NCs that do not contain copper dopants.[22] In order to both address and take advantage of the high dopant mobility, I examined the synthesis of CdSe/CdS NCs, which were then post-synthetically doped via cation exchange to obtain Cu^+:CdSe/CdS NCs.[23] The shell on the surface of the NCs helps eliminate surface trapping at early times and allows for the observation of hole trapping at copper. In this way, implementation of copper into the NC lattice results in an efficient hole localization method.

In addition to being efficient, hole localization at copper is robust and irreversible, as the hole does not repopulate the VB after formation of the $ML_{CB}CT$ excited state. A robust, long-lived $ML_{CB}CT$ excited state allows for transient observation of absorption transitions involving the copper-localized hole, or the Cu^{2+} species. This had never before been demonstrated in copper-doped NCs but is consistent with the mechanism described for bulk materials. When bulk Cu^+,Al^{3+}:ZnS is photoexcited, the copper localizes the photoexcited hole while the aluminum localizes the photoexcited electron.[16] Due to the spatial separation of these dopants, the lifetime of the excited state can be prolonged, which allows for the observation of a low-energy absorption feature associated with an electronic transition from the VB to the hole on Cu^{2+} ($L_{VB}MCT$ transition, where the "ligand" is the VB and the metal is Cu^{2+}). Consistent with the observed VB to Cu^{2+} transition in bulk crystals, a calculated absorption spectrum[20] for Cu^{2+}:$Cd_{33}Se_{34}$ NCs also

shows a broad absorption feature with an extinction coefficient of ~2000 $M^{-1}cm^{-1}$ that extends through the visible down to ~1.0 eV. This transition in Cu^{2+}:$Cd_{33}Se_{34}$ NCs is akin to the transition expected in photoexcited Cu^{+}:CdSe NCs after the hole localizes at the copper forming Cu^{2+}, as shown in Scheme 1.2.

Scheme 1.2. $ML_{CB}CT$ Excited State and $L_{VB}MCT$ Transitions in Copper-Doped NCs.

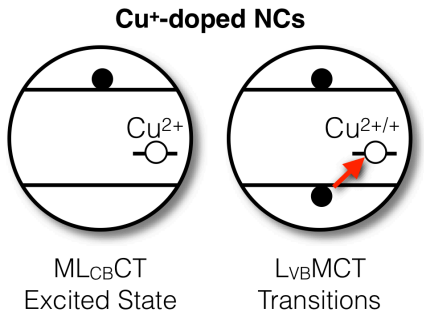

The robust localization of a hole on copper also sets the stage for further investigation of the $ML_{CB}CT$ excited state, including behavior in the presence of extra charge-carriers. The Gamelin group has previously shown that delocalized electrons can be added to the CB of NCs through a process called photodoping.[24-26] Photodoping imparts specific changes to the absorption and PL spectra as a response to the addition of excess delocalized CB electrons. Even more interesting, however, is the Auger recombination that happens upon photoexcitation in the presence of an extra CB electron. Auger recombination has very unique spectroscopic signatures that can be monitored by TRPL and is the process by which a CB electron and VB hole recombine nonradiatively, transferring energy to the extra charge-carrier.[27] Since the hole is localized at copper in the $ML_{CB}CT$ excited state of copper-doped NCs and not in the VB, photodoping these materials would result in a different dependence on the presence of excess CB electrons and therefore rate of Auger recombination.

1.3.3. Stoichiometric Copper Ions in Semiconductor Nanocrystals. $CuInS_2$ NCs have been widely studied as a non-toxic alternative to Cd-based chalcogenide NCs, specifically for incorporation into LSCs,[6] but the photophysical mechanism of these Cu^+-based materials has remained somewhat elusive. There are many reports invoking donor-acceptor pair (DAP) emission as the mechanism responsible for luminescence,[28-31] similar to that of bulk $CuInS_2$, which has been ascribed to lattice vacancies and antisite defects.[18] Excitonic and narrow luminescence can be observed for bulk crystals,[32] however, while the characteristic $CuInS_2$ NC luminescence is broad and red-shifted from the absorption.[13] Direct comparison with Cu^+:CdSe and Cu^+:InP NCs[18] indicates that lattice defects are not responsible for the $CuInS_2$ luminescence at all. All observed spectroscopic characteristics such as Stokes shifts, PL linewidths, and lifetimes of the ternary material are nearly indistinguishable from those of the doped NCs, exemplified by the absorption and PL spectra in Figure 1.2 for Cu^+:CdSe, Cu^+:InP, and $CuInS_2$ NCs.

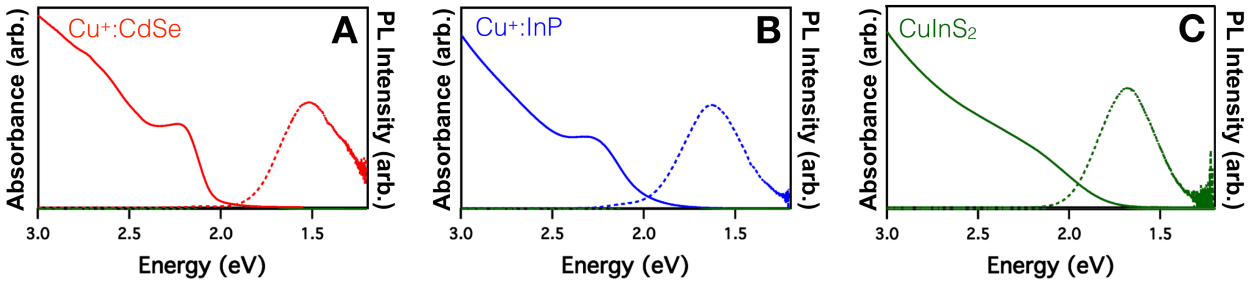

Figure 1.2. Absorption (solid lines, left) and PL (dotted lines, right) spectra of Cu^+:CdSe (**A**), Cu^+:InP (**B**), and $CuInS_2$ **(C)** NCs. All three samples show broad and red-shifted PL, characteristic of hole localization at copper after photoexcitation. Figure adapted from ref. 18.

Therefore, the Gamelin group proposed an alternate hypothesis of exciton self-trapping was proposed to explain the luminescence mechanism of $CuInS_2$ NCs.[18] In a self-trapped exciton, a lattice copper localizes the photogenerated hole, a favorable process due to strong electron-phonon coupling that induces a large reorganization energy of the lattice around the oxidized copper.[18]

Exciton self-trapping has also been demonstrated in AgCl, where silver exists as a d^{10} cation as well and undergoes a Jahn-Teller distortion upon photoexcitation and hole localization.[33] As a result, $CuInS_2$ NCs are often referred to as "heavily copper-doped" NCs due to the spectroscopic indistinguishability from the doped materials.

To gain information about the luminescent excited state and exciton self-trapping process in $CuInS_2$ NCs, the highest occupied molecular orbital (HOMO) and lowest unoccupied molecular orbital (LUMO) contributions for a series of alloyed Cu-In-Zn-S NCs were calculated using DFT.[34] An alloyed material provides a bridge between the copper-doped species and the pure $CuInS_2$ structure with which to study the electronic landscape of the NCs. Calculations indicate that as soon as copper is incorporated into $Zn_{34}S_{34}$ to form $Zn_{32}(Cu,In)_1S_{34}$, the HOMO localizes around the copper dopant and remains so throughout the entire composition series to $Cu_{17}In_{17}S_{34}$, as shown in Figure 1.3. Despite a small contraction after initial incorporation of indium, the LUMO remains largely delocalized across the NC volume throughout the alloyed series.

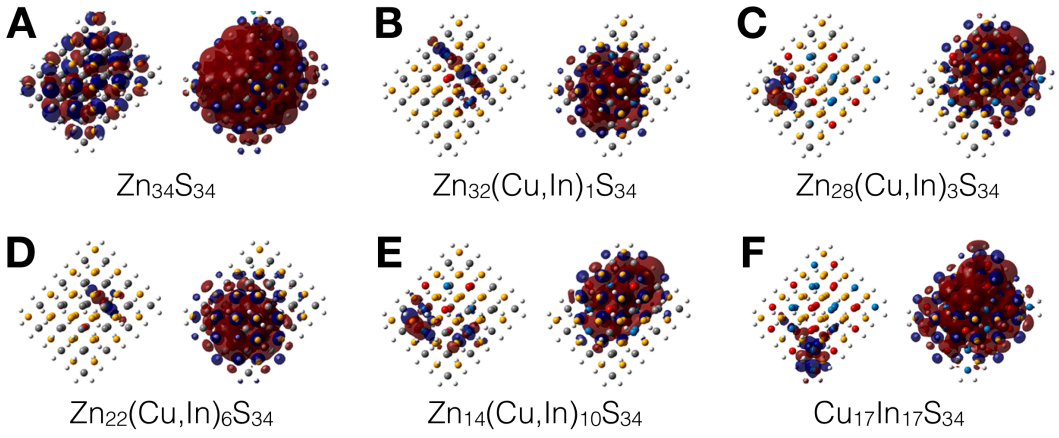

Figure 1.3. HOMO (left) and LUMO (right) DFT calculations for a series of alloyed Zn (grey)-Cu (blue)-In (red)-S (yellow) NCs from $Zn_{34}S_{34}$ to $CuInS_2$ shown in order of increasing copper and indium content. The HOMO remains localized after addition of copper, while the LUMO is delocalized. Figure adapted from ref. 34.

These observations further support the assignment that $CuInS_2$ NC PL arises as the recombination of a delocalized CB electron and a copper-localized hole while also disputing the previous assignment of recombination between a CB electron and a defect-localized hole.[35] Therefore, even though copper is present in stoichiometric amounts, it can still serve as an efficient localization center for photoexcited holes without the need to invoke defects in the luminescence mechanism. Computations such as these are powerful and help set the path for experimental investigation of the self-trapping mechanism. Monitoring spectroscopic markers such as PL energy as the copper concentration is increased from dopant to stoichiometric quantities in a series of alloyed ternary NC samples, then, can provide extra support for efficient hole localization in $CuInS_2$ NCs.

1.4 Intrinsic Traps in Semiconductor Nanocrystals

1.4.1. Surfaces of Indium Phosphide Semiconductor Nanocrystals. Semiconductor NC surfaces can greatly influence the material's photophysical properties due to their high surface-to-volume ratios.[36] NC surfaces are commonly passivated with long-chain organic ligands that coordinate to surface cations and anions. While these ligand-covered surfaces afford the NC colloidal stability, ligands do not always bind at all of the available surface atoms, leading to uncoordinated or under-coordinated ions that can act as charge-carrier trap sites.[37] When an electron or hole traps at the surface, the likelihood of non-radiative recombination increases, decreasing the radiative excitonic PL of the NC and lowering the PLQY.

InP NCs are highly susceptible to surface trapping but are of great interest to researchers as they are a proven less toxic alternative to the traditional lead (Pb)- and Cd-chalcogenide NCs.[10] However, before widespread penetration of InP NCs into everyday products can occur, a multitude

of problems must be overcome. Directly out of synthesis, InP NCs exhibit low (~1%) PLQYs and broad trap luminescence, in stark contrast to CdSe NCs, which can have with narrow linewidths and PLQYs of ~20-30% directly out of synthesis.[38-39] Figure 1.4 shows typical absorption and PL spectra for as-synthesized InP NCs with schematics illustrating the absorption, band-edge, and trap PL processes.

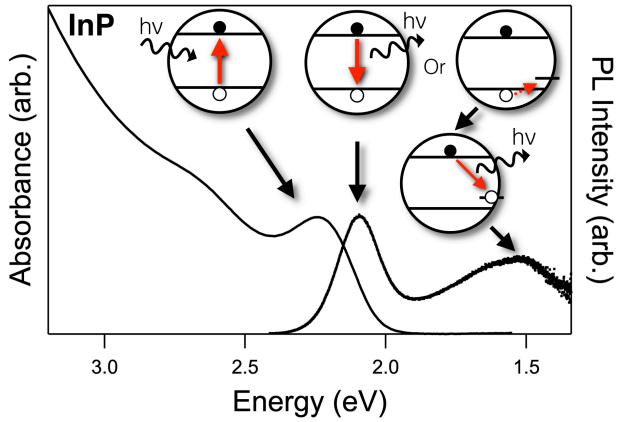

Figure 1.4. Absorption (left) and PL (right) spectra of InP NCs with schematics detailing the observed absorption and emission processes. The black arrows point to the corresponding transitions.

Numerous research groups have been working to increase the PLQY of InP NCs, and a variety of methods have been employed, all of which aim to passivate the surface of the NCs and reduce trap site density. Adding multiple layers, alloying, or using a combination of different semiconductor materials eliminates traps and increases PLQYs. Shell growth is a popular, albeit time and material intensive method of eliminating traps on NC surfaces, and the highest PLQYs of InP NCs thus far have been obtained through this method; the highest to-date was reported in early 2019 for InP/ZnSe/ZnS NCs at 95% PLQY.[40] Close competitors are InP/GaP/ZnS NCs with 85% PLQY[41] and InP/$ZnSe_xS_{1-x}$/ZnS NCs with 80% PLQY.[42]

Another common way of eliminating traps on the surface of InP NCs is through surface-etching with HF acid.[43-50] While this slightly reduces the NC size, it also removes under-

coordinated surface ions and forms In–F bonds.[51] Despite the highly toxic nature of HF, this post-synthetic treatment is likely a close second to shell growth as a preferred method to increase PLQYs. That said, a recent report detailed a microwave synthesis method using fluorinated ionic liquids (ILs) to obtain InP NCs with 30% PLQY directly out of synthesis without the use of HF.[52] Microwave syntheses appear to be gaining momentum[53-54] due to the ease with which NCs can be fabricated and the higher PLQYs attained directly out of synthesis.[52]

The Cossairt group has also shown that a simple post-synthetic surface annealing with Lewis acids can increase the PLQY of InP NCs.[55] Addition of Cd- and Zn-carboxylate results in sub-monolayer surface coverage, but the increase in PLQY rivals some shelled samples at ~50%. Through transmission electron microscopy (TEM), inductively-coupled plasma optical emission spectrometry (ICP-OES), and X-ray absorption spectroscopy (XAS) methods, it was demonstrated that the Cd^{2+} and Zn^{2+} ions displace In^{3+} ions at the NC surface. So rather than attempting to either grow shell layers on top of the surface or just completely etch it away, the traps can be eliminated, and the NC size can be retained. Interestingly, despite the consistency in NC size, it was observed that these surface treatments could still alter the NC absorption and emission energies, as seen in Figure 1.5, something that has only been reported a couple of times before for InP NCs[56] and has great implications for display technologies.

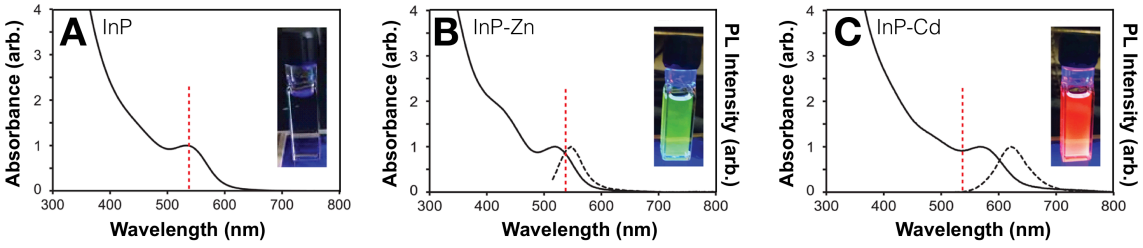

Figure 1.5. Absorption (left) and PL (right) spectra of InP NCs **(A)** and the same NCs after post-synthetic surface annealing with Zn-carboxylate (16 ± 4% PLQY) **(B)** and Cd-carboxylate (30 ± 11% PLQY) **(C).** The dashed red line corresponds to the first excitonic transition of the un-treated InP NCs in **A**, showing a clear blue-shift or red-shift when the NCs are treated with Zn^{2+} or Cd^{2+}, respectively. The

luminescence of each NC sample is shown in the inset photos. Figure adapted from ref. 55.

1.4.2. Charge-Carrier Trapping Implications on the PLQY of Indium Phosphide Nanocrystals. The aforementioned reports detail increases in NC PLQY. However, work to systematically analyze how changes in surface chemistry affect the mechanism by which charge-carrier trapping is reduced and the PLQY is increased are limited. As a result, low PLQYs have been attributed to both electron trapping[42,57-58] at under-coordinated indium sites (*a.k.a.* phosphorus vacancies)[59] and/or hole trapping[44,48-49] at under-coordinated phosphorus sites.[60] While researchers have obtained InP NCs with PLQYs close to 100%, it is still paramount we understand the exact microscopic changes that occur as surface traps are eliminated. This understanding will allow for creation of more targeted synthetic routes with which to obtain the highest-quality NCs.

One comprehensive report analyzed defect emission in both as-synthesized and HF-etched InP NCs using optically detected magnetic resonance (ODMR) spectroscopy.[59] Data showed a broadened resonance due to hyperfine coupling with indium nuclei. This led the authors to conclude that the defect emission is due to recombination of a VB hole with an electron trapped at an under-coordinated indium site. Another more recent work[48] invoked hole trapping as the sole determining factor of PLQYs in InP NCs. This conclusion was based on data from a combination of TRPL and transient absorption (TA) spectroscopy. A fast decay in the TRPL (~600 ps timescale) absent from the TA bleach recovery dynamics indicates fast hole trapping in the un-treated InP NC sample that disappears upon growth of a ZnS shell. Also, due to lack of correlation between the sample PLQY and TA bleach recovery dynamics, the authors specifically state that electron trapping is non-existent.

This being said, reports detailing the relative amounts of either electron or hole trapping processes may not apply to all InP NCs. There are many routes to make InP NCs, all with different synthetic conditions, precursors, and ligands. It is then reasonable to assume that the surfaces, and therefore trap-state densities of the resulting NCs are as different as the synthetic pathways taken to obtain them. However, we would expect the mechanism by which electron and hole trapping is eliminated, as well as the signatures of each to be the same. Charge-carrier trapping is a dynamic process; therefore, it makes sense to use time-resolved spectroscopy to study the photophysics of these materials. Interestingly, few reports have analyzed the full decay dynamics of multiple different InP NC samples. Only through vigorous analysis of the PL in samples with varying surface chemistries can we learn about the overall impact of surface chemistry modification on the PLQY of InP NCs.

1.4.3. Excitonic Fine Structure of Indium Phosphide Nanocrystals. While recent work has mainly focused on increasing InP NC PLQY, a few reports have examined the excitonic fine structure of these materials using low-temperature TRPL experiments.[61-62] The PL dynamics of as-synthesized InP NCs are dominated by non-radiative recombination resulting in fast-initial decays, which complicates analysis of time-resolved data necessary to study excitonic fine structure. These fast decays can be eliminated upon shelling the NC, however, which has led to the observation of bright-dark (B-D) splitting features in shelled samples.[61-62]

It has been shown that the lowest energy excited state in InP NCs is a dark state.[61] Radiative emission originates from this dark state at low temperatures. A brighter state lies higher in energy, from which recombination occurs at higher temperatures.[62] At low temperatures, the B-D splitting manifests itself as a biexponential decay, as can be seen in Figure 1.6. The fast, initial decay is due

to emission from the bright state prior to thermalization into the dark state. The slower component of the biexponential is the emission from a thermal equilibrium between the formally-forbidden dark state and the upper bright state. As the temperature is increased, the fast-initial decay disappears, and the slower component gets faster.

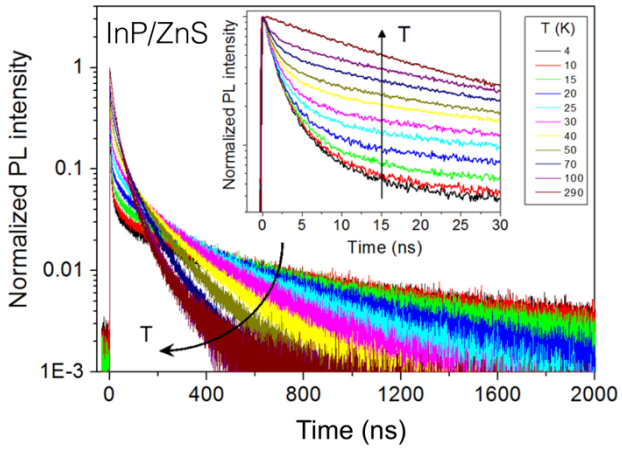

Figure 1.6. TRPL decay dynamics collected as a function of temperature for InP/ZnS NCs. At low temperatures (4 K, black), there is a fast-initial decay followed by a slower component. As the temperature increases (black to maroon), the fast-initial decay disappears, and the overall lifetime decreases. Inset: the same decay dynamics shown out to only 30 ns. Figure adapted from ref. 61.

As evident by the observation of B-D splitting, high-quality samples afford us the opportunity to study and begin to manipulate the photophysics of InP NCs to further elucidate the electronic structure of this important class of materials.

1.5 Summary and Conclusions

In summary, understanding and controlling the energetic landscape of semiconductor NCs is crucial to obtaining samples with high PLQYs. Non-radiative recombination is detrimental to a NC's PL efficiency, and unwanted trap states can drastically inhibit luminescence. One way this issue has been addressed is through the use of "engineered" trap sites within the NC core. An

engineered trap site, like copper(I), results in efficient charge-carrier localization, minimizing surface trapping and subsequent non-radiative charge-carrier recombination. Another way to reduce non-radiative recombination is by developing targeted synthetic strategies to eliminate surface electron and hole trapping. Only through careful study of how different surface chemistries affect the PL mechanism can we create routes to obtain high-quality samples. Overall, there is still much to gain from studying the luminescence mechanism of semiconductor NCs from the standpoints of both applications and fundamental materials research.

1.6 References

1. Smith, A. M.; Nie, S., Semiconductor Nanocrystals: Structure, Properties, and Band Gap Engineering. *Acc. Chem. Res.* **2010,** *43* (2), 190-200.
2. Talapin, D. V.; Lee, J.-S.; Kovalenko, M. V.; Shevchenko, E. V., Prospects of Colloidal Nanocrystals for Electronic and Optoelectronic Applications. *Chem. Rev.* **2010,** *110* (1), 389-458.
3. Ropp, R. C., *Luminescence and the Solid State*. Elsevier Science: 2013.
4. Bruchez, M.; Moronne, M.; Gin, P.; Weiss, S.; Alivisatos, A. P., Semiconductor Nanocrystals as Fluorescent Biological Labels. *Science* **1998,** *281* (5385), 2013.
5. Bradshaw, L. R.; Knowles, K. E.; McDowall, S.; Gamelin, D. R., Nanocrystals for Luminescent Solar Concentrators. *Nano Lett.* **2015,** *15* (2), 1315-1323.
6. Knowles, K. E.; Kilburn, T. B.; Alzate, D. G.; McDowall, S.; Gamelin, D. R., Bright CuInS2/CdS nanocrystal phosphors for high-gain full-spectrum luminescent solar concentrators. *Chem. Commun.* **2015,** *51* (44), 9129-9132.
7. Yoon, H. C.; Oh, J. H.; Ko, M.; Yoo, H.; Do, Y. R., Synthesis and Characterization of Green Zn–Ag–In–S and Red Zn–Cu–In–S Quantum Dots for Ultrahigh Color Quality of Down-Converted White LEDs. *ACS Appl. Mater. & Interf.* **2015,** *7* (13), 7342-7350.
8. Talapin, D. V.; Steckel, J., Quantum dot light-emitting devices. *MRS Bulletin* **2013,** *38* (9), 685-691.
9. Rossetti, R.; Brus, L., Electron-hole recombination emission as a probe of surface chemistry in aqueous cadmium sulfide colloids. *J. Phys. Chem.* **1982,** *86* (23), 4470-4472.
10. Tamang, S.; Lincheneau, C.; Hermans, Y.; Jeong, S.; Reiss, P., Chemistry of InP Nanocrystal Syntheses. *Chem. Mater.* **2016,** *28* (8), 2491-2506.
11. Ekimov, A. I.; Efros, A. L.; Onushchenko, A. A., Quantum size effect in semiconductor microcrystals. *Solid State Commun.* **1985,** *56* (11), 921-924.
12. Yen, W. M.; Shionoya, S.; Yamamoto, H., *Phosphor Handbook*. Second ed.; CRC Press: New York, 2007.
13. Knowles, K. E.; Hartstein, K. H.; Kilburn, T. B.; Marchioro, A.; Nelson, H. D.; Whitham, P. J.; Gamelin, D. R., Luminescent Colloidal Semiconductor Nanocrystals Containing

Copper: Synthesis, Photophysics, and Applications. *Chem. Rev.* **2016,** *116* (18), 10820-10851.
14. Harvey, E. N., *A History of Luminescence: From the Earliest Times Until 1900*. CreateSpace Independent Publishing Platform: 2015.
15. Shionoya, S.; Koda, T.; Era, K.; Fujiwara, H., Nature of Luminescence Transitions in ZnS Crvstals. *J. Phys. Soc. Jpn.* **1964,** *19* (7), 1157-1167.
16. Suzuki, A.; Shionoya, S., Mechanism of the Green-Copper Luminescence in ZnS Crystals. I. Direct Evidence for the Pair Emission Mechanism. *J. Phys. Soc. Jpn.* **1971,** *31*, 1455-1461.
17. Erickson, C. S.; Bradshaw, L. R.; McDowall, S.; Gilbertson, J. D.; Gamelin, D. R.; Patrick, D. L., Zero-Reabsorption Doped-Nanocrystal Luminescent Solar Concentrators. *ACS Nano* **2014,** *8* (4), 3461-3467.
18. Knowles, K. E.; Nelson, H. D.; Kilburn, T. B.; Gamelin, D. R., Singlet–Triplet Splittings in the Luminescent Excited States of Colloidal Cu+:CdSe, Cu+:InP, and CuInS2 Nanocrystals: Charge-Transfer Configurations and Self-Trapped Excitons. *J. Am. Chem. Soc.* **2015,** *137* (40), 13138-13147.
19. Grandhi, G. K.; Tomar, R.; Viswanatha, R., Study of Surface and Bulk Electronic Structure of II–VI Semiconductor Nanocrystals Using Cu as a Nanosensor. *ACS Nano* **2012,** *6* (11), 9751-9763.
20. Nelson, H. D.; Li, X.; Gamelin, D. R., Computational Studies of the Electronic Structures of Copper-Doped CdSe Nanocrystals: Oxidation States, Singlet-Triplet Splittings, Jahn-Teller Distortions, and Vibronic Bandshapes. *J. Phys. Chem. C* **2016,** *120*, 5714–5723.
21. Viswanatha, R.; Brovelli, S.; Pandey, A.; Crooker, S. A.; Klimov, V. I., Copper Doped Inverted Core/Shell Nanocrystals with "Permanent" Optically Active Holes. *Nano Lett.* **2011,** *11* (11), 4753-4758.
22. Yang, L.; Knowles, K. E.; Gopalan, A.; Hughes, K. E.; James, M. C.; Gamelin, D. R., One-Pot Synthesis of Monodisperse Colloidal Copper-Doped CdSe Nanocrystals Mediated by Ligand–Copper Interactions. *Chem. Mater.* **2016,** *28* (20), 7375-7384.
23. Hughes, K. E.; Hartstein, K. H.; Gamelin, D. R., Photodoping and Transient Spectroscopies of Copper-Doped CdSe/CdS Nanocrystals. *ACS Nano* **2018,** *12* (1), 718-728.
24. Rinehart, J. D.; Schimpf, A. M.; Weaver, A. L.; Cohn, A. W.; Gamelin, D. R., Photochemical Electronic Doping of Colloidal CdSe Nanocrystals. *J. Am. Chem. Soc.* **2013,** *135* (50), 18782-18785.
25. Schimpf, A. M.; Gunthardt, C. E.; Rinehart, J. D.; Mayer, J. M.; Gamelin, D. R., Controlling Carrier Densities in Photochemically Reduced Colloidal ZnO Nanocrystals: Size Dependence and Role of the Hole Quencher. *J. Am. Chem. Soc.* **2013,** *135* (44), 16569-16577.
26. Hartstein, K. H.; Erickson, C. S.; Tsui, E. Y.; Marchioro, A.; Gamelin, D. R., Electron Stability and Negative-Tetron Luminescence in Free-Standing Colloidal n-Type CdSe/CdS Quantum Dots. *ACS Nano* **2017,** *11* (10), 10430-10438.
27. Cohn, A. W.; Rinehart, J. D.; Schimpf, A. M.; Weaver, A. L.; Gamelin, D. R., Size Dependence of Negative Trion Auger Recombination in Photodoped CdSe Nanocrystals. *Nano Lett.* **2014,** *14* (1), 353-358.
28. Leach, A. D. P.; Macdonald, J. E., The Optoelectronic Properties of $CuInS_2$ Nanocrystals and their Origin. *J. Phys. Chem. Lett.* **2016,** *7*, 572-583.

29. Leach, A. D. P.; Shen, X.; Faust, A.; Cleveland, M. C.; La Croix, A. D.; Banin, U.; Pantelides, S. T.; Macdonald, J. E., Defect Luminescence from Wurtzite $CuInS_2$ Nanocrystals: Combined Experimental and Theoretical Analysis. *J. Phys. Chem. C* **2016,** *120*, 5207-5212.
30. Rice, W. D.; McDaniel, H.; Klimov, V. I.; Crooker, S. A., Magneto-Optical Properties of CuInS2 Nanocrystals. *J. Phys. Chem. Lett.* **2014,** *5* (23), 4105-4109.
31. Kraatz, I. T.; Booth, M.; Whitaker, B. J.; Nix, M. G. D.; Critchley, K., Sub-Bandgap Emission and Intraband Defect-Related Excited-State Dynamics in Colloidal CuInS2/ZnS Quantum Dots Revealed by Femtosecond Pump−Dump−Probe Spectroscopy. *J. Phys. Chem. C* **2014,** *118*, 24102−24109.
32. Tell, B.; Shay, J. L.; Kasper, H. M., Electrical Properties, Optical Properties, and Band Structure of CuGa${\mathrm{S}}_{2}$ and CuIn${\mathrm{S}}_{2}$. *Phys. Rev. B* **1971,** *4* (8), 2463-2471.
33. Vogelsang, H.; Husberg, O.; Köhler, U.; von der Osten, W.; Marchetti, A. P., Exciton self-trapping in AgCl nanocrystals. *Phys. Rev. B* **2000,** *61* (3), 1847-1852.
34. Nelson, H. D.; Gamelin, D. R., Valence-Band Electronic Structures of Cu+-Doped ZnS, Alloyed Cu−In−Zn−S, and Ternary CuInS2 Nanocrystals: A Unified Description of Photoluminescence across Compositions. *J. Phys. Chem. C* **2018,** *122*, 18124–18133.
35. Li, L.; Pandey, A.; Werder, D. J.; Khanal, B. P.; Pietryga, J. M.; Klimov, V. I., Efficient Synthesis of Highly Luminescent Copper Indium Sulfide-Based Core/Shell Nanocrystals with Surprisingly Long-Lived Emission. *J. Am. Chem. Soc.* **2011,** *133* (5), 1176-1179.
36. Boles, M. A.; Ling, D.; Hyeon, T.; Talapin, D. V., The surface science of nanocrystals. *Nat. Mat.* **2016,** *15*, 141.
37. Chadi, D. J., Atomic and Electronic Structures of Reconstructed Si(100) Surfaces. *Phys. Rev. Lett.* **1979,** *43* (1), 43-47.
38. Qu, L.; Peng, Z. A.; Peng, X., Alternative Routes toward High Quality CdSe Nanocrystals. *Nano Lett.* **2001,** *1* (6), 333-337.
39. Cossairt, B. M., Shining Light on Indium Phosphide Quantum Dots: Understanding the Interplay among Precursor Conversion, Nucleation, and Growth. *Chem. Mater.* **2016,** *28* (20), 7181-7189.
40. Kim, Y.; Ham, S.; Jang, H.; Min, J. H.; Chung, H.; Lee, J.; Kim, D.; Jang, E., Bright and Uniform Green Light Emitting InP/ZnSe/ZnS Quantum Dots for Wide Color Gamut Displays. *ACS Appl. Nano Mater.* **2019,** *2* (3), 1496-1504.
41. Kim, S.; Kim, T.; Kang, M.; Kwak, S. K.; Yoo, T. W.; Park, L. S.; Yang, I.; Hwang, S.; Lee, J. E.; Kim, S. K.; Kim, S.-W., Highly Luminescent InP/GaP/ZnS Nanocrystals and Their Application to White Light-Emitting Diodes. *J. Am. Chem. Soc.* **2012,** *134* (8), 3804-3809.
42. Hahm, D.; Chang, J. H.; Jeong, B. G.; Park, P.; Kim, J.; Lee, S.; Choi, J.; Kim, W. D.; Rhee, S.; Lim, J.; Lee, D. C.; Lee, C.; Char, K.; Bae, W. K., Design Principle for Bright, Robust, and Color-Pure InP/ZnSexS1–x/ZnS Heterostructures. *Chem. Mater.* **2019**.
43. Mićić, O. I.; Cheong, H. M.; Fu, H.; Zunger, A.; Sprague, J. R.; Mascarenhas, A.; Nozik, A. J., Size-Dependent Spectroscopy of InP Quantum Dots. *J. Phys. Chem. B* **1997,** *101* (25), 4904-4912.
44. Blackburn, J. L.; Ellingson, R. J.; Mićić, O. I.; Nozik, A. J., Electron Relaxation in Colloidal InP Quantum Dots with Photogenerated Excitons or Chemically Injected Electrons. *J.Phys. Chem. B* **2003,** *107* (1), 102-109.

45. Ellingson, R. J.; Blackburn, J. L.; Yu, P.; Rumbles, G.; Mićić, O. I.; Nozik, A. J., Excitation Energy Dependent Efficiency of Charge Carrier Relaxation and Photoluminescence in Colloidal InP Quantum Dots. *J.Phys. Chem. B* **2002,** *106* (32), 7758-7765.
46. Mićić, O. I.; Sprague, J.; Lu, Z.; Nozik, A. J., Highly efficient band-edge emission from InP quantum dots. *Appl. Phys. Lett.* **1996,** *68* (22), 3150-3152.
47. Poles, E.; Selmarten, D. C.; Mićić, O. I.; Nozik, A. J., Anti-Stokes photoluminescence in colloidal semiconductor quantum dots. *Appl. Phys. Lett.* **1999,** *75* (7), 971-973.
48. Janke, E. M.; Williams, N. E.; She, C.; Zherebetskyy, D.; Hudson, M. H.; Wang, L.; Gosztola, D. J.; Schaller, R. D.; Lee, B.; Sun, C.; Engel, G. S.; Talapin, D. V., Origin of Broad Emission Spectra in InP Quantum Dots: Contributions from Structural and Electronic Disorder. *J. Am. Chem. Soc.* **2018,** *140* (46), 15791-15803.
49. Adam, S.; Talapin, D. V.; Borchert, H.; Lobo, A.; McGinley, C.; Castro, A. R. B. d.; Haase, M.; Weller, H.; Möller, T., The effect of nanocrystal surface structure on the luminescence properties: Photoemission study of HF-etched InP nanocrystals. *J. Chem. Phys.* **2005,** *123* (8), 084706.
50. Talapin, D. V.; Gaponik, N.; Borchert, H.; Rogach, A. L.; Haase, M.; Weller, H., Etching of Colloidal InP Nanocrystals with Fluorides: Photochemical Nature of the Process Resulting in High Photoluminescence Efficiency. *J. Phys. Chem. B* **2002,** *106* (49), 12659-12663.
51. Kim, T.-G.; Zherebetskyy, D.; Bekenstein, Y.; Oh, M. H.; Wang, L.-W.; Jang, E.; Alivisatos, A. P., Trap Passivation in Indium-Based Quantum Dots through Surface Fluorination: Mechanism and Applications. *ACS Nano* **2018,** *12* (11), 11529-11540.
52. Siramdas, R.; McLaurin, E. J., InP Nanocrystals with Color-Tunable Luminescence by Microwave-Assisted Ionic-Liquid Etching. *Chem. Mater.* **2017,** *29* (5), 2101-2109.
53. Baghbanzadeh, M.; Carbone, L.; Cozzoli, P. D.; Kappe, C. O., Microwave-Assisted Synthesis of Colloidal Inorganic Nanocrystals. *Angew. Chem., Int. Ed.* **2011,** *50* (48), 11312-11359.
54. Zhu, Y.-J.; Chen, F., Microwave-Assisted Preparation of Inorganic Nanostructures in Liquid Phase. *Chem. Rev.* **2014,** *114* (12), 6462-6555.
55. Stein, J. L.; Mader, E. A.; Cossairt, B. M., Luminescent InP Quantum Dots with Tunable Emission by Post-Synthetic Modification with Lewis Acids. *J. Phys. Chem. Lett.* **2016,** *7* (7), 1315-1320.
56. Kirkwood, N.; Monchen, J. O. V.; Crisp, R. W.; Grimaldi, G.; Bergstein, H. A. C.; du Fossé, I.; van der Stam, W.; Infante, I.; Houtepen, A. J., Finding and Fixing Traps in II–VI and III–V Colloidal Quantum Dots: The Importance of Z-Type Ligand Passivation. *J. Am. Chem. Soc.* **2018,** *140* (46), 15712-15723.
57. Thomas, A.; Sandeep, K.; Somasundaran, S. M.; Thomas, K. G., How Trap States Affect Charge Carrier Dynamics of CdSe and InP Quantum Dots: Visualization through Complexation with Viologen. *ACS Energy Lett.* **2018,** *3* (10), 2368-2375.
58. Kim, S. H.; Wolters, R. H.; Heath, J. R., Photophysics of size-selected InP nanocrystals: Exciton recombination kinetics. *J. Chem. Phys.* **1996,** *105* (18), 7957-7963.
59. Langof, L.; Ehrenfreund, E.; Lifshitz, E.; Micic, O. I.; Nozik, A. J., Continuous-Wave and Time-Resolved Optically Detected Magnetic Resonance Studies of Nonetched/Etched InP Nanocrystals. *J. Phys. Chem. B* **2002,** *106* (7), 1606-1612.
60. Fu, H.; Zunger, A., InP quantum dots: Electronic structure, surface effects, and the redshifted emission. *Phys. Rev. B* **1997,** *56* (3), 1496-1508.

61. Biadala, L.; Siebers, B.; Beyazit, Y.; Tessier, M. D.; Dupont, D.; Hens, Z.; Yakovlev, D. R.; Bayer, M., Band-Edge Exciton Fine Structure and Recombination Dynamics in InP/ZnS Colloidal Nanocrystals. *ACS Nano* **2016,** *10* (3), 3356-3364.
62. Brodu, A.; Ballottin, M. V.; Buhot, J.; van Harten, E. J.; Dupont, D.; La Porta, A.; Prins, P. T.; Tessier, M. D.; Versteegh, M. A. M.; Zwiller, V.; Bals, S.; Hens, Z.; Rabouw, F. T.; Christianen, P. C. M.; de Mello Donega, C.; Vanmaekelbergh, D., Exciton Fine Structure and Lattice Dynamics in InP/ZnSe Core/Shell Quantum Dots. *ACS Photonics* **2018,** *5* (8), 3353-3362.

Chapter 2: Photodoping and Transient Spectroscopies of Copper-Doped CdSe/CdS Nanocrystals

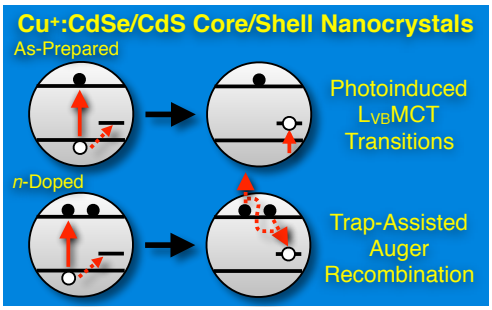

Adapted with permission from:
Hughes, K. E.; Hartstein, K. H., Gamelin, D. R. *ACS Nano* **2018**, *12*, 718–728.

2.1 Overview

Colloidal Cu^+-doped CdSe/CdS core/shell semiconductor nanocrystals (NCs) are investigated in their as-prepared and degenerately *n*-doped forms using time-resolved photoluminescence and transient-absorption spectroscopies. Photoluminescence from Cu^+:CdSe/CdS NCs is dominated by recombination of delocalized conduction-band (CB) electrons with copper-localized holes. In addition to prominent bleaching of the first excitonic absorption feature, transient-absorption measurements show bleaching of the sub-bandgap copper-to-CB charge-transfer ($ML_{CB}CT$) absorption band and also reveal a photoinduced mid-gap valence-band (VB)-to-copper charge transfer ($L_{VB}MCT$) absorption band that extends into the near-infrared, as predicted by recent computations. The photoluminescence of these NCs is substantially diminished upon introduction of excess CB electrons *via* photodoping. Time-resolved photoluminescence measurements reveal that the $ML_{CB}CT$ excited state is still formed upon photoexcitation of the *n*-doped Cu^+:CdSe/CdS NCs, but its luminescence is quenched by a fast (picosecond) three-carrier trap-assisted Auger recombination process involving two CB electrons and one copper-bound hole.

2.2 Introduction

Copper-doped semiconductors have played a central role in the history of phosphors for lighting and display technologies.[1] The classic green phosphor Cu^+-doped ZnS has been studied

in great detail and represents a paradigmatic example of donor-acceptor pair (DAP) emission in the solid state.[1-3] In this bulk material, excitation of the host semiconductor to generate band-like charge carriers is followed by rapid and deep hole localization around copper and shallow electron binding to donors near the conduction-band (CB) edge. Radiative recombination of those electrons with the deeply trapped holes generates broad emission at energies well below the onset of the host's absorption.

In recent years, luminescent colloidal copper-doped semiconductor nanocrystals[4-10] (NCs) have been attracting attention for applications such as light-emitting diodes,[11-12] bio-labels,[13-14] or luminescent solar concentrators (LSCs).[15-16] Although the specific photoluminescence (PL) mechanism of copper-doped NCs is still sometimes debated, a great deal of evidence now points to the photophysical sequence outlined in Scheme 2.1.[4] Here, NC photoexcitation is followed by rapid hole capture by copper and subsequent slow recombination of this trapped hole with a delocalized CB-like electron. The electron in this process is subject to quantum confinement, affording attractive PL tunability through NC size or composition. This PL is characteristically broad, not simply because of inhomogeneous effects (*e.g.*, size distributions, copper radial distributions, *etc.*), but also because of strong electron-phonon coupling in the luminescent excited state that accompanies hole localization. Computational studies on Cu^{+}:CdSe NCs have shown that this hole localizes almost entirely within a highly covalent [$CuSe_4$] cluster, causing this cluster's geometry to reorganize substantially *via* Cu-Se bond-length contractions and a Jahn-Teller low-symmetry deformation.[17] These distortions manifest themselves as Franck-Condon progressions that broaden the homogeneous PL bandshape.

Scheme 2.1. Proposed Sequence of Events Responsible for the Photoluminescence of Cu^+-Doped CdSe NCs.

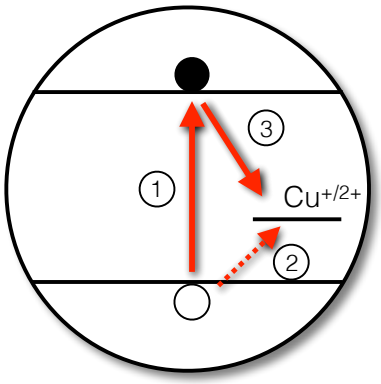

The rich chemical tunability and solution compatibility of this class of materials has driven research into luminescent copper-containing NCs of numerous compositions, shapes, and sizes.[4] For LSCs in particular, the large luminescence Stokes shifts displayed by copper-doped NCs lead to extremely low reabsorption losses,[15] even below those of other leading visible-light-absorbing nanocrystal LSC phosphors such as $CuInS_2$ or CdSe/CdS NCs.[15, 18] With recent improvements in photoluminescence quantum yields (PL QYs), reaching nearly 100% in Cu^+-doped CdSe nanoplatelets,[16] these materials show great promise for solution-processed optoelectronics.

An interesting chemical challenge in investigating copper-doped NCs is the high diffusivity of Cu^+ in semiconductor lattices. On one hand, high diffusivity is powerful because NCs like CdSe can be post-synthetically doped with rapidly diffusion cations like copper or silver *via* partial cation exchange.[19-22] The same high diffusivity can also be detrimental, however, because these dopants are easily lost again during sample purification or processing. For example, reliable shelling procedures for Cu^+-doped NCs would be attractive for many reasons, including surface passivation, heterostructure formation, and stabilization of *n*-doped configurations,[23] but we have observed that shelling Cu^+:CdSe NCs with CdS causes loss of $ML_{CB}CT$ PL and recovery of the NC band-edge PL because of copper loss. Amines, which are commonly used in many shelling procedures and also as NC surface-capping ligands, were found to extract copper from doped CdSe

NCs, even at room temperature.[21] Copper's high diffusivity thus complicates traditional routes for shelling copper-doped NCs, inhibiting spectroscopic and photophysical studies of Cu^+:CdSe/CdS core/shell NCs as well as investigation of stable *n*-doped Cu^+:CdSe/CdS NCs.

Here, we report the successful incorporation of copper directly into pre-formed CdSe/CdS core/shell NCs by post-synthetic partial cation exchange, circumventing the above challenges. The resulting NCs were examined through a series of spectroscopic and photochemical experiments to probe their electronic structure and photodynamics. Using a combination of transient-absorption (TA) and time-resolved PL (TRPL) spectroscopies, we have probed the critical processes of hole capture by Cu^+ and subsequent electron-hole recombination, both spectrally and temporally. TA measurements show signatures not only of the photogenerated electrons, as for most undoped NCs, but also of the photogenerated holes in the luminescent excited state *via* appearance of a new photoinduced mid-gap valence-band (VB)-to-copper charge-transfer ($L_{VB}MCT$) absorption band. We further examine the effect of photochemical *n*-doping on the photophysical properties of these Cu^+:CdSe/CdS core/shell NCs. These experiments show that excess delocalized CB electrons quench the characteristic copper-based PL by a picosecond three-particle trap-assisted Auger recombination mechanism, with implications for current-driven processes such as electroluminescence involving copper-containing semiconductor nanocrystals. Clear examples of trap-assisted Auger recombination in colloidal semiconductor NCs are relatively rare, and this observation points to opportunities for investigation of trap-assisted Auger processes using copper as a designer hole trap. Overall, these results clarify the microscopic photophysical processes that lead to both luminescence and carrier-mediated luminescence quenching in this class of nanomaterials, and may help to accelerate further development of such materials for application in future optoelectronic, sensing, or solar technologies.

2.3 Results and Analysis

2.3.1. Synthesis and General Characterization. Figure 2.1 presents TEM images of a representative series of core CdSe NCs, CdSe/CdS NCs grown from these cores, and Cu^+:CdSe/CdS NCs prepared by post-synthetic doping of these same core/shell NCs. The core CdSe NCs have an average diameter of 4.4 ± 0.3 nm. The NC diameter increases to 5.2 ± 0.4 nm upon addition of a CdS shell. These NCs remain the same size upon copper doping. The average amount of copper incorporated into these Cu^+:CdSe/CdS NCs was determined by ICP-AES to be 4.5% (total cations), which corresponds to roughly 65 copper ions per NC. The TEM images show no evidence of side-product formation.

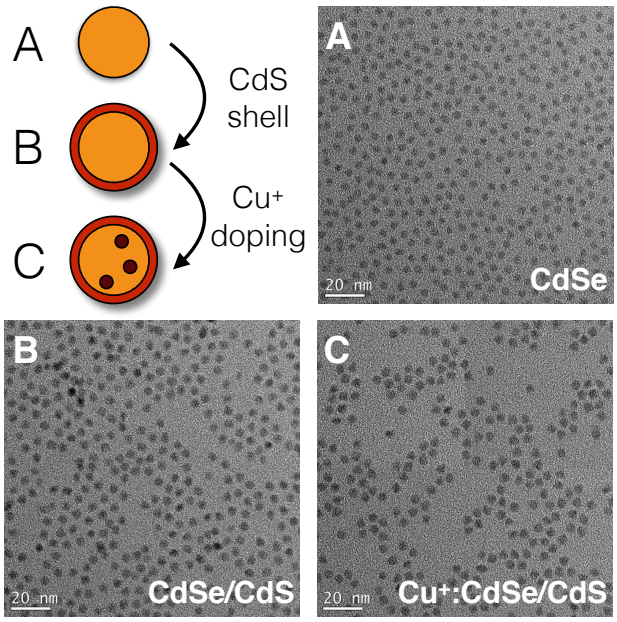

Figure 2.1. TEM images of a series of related nanocrystals. **(A)** CdSe NCs synthesized by hot injection. **(B)** The same NCs after growth of a thin (<2 ML) shell of CdS, *i.e.*, CdSe/CdS NCs. **(C)** The same CdSe/CdS NCs after doping with copper, *i.e.*, Cu^+:CdSe/CdS NCs.

2.3.2. Absorption and Photoluminescence. Figure 2.2A shows electronic absorption and steady-state PL spectra of the CdSe, CdSe/CdS, and Cu^+:CdSe/CdS NCs from Figure 2.1. The first

excitonic absorption maximum red-shifts by about 60 meV with the addition of the thin CdS shell (<2 monolayers). The absorption spectrum remains largely unchanged upon copper doping, but a small amount of new copper $ML_{CB}CT$ absorption is detectable below the first NC excitonic maximum, as detailed previously.[8, 21] The luminescence spectra of the CdSe and CdSe/CdS NCs are both dominated by excitonic PL. Copper incorporation changes this PL dramatically, yielding broad emission with a large effective Stokes shift of ~700 meV (between first excitonic absorption and PL maxima), assigned as the copper $ML_{CB}CT$ luminescence illustrated in Scheme 2.1. There is negligible excitonic PL from these Cu^+:CdSe/CdS NCs, consistent with doping of all NCs and rapid hole capture by copper. Figure 2.2B plots PL decay curves measured for the same CdSe, CdSe/CdS, and Cu^+:CdSe/CdS NCs. The PL decay time increases dramatically upon doping with copper, now having an average time constant of 1.4 ± 0.1 μs (*vide infra*). These spectroscopic data are consistent with observations for other copper-doped semiconductor NCs[4-8, 10] and establish these materials as suitable for more in-depth spectroscopic studies.

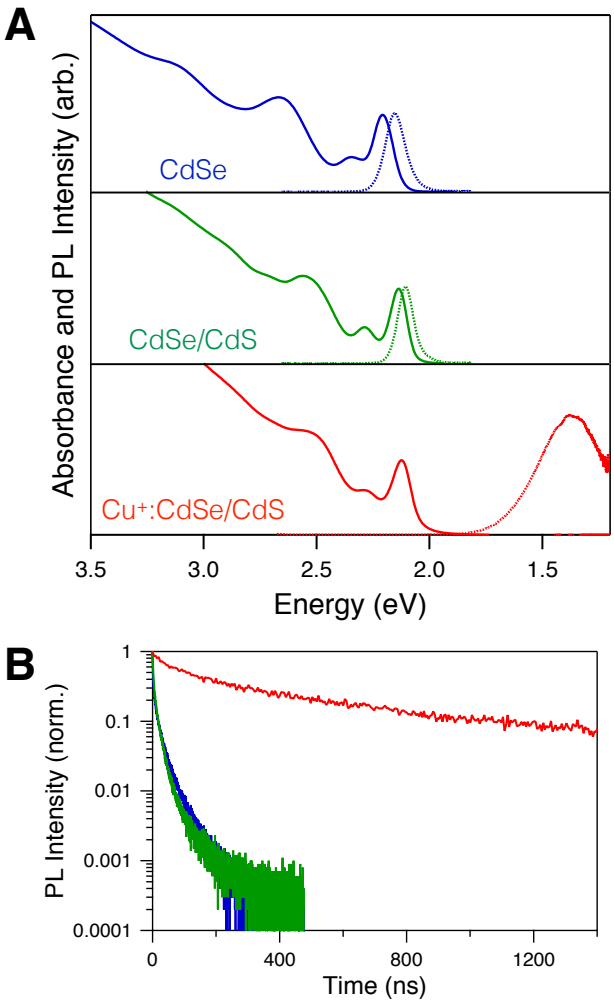

Figure 2.2. (A) Room-temperature absorption (solid) and PL (dotted) spectra of the CdSe (blue), CdSe/CdS (green), and Cu^+:CdSe/CdS (red) NCs from Figure 2.1, in toluene. A large effective Stokes shift and PL broadening are seen upon incorporation of copper into the NCs. There is negligible excitonic PL in the copper-doped NCs. **(B)** Room-temperature PL decay dynamics of the same CdSe (blue), CdSe/CdS (green), and Cu^+:CdSe/CdS (red) NCs.

Figure 2.3 presents room-temperature time-resolved PL (TRPL) data collected for the Cu^+:CdSe/CdS NCs of Figures 2.1 and 2.2, but now focusing on the sub-nanosecond timescale. Although essentially absent from the steady-state PL spectrum (Figure 2.2A), excitonic PL is detected by TRPL at short times following the excitation pulse. The blue curve in Figure 2.3A plots the TRPL dynamics measured for this excitonic PL (580–605 nm). The red curve in Figure 2.3A plots the TRPL dynamics measured for the copper-based $ML_{CB}CT$ PL (775–825 nm) of the

same sample. Note that the long $ML_{CB}CT$ PL lifetime (Figure 2.2B) means a small PL rate and hence few photons on these sub-nanosecond timescales. The dashed grey curve in Figure 2.3A shows the instrument response function (IRF, ~25 ps). The excitonic PL largely tracks the IRF, with only a slightly slower decay after photoexcitation, indicating that this PL is primarily present only during photoexcitation. The exciton lifetime is thus shortened from ~6 ns to ~25 ps upon introduction of Cu^+ into these CdSe/CdS NCs. In contrast with the excitonic PL, the $ML_{CB}CT$ PL intensity only grows during the IRF, and it decays slowly after excitation is terminated. Both the slow rise and the slow decay reflect the long lifetime of the luminescent $ML_{CB}CT$ excited state.

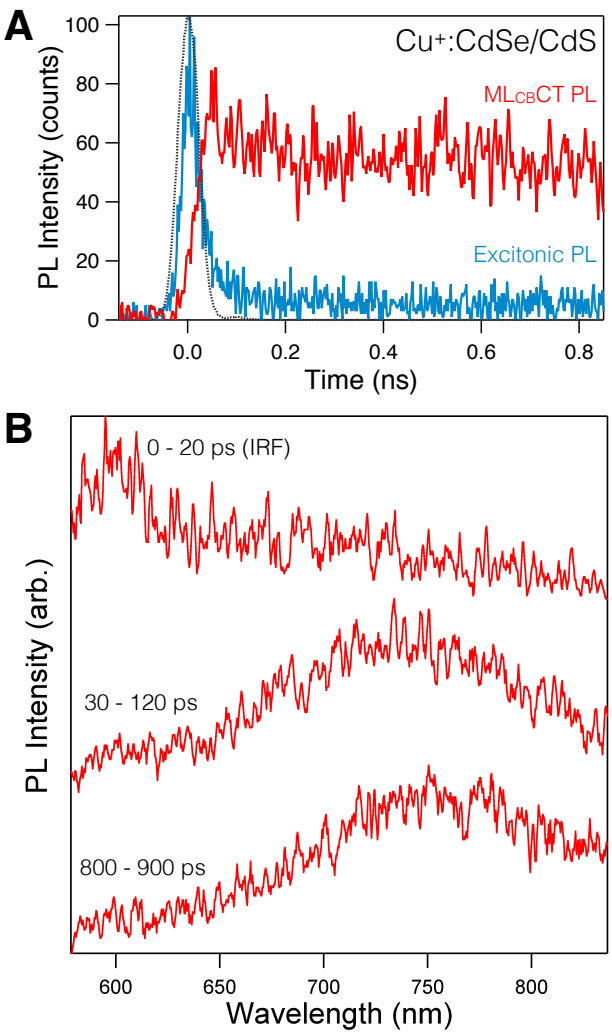

Figure 2.3. Data from room-temperature TRPL measurements of Cu^+:CdSe/CdS NCs. **(A)** TRPL dynamics of Cu^+:CdSe/CdS NCs. The blue curve shows the dynamics of the excitonic PL (580–605 nm), and the red curve shows the copper $ML_{CB}CT$ PL dynamics (775–825 nm). The black dashed curve shows the instrument response function (IRF). The excitonic PL largely tracks the instrument response function, but the $ML_{CB}CT$ PL grows in throughout the IRF. Fitting the IRF to a Gaussian function gives a response time of ~25 ps. **(B)** Gated TRPL spectra of Cu^+:CdSe/CdS NCs integrated for time windows between 0–20 ps (top), 30–120 ps (middle), and 800–900 ps (bottom). At early times, excitonic PL is present and $ML_{CB}CT$ PL is absent. As time evolves, the excitonic PL disappears and the $ML_{CB}CT$ PL appears.

Figure 2.3B presents three gated TRPL spectra of these Cu^+:CdSe/CdS NCs, representing the emission at different delay times following the photoexcitation pulse. The top curve represents integration between 0 and 20 ps (*i.e.*, during the IRF) and shows essentially only excitonic PL. The

middle curve represents integration between 30 and 120 ps and shows the emergence of copper $ML_{CB}CT$ PL alongside a small amount of excitonic PL. The bottom curve, integrated between 800 and 900 ps, shows exclusively $ML_{CB}CT$ PL, with no evident excitonic PL anymore. Together, the data in Figure 2.3A,B support the conclusion of very fast (~25 ps) energy relaxation from the excitonic state to the mid-gap $ML_{CB}CT$ excited state in these Cu^+:CdSe/CdS NCs, *i.e.*, rapid hole capture by copper as illustrated in Scheme 2.1.

2.3.3. Transient Absorption Spectroscopy of Cu^+:CdSe/CdS NCs. Figure 2.4 plots absorption and TA spectra of the Cu^+:CdSe/CdS NCs described in Figure 2.1. The TA spectrum is dominated by a pronounced bleach of the first excitonic absorption band. An additional small negative feature with an asymmetric shape is observed on the red side of this exciton bleach, centered at ~610 nm. The TA spectra of undoped CdSe and CdSe/CdS NCs typically show only a small positive (photoinduced) signal just below the first exciton (see Appendix A), reflecting Coulombically shifted biexciton or negative-trion absorption.[24-25] These and other Cu^+-doped NCs display weak $ML_{CB}CT$ absorption in this region (Figure 2.2).[8, 21] We thus assign the negative TA signal at ~610 nm in Figure 2.4 to the bleach of sub-bandgap $ML_{CB}CT$ absorption. The photoinduced absorption from multi-carrier excitonic configurations is superimposed upon this bleach, and together they give rise to the local maximum at ~605 nm in the TA spectrum. Very similar TA spectra are observed for all Cu^+:CdSe/CdS NCs examined in this study, as well as for Cu^+:CdS NCs examined here (see Appendix A). In some instances, we observe that the local maximum (~605 nm in Figure 2.4) has a positive value of ΔOD, supporting the interpretation presented above.

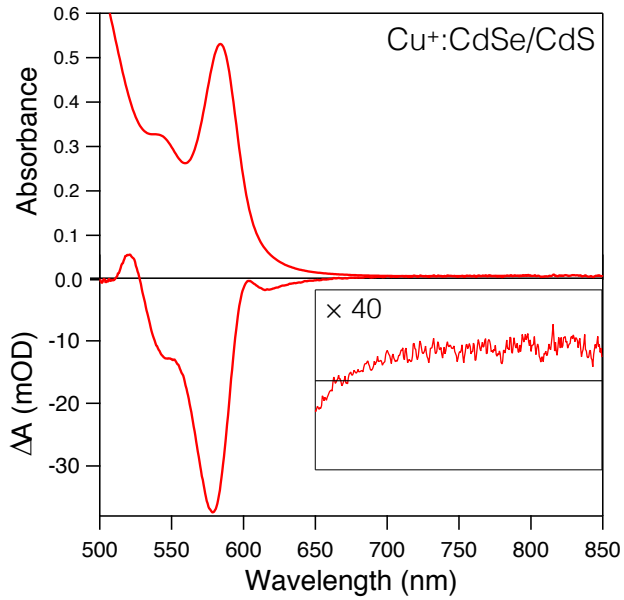

Figure 2.4. Room-temperature absorption spectrum (top) and transient absorption (TA) spectrum (bottom) of the Cu^+:CdSe/CdS NCs from Figure 2.1. Inset: TA spectrum between 650 and 850 nm magnified 40× to highlight the appearance of broad photoinduced absorption tailing into the near-infrared.

The inset to Figure 2.4 plots the same TA data between 650 and 850 nm but with magnified amplitudes. Weak photoinduced mid-gap absorption is observed in this region, extending into the near-IR beyond our instrumental range. This feature is reminiscent of the photoinduced mid-gap absorption observed in bulk Cu^+-doped ZnS phosphors, which has been assigned to L_{VB}MCT absorption made possible by capture of the photogenerated hole by a Cu^+ dopant.[3] We therefore assign this photoinduced mid-gap absorption to L_{VB}MCT transitions that promote VB electrons into the copper-localized holes in the luminescent excited states of these Cu^+:CdSe/CdS NCs. The amplitude of this photoinduced TA can be analyzed quantitatively by comparison to the exciton bleach. The extinction coefficient at the first excitonic absorption maximum of these NCs was estimated by absorption spectroscopy to be ~2.1 x 10^5 $M^{-1}cm^{-1}$. This absorption is bleached by ~50% upon occupation of the $1S_e$ CB orbital by one photogenerated electron,[26] such that the per-electron (bleach) extinction coefficient at the first excitonic maximum is ~1.0 x 10^5 $M^{-1}cm^{-1}$. From this value and the relative exciton and mid-gap TA amplitudes, we can thus estimate the per-hole

extinction coefficient of the photoinduced mid-gap absorption to be ~2000 $M^{-1}cm^{-1}$ between 750 and 850 nm. This value is very similar to the one predicted by density functional theory (DFT) for L_{VB}MCT transitions in Cu^{2+}-doped CdSe NCs (~1000 < ε < ~2000 $M^{-1}cm^{-1}$),[17] supporting our assignment of this low-energy photoinduced absorption to L_{VB}MCT transitions.

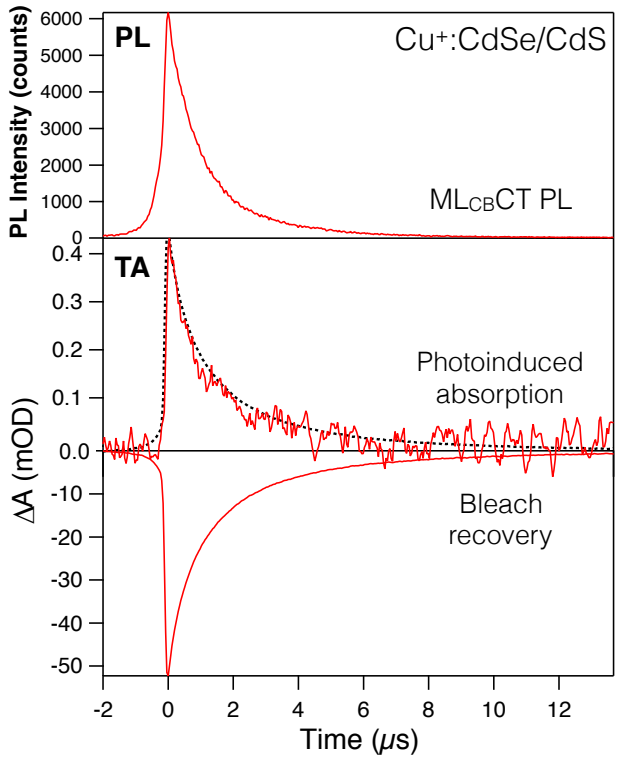

Figure 2.5. TRPL decay (top) and TA (middle, bottom) dynamics for Cu^{+}:CdSe/CdS NCs. The TRPL dynamics are integrated between 760 and 820 nm. The TA dynamics show the bleach recovery of the first exciton (bottom, integrated between 565 and 590 nm) and the photoinduced absorption feature at low energy (middle, integrated between 675 and 765 nm). The black dashed line shows the TA dynamics for the excitonic bleach superimposed on top of the dynamics for the photoinduced feature demonstrating that the two decays have very similar dynamics. Bi-exponential fitting yields an average time constant of 1.4 ± 0.1 μs for these processes.

Figure 2.5 plots TA dynamics measured for the exciton bleach and photoinduced mid-gap absorption seen in Figure 2.4, along with ML_{CB}CT PL decay dynamics of the same NCs. Whereas the PL reports on the subset of electron-hole pairs that recombine radiatively, the exciton TA bleach reports almost exclusively on the population of CB electrons in CdSe NCs, because of the

high valence-band degeneracy.[27-29] In contrast, the mid-gap L_{VB}MCT TA reports solely on the population of copper-bound holes. All three signals in Figure 2.5 show the same kinetics within experimental uncertainty, as emphasized by superimposing the (inverted) exciton bleach-recovery data upon the photoinduced absorption decay in the middle panel of Figure 2.5. Fitting these dynamics to a bi-exponential function yields an average time constant of 1.4 ± 0.1 μs, applicable to all three curves. The TA exciton-bleach data show a very small additional component at longer times that is not present in the PL data. We assign this component to CB electrons whose associated photogenerated holes were captured not by copper but by competing hole traps, for example at the NC surfaces. Overall, these time-resolved spectroscopic data show distinct signatures of delocalized CB electrons and deeply trapped holes, and both populations decay at essentially the same rate as the ML_{CB}CT luminescence. These observations provide insights into the individual microscopic components (CB electron, localized hole) of the photophysical mechanism summarized in Scheme 2.1.

It is interesting to note that the PL and TA kinetics observed in these Cu^+:CdSe/CdS core/shell NCs are ~3x slower than the PL decay kinetics measured previously for similar Cu^+-doped CdSe NCs without CdS shells.[8] These longer lifetimes were observed in all of the Cu^+-doped core/shell samples examined here. This difference is not correlated with any commensurate increase in PL QY in the Cu^+:CdSe/CdS core/shell NCs, indicating that this lifetime difference does not relate simply to suppression of slow non-radiative decay channels. Instead, we tentatively interpret this longer ML_{CB}CT lifetime as reflecting the effect of sulfide coordination to copper in these NCs. This hypothesis stems from our observation of even longer time constants (~2.3 μs) in the PL decay and TA recovery dynamics of Cu^+:CdS NCs (see Appendix A), all of which are again correlated. The Cu^+ ML_{CB}CT excited state may have a smaller radiative decay rate in sulfides than

selenides because of the smaller covalency of the former. We speculate that the multi-exponential dynamics described above may reflect mixed sulfide/selenide coordination environments, but it is unclear at this time whether Cu^+ ions are distributed statistically within these Cu^+:CdSe/CdS NCs or whether Cu^+ preferentially seeks sulfide coordination, preventing a more quantitative analysis of this observation.

2.3.4. Photodoping and Spectroscopy of n-doped Cu^+:CdSe/CdS NCs. In addition to investigating the spectroscopy of as-prepared Cu^+:CdSe/CdS NCs, we were also interested in exploring the spectroscopy of photochemically *n*-doped Cu^+:CdSe/CdS NCs to examine the effects that extra electrons may have on the above photodynamics. Such photodoping experiments may also relate to assertions that the mid-gap luminescence of copper-doped NCs actually requires Cu^{2+} as the active defect,[7, 30-33] rather than Cu^+ as illustrated in Scheme 2.1. Successful degenerate *n*-doping should shift the Fermi level sufficiently negative to eliminate any possibility of Cu^{2+}, providing a different perspective on the viability of this alternative mechanistic interpretation. To explore these concepts, samples of CdSe/CdS and Cu^+:CdSe/CdS NCs were photodoped under identical conditions using $Li[Et_3BH]$ as the terminal reductant, following methods we have detailed previously.[23, 34-36] For these experiments, the Cu^+:CdSe/CdS NCs were prepared with less copper than used in Figures 2.2-5, such that a small subset of undoped NCs remained, allowing both the copper-based $ML_{CB}CT$ PL of doped NCs and the excitonic PL of undoped NCs to be monitored simultaneously under identical conditions.

Figure 2.6 summarizes absorption and PL data collected during photodoping of these two NC samples. Figure 2.6A shows a series of absorption spectra collected at different stages of CdSe/CdS NC photodoping. Absorption at the first excitonic maximum decreases, ultimately reaching ~40% of its original value, which corresponds to addition of an average of 1.25 CB

electrons per NC $\langle n \rangle$ = 1.25) at maximum photodoping.[23, 26, 34] Figure 2.6B shows a concomitant decrease in excitonic PL intensity during photodoping. There is a small red-shift of both the absorption and PL maxima upon photodoping (<15 meV at $\langle n \rangle$ = 1.25), as described previously for trions in CdSe-based NCs.[34, 37-38] Similarly, Figure 2.6C shows absorption spectra collected during photodoping of the Cu^+:CdSe/CdS NCs. Like in Figure 2.6A, absorption at the first excitonic maximum decreases during photodoping, this time stopping at ~50% of its original value ($\langle n \rangle$ = 1.0). Figure 2.6D plots PL spectra of these NCs collected during photodoping. The excitonic and $ML_{CB}CT$ PL intensities both decrease during photodoping, but the $ML_{CB}CT$ PL intensity decreases by a greater percentage.

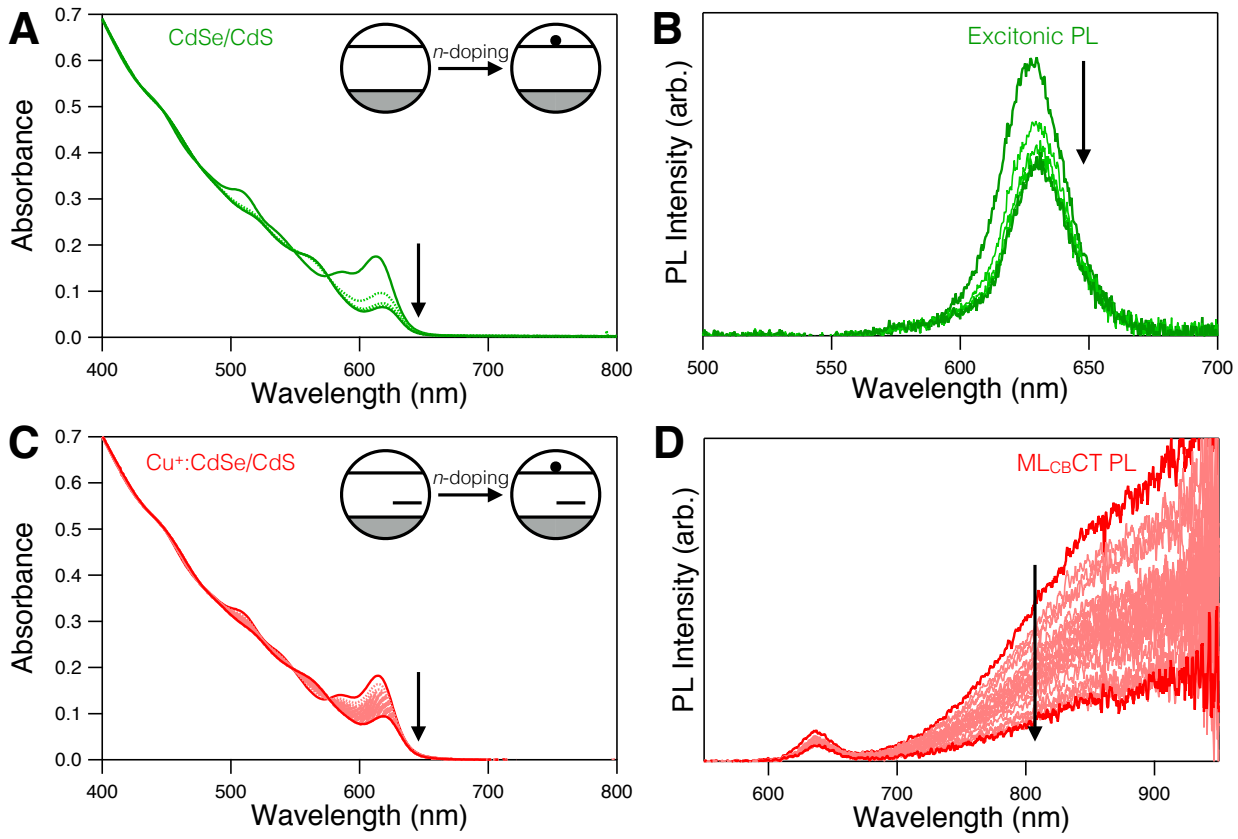

Figure 2.6. Photodoping of CdSe/CdS (green) and Cu^+:CdSe/CdS (red) NCs using Li[Et_3BH] as the sacrificial reductant. **(A)** Absorption spectra of CdSe/CdS NCs collected

during photodoping. The first excitonic absorption feature bleaches as electrons are added to the CB. These data are consistent with an average number of excess CB electrons per NC of $\langle n \rangle$ = 1.25 at maximum photodoping. **(B)** PL spectra of CdSe/CdS NCs collected during photodoping. Accumulation of CB electrons reduces the excitonic PL intensity. **(C)** Absorption spectra of Cu^+:CdSe/CdS NCs collected during photodoping. The first excitonic absorption feature bleaches with added electrons, as in the undoped core/shell NCs. These data are consistent with an average number of excess CB electrons per NC of $\langle n \rangle$ = 1.0 at maximum photodoping. **(D)** PL spectra of Cu^+:CdSe/CdS NCs collected during photodoping. This sample was deliberately prepared with a small subset of undoped NCs to allow both copper-based $ML_{CB}CT$ and excitonic PL to be monitored simultaneously. As excess CB electrons are added to the NCs, both PL intensities decrease but the $ML_{CB}CT$ PL decreases by a greater percentage.

Figure 2.7A quantifies the spectral changes observed in Figure 2.6, plotting these changes *vs* photodoping time for both the doped and undoped NCs. As described previously,[23, 34] photodoping of CdSe-based NCs is facile and rapid, and the spectral changes for the CdSe/CdS NCs here plateau after only ~5 min of continuous above-bandgap irradiation. In contrast, photodoping of the Cu^+:CdSe/CdS NCs takes much longer under identical conditions, reaching steady state only after ~100 min or more. This much slower photodoping of the Cu^+:CdSe/CdS NCs reflects a diminished quantum efficiency for hole capture at the NC surfaces after copper doping. Following Scheme 2.1, hole quenching that leads to successful photodoping must now compete with rapid (~25 ps, Figure 2.3) hole capture by Cu^+, decreasing the photodoping rates in Cu^+:CdSe/CdS NCs relative to the control CdSe/CdS NCs.

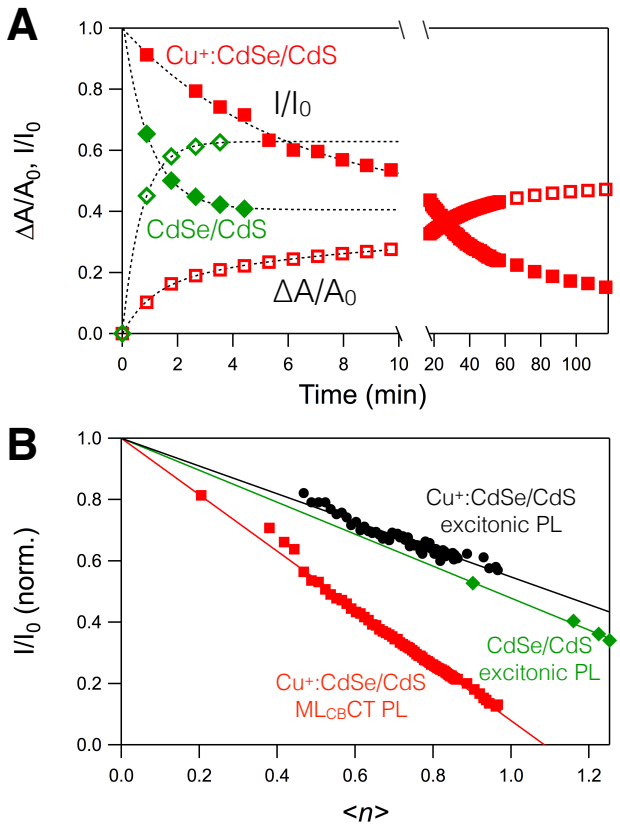

Figure 2.7. **(A)** Summary of the photodoping data shown in Figure 2.6. Green diamonds represent CdSe/CdS NC data, red squares represent Cu^+:CdSe/CdS NC data, empty symbols represent normalized absorbance of the first excitonic feature, and solid symbols represent normalized PL intensity. The dotted curves are guides to the eye. **(B)** The data from panel A, replotted as I/I_0 *vs* $\langle n \rangle$. The green diamonds represent the normalized CdSe/CdS NC excitonic PL intensities, and the red squares represent the normalized Cu^+:CdSe/CdS NC $ML_{CB}CT$ PL intensities. Normalized excitonic PL intensities from the Cu^+:CdSe/CdS NC data are also plotted (black symbols). The solid lines show linear fits to the data. Each plot is normalized to the extrapolated value at $\langle n \rangle = 0$.

Figure 2.7B replots the photodoping data from Figure 2.7A as I/I_0 *vs* $\langle n \rangle$, where $\langle n \rangle$ is determined from the first-exciton absorption bleach. Data are included for the excitonic PL of the CdSe/CdS NC sample, and for both the $ML_{CB}CT$ and excitonic PL of the Cu^+:CdSe/CdS NC sample. The solid lines show linear fits to the data for each PL feature. The slopes of the two excitonic PL data sets are essentially indistinguishable, both –0.49 ± 0.04, but the $ML_{CB}CT$ data set has a steeper slope of ~ –0.92. Beyond demonstrating a much greater sensitivity of $ML_{CB}CT$ PL to extra CB electrons, the data in Figure 2.7B confirm that the excitonic PL observed in the

ensemble of Cu^+:CdSe/CdS NCs derives from a subset of undoped CdSe/CdS NCs. From these data, one CB electron reduces the excitonic PL of the undoped CdSe/CdS NCs by about 50%, but almost completely eliminates the $ML_{CB}CT$ PL of the Cu^+:CdSe/CdS NCs.

Various processes could conceivably cause this reduction in $ML_{CB}CT$ PL upon *n*-doping, from redox changes of the copper ions themselves to modification of the NC surface traps. To clarify the origins of this reduced PL, we performed TRPL measurements on the sub-nanosecond timescale. Figure 2.8A plots absorption and steady-state PL spectra collected before and after photodoping of these Cu^+:CdSe/CdS NCs to $\langle n \rangle = 0.8$. At this photodoping level, the NC ensemble contains a mixture of NCs with zero and one excess CB electron, and the ensemble CW PL intensity is reduced by ~75%. Figure 2.8B shows sub-nanosecond TRPL decay curves measured for the $ML_{CB}CT$ PL of these NCs before and after this photodoping. As mentioned above, the long $ML_{CB}CT$ excited-state lifetime ($\tau \sim 1.4 \pm 0.1$ μs) means that few photons are emitted over sub-nanosecond time windows, but sufficient signal-to-noise could be achieved with long integration. Relative to the Cu^+:CdSe/CdS NCs, the *n*-doped Cu^+:CdSe/CdS NCs show increased PL intensities immediately after the excitation pulse, followed by more rapid PL decay over the first ~500 ps before converging to the same slow decay rates of the Cu^+:CdSe/CdS NCs without excess CB electrons. When these photodoped NCs are exposed to air, their excess CB electrons are removed and the original absorption spectra, PL spectra, and PL dynamics recover almost quantitatively (see Appendix A), confirming that these spectroscopic changes are indeed caused by the excess electrons.

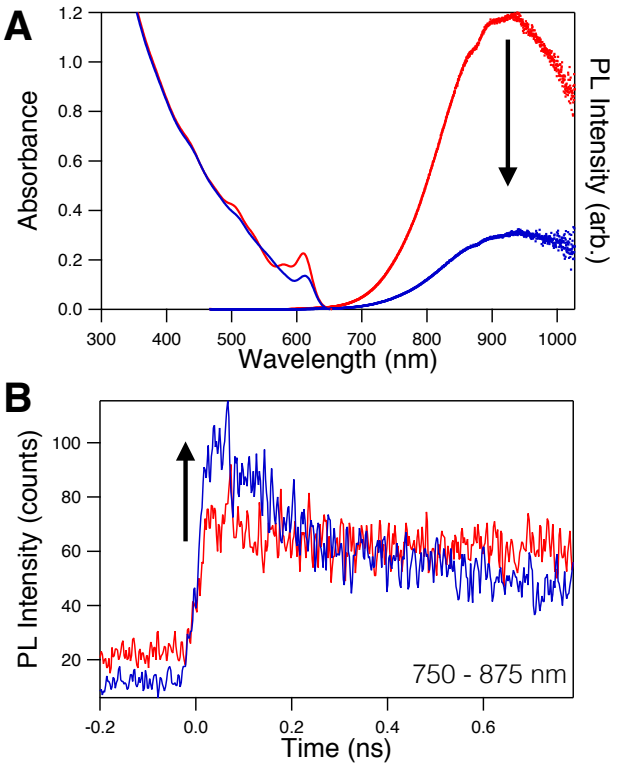

Figure 2.8. (A) Absorption (solid) and PL (dotted) spectra of Cu^{+}:CdSe/CdS NCs collected before (red) and after (blue) photodoping to an average of $\langle n \rangle$ = 0.8, as demonstrated by the bleach in the absorption of the first excitonic transition and the decrease in $ML_{CB}CT$ PL intensity. **(B)** TRPL dynamics measured on a 1 ns window. The $ML_{CB}CT$ PL intensity from the photodoped NCs (blue) increases in intensity at short times and has a faster decay than the $ML_{CB}CT$ PL intensity of the NCs before photodoping (red).

The TRPL data in Figure 2.8B for the *n*-doped Cu^{+}:CdSe/CdS NCs are characteristic of trions in NCs, in which an excess carrier (a CB electron in this case) generates increased PL at short times because of an increased probability of radiative recombination, but it also causes faster excited-state nonradiative decay *via* new Auger-recombination pathways, diminishing the overall PL intensity. Analysis of the fast decay in Figure 2.8B yields a time constant of ~260 ps for this Auger process, which is similar to the negative trion Auger time constants observed for excitonic PL in undoped CdSe/CdS QDs,[23, 39-40] except in this case it is detected while monitoring $ML_{CB}CT$ PL intensity. The data in Figures 2.6 and 2.7 demonstrate that *n*-doping reduces $ML_{CB}CT$ PL intensities not by suppressing formation of the luminescent $ML_{CB}CT$ excited state, but instead by quenching this excited-state population *after* it has been formed. Moreover, these data demonstrate

that trion Auger recombination more effectively reduces $ML_{CB}CT$ luminescence than excitonic luminescence; because the two Auger rate constants are comparable, this difference primarily reflects the slow $ML_{CB}CT$ radiative decay.

2.4 Discussion

Although the PL dynamics of copper-doped semiconductor NCs have been described in many publications, their TA spectra and dynamics contain a large amount of mechanistic information but have not yet been thoroughly explored. Exciton TA data from InAs NCs doped with interstitial copper as shallow donors have been reported,[41] but those samples apparently represent a very different electronic structure from the luminescent copper-doped NCs investigated here. Transient X-ray absorption data for copper-doped CdS NCs have been reported[10] that support the photophysical mechanism described by Scheme 2.1, showing both copper oxidation and the appearance of new pre-edge 1s → 3d transitions at the copper K edge. While this manuscript was under review, a report was published[42] that discusses exciton TA dynamics of copper-doped CdSe NCs at times < 1 ns. This report does not address the photoinduced mid-gap charge-transfer absorption described here. Mid-gap features in the TA spectra of luminescent copper-doped NCs have not been reported.

As described in the introduction, one signature of the metastable Cu^{2+}-like intermediate formed upon localization of a photogenerated hole in bulk Cu^{+}:ZnS[1-3] is the appearance of a new, broad low-energy electronic absorption band associated with promotion of VB electrons to the photogenerated copper-localized hole, *i.e.*, $L_{VB}MCT$ transitions. This band extends as low as ~1.3 eV in ZnS, and is predicted by DFT to extend to even lower energies in Se^{2-}-based lattices because of the smaller Se^{2-} electronegativity and hence shallower VB edges.[17] To our knowledge, this

L_{VB}MCT band has not been identified in other copper-doped semiconductor NCs. Even samples described as preferentially doped with Cu^{2+} rather than Cu^{+} have not shown this anticipated mid-gap absorption.[7, 30, 33, 43-44] We assign the broad, photoinduced mid-gap absorption as arising from these predicted L_{VB}MCT transitions. The appearance of this mid-gap L_{VB}MCT absorption in the TA measurement is summarized in Scheme 2.2 (left). Importantly, the appearance of this L_{VB}MCT absorption as a *photoinduced* signal confirms the hole-trapping step of the PL mechanism in Scheme 2.1, and hence also the Cu^{+} starting oxidation state of the copper ions involved in the PL of these NCs. Decay of this photoinduced TA signal coincides with the exciton bleach recovery, also consistent with the PL mechanism of Scheme 2.1. The L_{VB}MCT per-copper extinction coefficient of ~2000 $M^{-1}cm^{-1}$ at wavelengths between 700 and 850 nm is consistent with predictions made by DFT.[17] The analogous photoinduced absorption is also observed in Cu^{+}-doped CdS NCs (Appendix A), supporting this interpretation. Because the photoinduced mid-gap L_{VB}MCT absorption is specifically associated with photogenerated holes, and because the exciton bleach TA signal is dominated by photogenerated electrons, these results demonstrate that photogenerated electrons and holes can both be monitored independently in these samples, which may prove attractive for future studies of photochemical processes such as photoinduced interfacial charge injection or photocatalysis using copper-doped NCs.

Scheme 2.2. (Left) Depiction of the Transient-Absorption Experiment, Showing Pump Excitation, Hole Trapping at Copper to Form the Luminescent $ML_{CB}CT$ Excited State, and the Appearance of New (Photoinduced) $L_{VB}MCT$ Absorption. (Right) Depiction of the Trap-Assisted Auger Recombination Process that Reduces $ML_{CB}CT$ Luminescence in *n*-doped Cu^+:CdSe/CdS NCs.

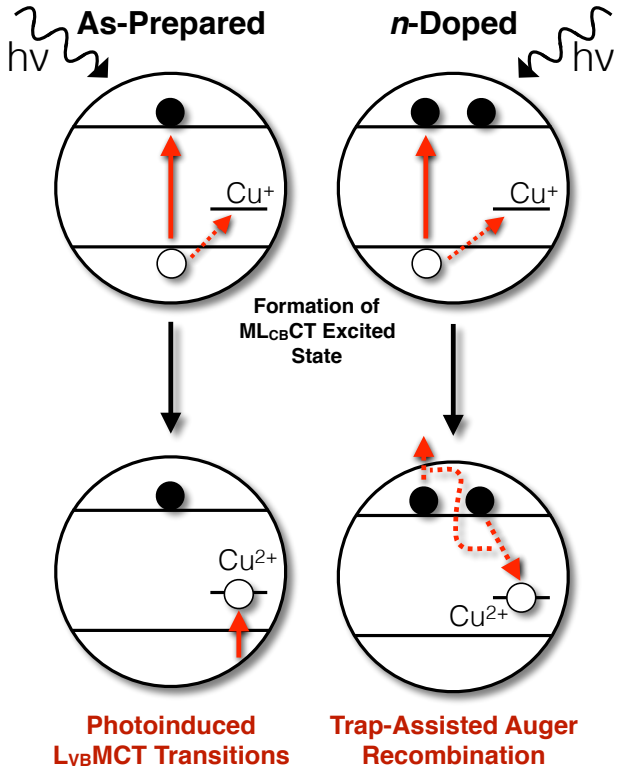

These results also contribute to our understanding of the relationship between copper-doped and copper-based semiconductor NCs. Recent experiments have highlighted strong spectroscopic similarities between copper-doped semiconductor NCs and ternary $CuInE_2$ (E = S, Se) NCs.[8, 33] The TA data presented here represent an additional way in which these two classes of NCs are spectroscopically quite similar. $CuInS_2$ and related ternary NCs have been studied extensively by TA,[45-47] and they always show a broad photoinduced mid-gap absorption band tailing into the near-IR. The similarity of that TA feature to the photoinduced $L_{VB}MCT$ absorption of bulk Cu^+-doped ZnS (ref. 3), and to that of the Cu^+-doped CdSe/CdS and CdS NCs reported here, strongly supports the description of $CuInS_2$ NCs as behaving like heavily Cu^+-doped semiconductor NCs,[4, 8] in which photoexcitation is followed by hole localization at one or a small

number of lattice Cu^+ ions (exciton self-trapping), analogous to the mechanism depicted in Scheme 2.1 in the dilute-Cu^+ limit.

Finally, two major effects of Cu^+ doping were observed in the photochemical *n*-doping and spectroscopy of the resulting *n*-doped NCs. First, the Cu^+:CdSe/CdS NCs accumulate CB electrons much slower than the same NCs in the absence of copper. This result reflects the fact that the copper dopants compete with the surface hole quenchers for capture of photogenerated holes (Scheme 2.1). Second, *n*-doping reduces the $ML_{CB}CT$ PL intensities of Cu^+:CdSe/CdS NCs more than it reduces the excitonic PL intensities of undoped CdSe/CdS NCs, and our TRPL investigations show that the $ML_{CB}CT$ PL intensity is attenuated specifically by a picosecond non-radiative trion Auger recombination process. The data indicate that photoexcitation of *n*-doped Cu^+:CdSe/CdS NCs still generates the same emissive $ML_{CB}CT$ excited state with similar efficiency as seen prior to *n* doping. Intriguingly, these unusual trions involve two delocalized CB electrons and one copper-bound hole, making this process formally a "trap-assisted" Auger recombination, as illustrated in Scheme 2.2 (right). This Auger process is remarkably fast ($\tau = 260$ ps) given that one of the three carriers is highly localized. In fact, its time constant is comparable to those of negative trions in undoped CdSe/CdS and related NCs,[23, 39-40] where all participating carriers are delocalized. This time constant is also similar to the time constants measured for trap-assisted Auger recombination in *n*-doped ZnO NCs (*e.g.*, ~270 ps for $d \sim 6.6$ nm *n*-ZnO NCs),[48] which involves two CB electrons and one surface-trapped hole. The rapidity of these trap-assisted Auger recombination processes may reflect facile momentum conservation when trapped-carriers are involved. These results contribute to the growing evidence of fast multi-carrier trap-assisted Auger dynamics in NCs,[48-51] and raise the possibility that such processes may have been underappreciated in favor of core delocalized trion Auger when interpreting the effect of, for

example, NC photoionization and surface trapping in photoluminescence blinking. From a practical standpoint, the rapid Auger recombination process observed here can also be expected to cause efficiency droop at lower current densities in electroluminescence devices based on copper-doped NCs (or, by extension, $CuInS_2$ NCs) than found in analogous undoped NCs, due primarily to the longer PL lifetimes of the former, and this consideration may ultimately define the performance ceiling for copper-based NC emitters in devices of this type.

2.5 Summary and Conclusions

In summary, we have investigated the synthesis, spectroscopy, photodoping, and photodynamics of Cu^+-doped CdSe/CdS core/shell NCs. We have used a post-synthetic doping strategy to insert copper into pre-formed CdSe/CdS core/shell NCs, yielding Cu^+:CdSe/CdS core/shell NCs that exhibit strong $ML_{CB}CT$ luminescence and little or no excitonic luminescence, an indication that essentially every NC contains copper. Spectroscopic and photochemical experiments on these Cu^+:CdSe/CdS NCs have revealed previously unexplored aspects of their electronic structure and photophysical properties relevant to their potential application in various technologies. In particular, TA measurements show new photoinduced $L_{VB}MCT$ absorption in the luminescent excited state, reflecting low-energy electronic transitions triggered by hole trapping at the copper dopants. This TA feature allows decay of the photogenerated holes to be probed in parallel with that of the delocalized CB electrons during the lifetime of the luminescent Cu^+:CdSe/CdS NC excited state because of their different energies; this capability may prove advantageous for future photochemical investigations of copper-doped semiconductor NCs.

Photochemical *n*-doping of Cu^+-doped NCs has also been examined. Cu^+ dopants compete with the sacrificial reductant for capture of the photogenerated holes, making photodoping roughly

an order of magnitude slower for the doped NCs relative to analogous undoped NCs. The mid-gap PL of Cu^+:CdSe/CdS NCs is also greatly reduced upon addition of excess delocalized CB electrons. Fast TRPL measurements show that the same luminescent $ML_{CB}CT$ excited state is still formed in *n*-doped Cu^+:CdSe/CdS NCs, but this excited state is quenched by a picosecond three-carrier trap-assisted Auger recombination process. Overall, the results presented here advance our understanding of the photophysical properties of this important class of luminescent nanomaterials and extend such studies to include measurements of their response to changes in excess carrier density, with potential ramifications for the use of copper-containing luminescent NCs in future optoelectronic, photochemical, or solar-energy-conversion technologies.

2.6 Experimental Methods

2.6.1. Synthesis and Photodoping. CdSe NC cores and CdSe/CdS core/shell NCs were synthesized by procedures adapted from previous literature reports.[52-53] For the synthesis of the CdSe NC cores, a cadmium precursor solution (1.12 mmol CdO, 1 g oleylamine (OA), and 12 g octadecene (ODE)) was degassed at 105 ºC for ~1 h, after which it was heated to 280 ºC under nitrogen. Once the solution turned clear and colorless (indicating cadmium oleate formation), it was cooled to 100 ºC and placed under vacuum for ~30 min. The flask was filled with nitrogen, and 2 g hexadecylamine (HDA) and 2 g trioctylphosphine oxide (TOPO, 99%) were added. The solution was placed under vacuum for ~10 min. The temperature of the flask was raised to 300 ºC, and a selenium precursor (2.4 mmol Se and ~4 mL trioctylphosphine (TOP); sonicated) was rapidly injected. The reaction was allowed to proceed for 30 s, after which it was cooled. At ~80 ºC, ~4 mL toluene was added to the flask. CdSe NCs were washed with ethanol and small amounts of methanol and re-suspended in toluene.

For the shelling synthesis, both cadmium and sulfur precursors needed to be prepared. For the cadmium shell precursor, 1.6 mmol CdO, 2 g OA, and 6 g ODE were degassed at 110 ºC for ~1 h, after which the solution was heated to 300 ºC under nitrogen. Once the solution turned clear and colorless, the temperature was reduced to 100 ºC, at which point the flask was cooled back to room temperature under vacuum. For the sulfur shell precursor, 4 mmol octanethiol and 15 g ODE were purged with nitrogen for a minimum of one hour. The shelling reaction flask was prepared with 0.2 mmol dried CdSe cores, 4 g ODE and 2 g HDA. This flask was heated to 50 ºC in order to melt HDA (under nitrogen), and then was placed under vacuum. The temperature was increased to 100 ºC and degassed for ~1 h. The shelling precursors were added to the flask under nitrogen at 200 ºC, and the temperature was ramped to 300 ºC after the start of addition of precursors. The shelling was stopped and the heat was removed after 30 min. ~4 mL toluene was added when the solution reached 80 ºC upon cooling. CdSe/CdS NCs were washed four times with ethanol and methanol and re-suspended in toluene.

The synthesis of Cu^{+}:CdSe/CdS core/shell NCs was adapted from a previous literature report.[21] 0.055 mmol CuI (90% Cu^{+}:Cd^{2+} ratio) in 9.9 g ODE was purged with nitrogen for 20 minutes before addition of 0.067 mmol TOP to make a copper precursor solution. The solution was sonicated until all CuI dissolved. The doping synthesis is as follows: 0.06 mmol Cd^{2+} of CdSe/CdS NCs were dried and re-suspended in 3.35 g ODE and 0.1 mL OA. The solution temperature was raised to 60 ºC, and three ~10 min pump-purge cycles were performed. The solution was heated to 235 ºC under nitrogen. 1.4 mL of the copper solution (10% Cu^{+}:Cd^{2+}) was quickly injected into the flask and allowed to react for 10 minutes. The flask was then rapidly cooled to room temperature. Cu^{+}:CdSe/CdS NCs were washed with 3:1 ethanol:acetone, resulting in an oily pellet. The sample was precipitated using acetone, and the resulting solid pellet was

dried and re-suspended in toluene. Typical PL quantum yields for the Cu^{+}:CdSe/CdS NC samples examined here were on the order of 10%.

NC photodoping was performed according to methods detailed previously.[19,22,23,27] NCs were dried and resuspended in anhydrous toluene in a nitrogen-filled glovebox. Briefly, NCs were diluted in anhydrous toluene with ~100 equiv $Li[Et_3BH]$ and sealed with a Teflon stopper in a fluorescence cuvette equipped with a magnetic stir bar. The NCs were excited with a 405 nm laser (P = 0.5 mW) focused onto the cuvette, while the solution was continuously stirred in the absorption spectrophotometer. Absorption and PL spectra were collected *in situ* during illumination. For Auger measurements, only ~50 equiv $Li[Et_3BH]$ were added to limit $\langle n \rangle$ to values <1, and TRPL measurements were also performed under continuous stirring. Our prior work has demonstrated that this photodoping involves a non-photochemical NC surface reduction by $Li[Et_3BH]$ followed by capture of photogenerated holes by these reduced surface moieties.[35]

2.6.2. Physical Measurements. Absorption spectra were collected at room temperature on a Cary 5000 spectrophotometer (Varian). For continuous-wave (CW) PL measurements, colloidal NCs were excited using a 405 nm laser diode, and the spectra were collected using an OceanOptics 2000+ spectrometer. Transmission electron microscope (TEM) images were obtained using a FEI Tecnai G2 F20 operating at 200 kV, and size distribution analysis was performed on 300 individual NCs per sample. Concentrations of copper and cadmium were determined by analysis of dried nanocrystals digested in ultrapure nitric acid (EMD Chemicals) using inductively coupled plasma atomic emission spectrometry (ICP-AES; Perkin-Elmer). PL quantum yields were measured using an External Quantum Efficiency Measurement System with a Hamamatsu Integrating Sphere (C9920-12) and a Hamamatsu high-sensitivity photonic multi-channel analyzer (C10027-01). PL dynamics (hole trapping and Auger studies) were measured by exciting the colloidal NCs at room

temperature with the frequency-doubled output of a Ti:Sapphire laser (405 nm, 150 fs pulse, power ~390 μW, repetition rate either 200 kHz or 250 kHz). PL decay curves were recorded using a monochromator and streak camera with an instrument response time of ~25 ps. Parallel TA and TRPL measurements were performed using an Ekspla Nd:YAG laser operating at a 25 Hz repetition rate. Samples were pumped with the third harmonic of the 1064 nm fundamental, using an excitation energy of ~100 μJ/pulse. For TA, a 150W CW Xe lamp was used as the white-light probe. The pump and probe beams intersected the colloidal sample at a 90^{o} angle. TA spectra and dynamics were collected using a monochromator and streak camera with an instrument response of ~20 ps.

2.7 References

1. Shionoya, S.; Yen, W. M.; Yamamoto, H., *Phosphor Handbook*. CRC Press: 2006.
2. Shionoya, S.; Koda, T.; Era, K.; Fujiwara, H., Nature of Luminescence Transitions in ZnS Crystals. *J. Phys. Soc. Jpn.* **1964,** *19* (7), 1157-1167.
3. Suzuki, A.; Shionoya, S., Mechanism of the Green-Copper Luminescence in ZnS Crystals. I. Direct Evidence for the Pair Emission Mechanism. *J. Phys. Soc. Jpn.* **1971,** *31* (5), 1455-1461.
4. Knowles, K. E.; Hartstein, K. H.; Kilburn, T. B.; Marchioro, A.; Nelson, H. D.; Whitham, P. J.; Gamelin, D. R., Luminescent Colloidal Semiconductor Nanocrystals Containing Copper: Synthesis, Photophysics, and Applications. *Chem. Rev.* **2016,** *116* (18), 10820-10851.
5. Xie, R.; Peng, X., Synthesis of Cu-Doped InP Nanocrystals (d-dots) with ZnSe Diffusion Barrier as Efficient and Color-Tunable NIR Emitters. *J. Am. Chem. Soc.* **2009,** *131* (30), 10645-10651.
6. Srivastava, B. B.; Jana, S.; Pradhan, N., Doping Cu in Semiconductor Nanocrystals: Some Old and Some New Physical Insights. *J. Am. Chem. Soc.* **2011,** *133* (4), 1007-1015.
7. Grandhi, G. K.; Viswanatha, R., Tunable Infrared Phosphors Using Cu Doping in Semiconductor Nanocrystals: Surface Electronic Structure Evaluation. *J. Phys. Chem. Lett.* **2013,** *4* (3), 409-415.
8. Knowles, K. E.; Nelson, H. D.; Kilburn, T. B.; Gamelin, D. R., Singlet–Triplet Splittings in the Luminescent Excited States of Colloidal Cu+:CdSe, Cu+:InP, and CuInS2 Nanocrystals: Charge-Transfer Configurations and Self-Trapped Excitons. *J. Am. Chem. Soc.* **2015,** *137* (40), 13138-13147.
9. Cooper, J. K.; Gul, S.; Lindley, S. A.; Yano, J.; Zhang, J. Z., Tunable Photoluminescent Core/Shell Cu+-Doped ZnSe/ZnS Quantum Dots Codoped with Al3+, Ga3+, or In3+. *ACS Appl. Mater. Interfaces* **2015,** *7* (18), 10055-10066.

10. Hassan, A.; Zhang, X.; Liu, X.; Rowland, C. E.; Jawaid, A. M.; Chattopadhyay, S.; Gulec, A.; Shamirian, A.; Zuo, X.; Klie, R. F.; Schaller, R. D.; Snee, P. T., Charge Carriers Modulate the Bonding of Semiconductor Nanoparticle Dopants As Revealed by Time-Resolved X-ray Spectroscopy. *ACS Nano* **2017,** *11*, 10070-10076.
11. Huang, J.; Yang, Y.; Xue, S.; Yang, B.; Liu, S.; Shen, J., Photoluminescence and electroluminescence of ZnS:Cu nanocrystals in polymeric networks. *Appl. Phys. Lett.* **1997,** *70* (18), 2335-2337.
12. Zhang, W.; Lou, Q.; Ji, W.; Zhao, J.; Zhong, X., Color-Tunable Highly Bright Photoluminescence of Cadmium-Free Cu-Doped Zn–In–S Nanocrystals and Electroluminescence. *Chem. Mater.* **2014,** *26* (2), 1204-1212.
13. Wu, P.; Yan, X.-P., Doped quantum dots for chemo/biosensing and bioimaging. *Chem. Soc. Rev.* **2013,** *42* (12), 5489-5521.
14. Jiang, T.; Song, J.; Wang, H.; Ye, X.; Wang, H.; Zhang, W.; Yang, M.; Xia, R.; Zhu, L.; Xu, X., Aqueous synthesis of color tunable Cu doped Zn-In-S/ZnS nanoparticles in the whole visible region for cellular imaging. *J. Mater. Chem. B* **2015,** *3* (11), 2402-2410.
15. Bradshaw, L. R.; Knowles, K. E.; McDowall, S.; Gamelin, D. R., Nanocrystals for Luminescent Solar Concentrators. *Nano Lett.* **2015,** *15* (2), 1315-1323.
16. Sharma, M.; Gungor, K.; Yeltik, A.; Olutas, M.; Guzelturk, B.; Kelestemur, Y.; Erdem, T.; Delikanli, S.; McBride, J. R.; Demir, H. V., Near-Unity Emitting Copper-Doped Colloidal Semiconductor Quantum Wells for Luminescent Solar Concentrators. *Adv. Mater.* **2017,** *29* (30), 1700821.
17. Nelson, H. D.; Li, X.; Gamelin, D. R., Computational Studies of the Electronic Structures of Copper-Doped CdSe Nanocrystals: Oxidation States, Jahn–Teller Distortions, Vibronic Bandshapes, and Singlet–Triplet Splittings. *J. Phys. Chem. C* **2016,** *120* (10), 5714-5723.
18. Knowles, K. E.; Kilburn, T. B.; Alzate, D. G.; McDowall, S.; Gamelin, D. R., Bright CuInS2/CdS nanocrystal phosphors for high-gain full-spectrum luminescent solar concentrators. *Chem. Commun.* **2015,** *51* (44), 9129-9132.
19. Sahu, A.; Kang, M. S.; Kompch, A.; Notthoff, C.; Wills, A. W.; Deng, D.; Winterer, M.; Frisbie, C. D.; Norris, D. J., Electronic Impurity Doping in CdSe Nanocrystals. *Nano Lett.* **2012,** *12*, 2587-2594.
20. Gopal, M. B., Ag and Cu doped colloidal CdSe nanocrystals: partial cation exchange and luminescence. *Mater. Res. Express* **2015,** *2*, 085004.
21. Yang, L.; Knowles, K. E.; Gopalan, A.; Hughes, K. E.; James, M. C.; Gamelin, D. R., One-Pot Synthesis of Monodisperse Colloidal Copper-Doped CdSe Nanocrystals Mediated by Ligand–Copper Interactions. *Chem. Mater.* **2016,** *28* (20), 7375-7384.
22. Nelson, H. D.; Hinterding, S. O. M.; Fainblat, R.; Creutz, S. E.; Li, X.; Gamelin, D. R., Mid-Gap States and Normal vs Inverted Bonding in Luminescent Cu+- and Ag+-Doped CdSe Nanocrystals. *J. Am. Chem. Soc.* **2017,** *139*, 6411–6421.
23. Hartstein, K. H.; Erickson, C. S.; Tsui, E. Y.; Marchioro, A.; Gamelin, D. R., Electron Stability and Negative-Tetron Luminescence in Free-Standing Colloidal n-Type CdSe/CdS Quantum Dots. *ACS Nano* **2017,** *11*, 10430–10438.
24. McArthur, E. A.; Morris-Cohen, A. J.; Knowles, K. E.; Weiss, E. A., Charge Carrier Resolved Relaxation of the First Excitonic State in CdSe Quantum Dots Probed with Near-Infrared Transient Absorption Spectroscopy. *J. Phys. Chem. B* **2010,** *114* (45), 14514-14520.

25. Klimov, V. I., Optical Nonlinearities and Ultrafast Carrier Dynamics in Semiconductor Nanocrystals. *J. Phys. Chem. B* **2000,** *104* (26), 6112-6123.
26. Shim, M.; Wang, C. J.; Guyot-Sionnest, P., Charge-tunable optical properties in colloidal semiconductor nanocrystals. *J. Phys. Chem. B* **2001,** *105*, 2369-2373.
27. Hunsche, S.; Dekorsy, T.; Klimov, V.; Kurz, H., Ultrafast dynamics of carrier-induced absorption changes in highly-excited CdSe nanocrystals. *Appl. Phys. B* **1996,** *62* (1), 3-10.
28. Klimov, V. I.; McBranch, D. W.; Leatherdale, C. A.; Bawendi, M. G., Electron and hole relaxation pathways in semiconductor quantum dots. *Phys. Rev. B* **1999,** *60*, 13740-13749.
29. Knowles, K. E.; Frederick, M. T.; Tice, D. B.; Morris-Cohen, A. J.; Weiss, E. A., Colloidal Quantum Dots: Think Outside the (Particle-in-a-)Box. *J. Phys. Chem. Lett.* **2012,** *3*, 18-26.
30. Viswanatha, R.; Brovelli, S.; Pandey, A.; Crooker, S. A.; Klimov, V. I., Copper-Doped Inverted Core/Shell Nanocrystals with "Permanent" Optically Active Holes. *Nano Lett.* **2011,** *11*, 4753-4758.
31. Brovelli, S.; Galland, C.; Viswanatha, R.; Klimov, V. I., Tuning Radiative Recombination in Cu-doped Nanocrystals via Electrochemical Control of Surface Trapping. *Nano Lett.* **2012,** *12* (8), 4372-4379.
32. Grandhi, G. K.; Tomar, R.; Viswanatha, R., Study of Surface and Bulk Electronic Structure of II-VI Semiconductor Nanocrystals Using Cu as a Nanosensor. *ACS Nano* **2012,** *6* (11), 9751-9763.
33. Rice, W. D.; McDaniel, H.; Klimov, V. I.; Crooker, S. A., Magneto-Optical Properties of CuInS2 Nanocrystals. *J. Phys. Chem. Lett.* **2014,** *5* (23), 4105-4109.
34. Rinehart, J. D.; Schimpf, A. M.; Weaver, A. L.; Cohn, A. W.; Gamelin, D. R., Photochemical Electronic Doping of Colloidal CdSe Nanocrystals. *J. Am. Chem. Soc.* **2013,** *135*, 18782-18785.
35. Tsui, E. Y.; Hartstein, K. H.; Gamelin, D. R., Selenium Redox Reactivity on Colloidal CdSe Quantum Dot Surfaces. *J. Am. Chem. Soc.* **2016,** *138*, 11105–11108.
36. Carroll, G. M.; Tsui, E. Y.; Brozek, C. K.; Gamelin, D. R., Spectroelectrochemical Measurement of Surface Electrostatic Contributions to Colloidal CdSe Nanocrystal Redox Potentials. *Chem. Mater.* **2016,** *28*, 7912–7918.
37. Franceschetti, A.; Zunger, A., Optical transitions in charged CdSe quantum dots. *Phys. Rev. B* **2000,** *62*, R16287-R16290.
38. Shimizu, K. T.; K.Woo, W.; Fisher, B. R.; Eisler, H. J.; Bawendi, M. G., Surface-Enhanced Emission from Single Semiconductor Nanocrystals. *Phys. Rev. Lett.* **2002,** *89*, 117401.
39. Jha, P. P.; Guyot-Sionnest, P., Trion Decay in Colloidal Quantum Dots. *ACS Nano* **2009,** *3*, 1011–1015.
40. Cohn, A. W.; Rinehart, J. D.; Schimpf, A. M.; Weaver, A. L.; Gamelin, D. R., Size Dependence of Negative Trion Auger Recombination in Photodoped CdSe Nanocrystals. *Nano Lett.* **2014,** *14*, 353−358.
41. Yang, C.; Faust, A.; Amit, Y.; Gdor, I.; Banin, U.; Ruhman, S., Impurity Sub-Band in Heavily Cu-Doped InAs Nanocrystal Quantum Dots Detected by Ultrafast Transient Absorption. *J. Phys. Chem. A* **2016,** *120* (19), 3088-3097.
42. Maiti, S.; Dana, J.; Jadhav, Y.; Debnath, T.; Haram, S. K.; Ghosh, H. N., Electrochemical Evaluation of Dopant Energetics and the Modulation of Ultrafast Carrier Dynamics in Cu-Doped CdSe Nanocrystals. *J. Phys. Chem. C* **2017,** *121*, 27233-27240.

43. Jana, S.; Srivastava, B. B.; Acharya, S.; Santra, P. K.; Jana, N. R.; Sarma, D. D.; Pradhan, N., Prevention of photooxidation in blue-green emitting Cu doped ZnSe nanocrystals. *Chem. Commun.* **2010,** *46* (16), 2853-2855.
44. Pandey, A.; Brovelli, S.; Viswanatha, R.; Li, L.; Pietryga, J. M.; Klimov, V. I.; Crooker, S. A., Long-lived photoinduced magnetization in copper-doped ZnSe-CdSe core-shell nanocrystals. *Nat. Nanotech.* **2012,** *7* (12), 792-797.
45. Berends, A. C.; Rabouw, F. T.; Spoor, F. C. M.; Bladt, E.; Grozema, F. C.; Houtepen, A. J.; Siebbeles, L. D. A.; de Mello Donegá, C., Radiative and Nonradiative Recombination in CuInS2 Nanocrystals and CuInS2-Based Core/Shell Nanocrystals. *J. Phys. Chem. Lett.* **2016,** *7* (17), 3503-3509.
46. Jara, D. H.; Stamplecoskie, K. G.; Kamat, P. V., Two Distinct Transitions in CuxInS2 Quantum Dots. Bandgap versus Sub-Bandgap Excitations in Copper-Deficient Structures. *J. Phys. Chem. Lett.* **2016,** *7* (8), 1452-1459.
47. Debnath, T.; Maiti, S.; Maity, P.; Ghosh, H. N., Subpicosecond Exciton Dynamics and Biexcitonic Feature in Colloidal CuInS2 Nanocrystals: Role of In–Cu Antisite Defects. *J. Phys. Chem. Lett.* **2015,** *6* (17), 3458-3465.
48. Cohn, A. W.; Schimpf, A. M.; Gunthardt, C. E.; Gamelin, D. R., Size-Dependent Trap-Assisted Auger Recombination in Semiconductor Nanocrystals. *Nano Lett.* **2013,** *13* (4), 1810-1815.
49. White, M. A.; Weaver, A. L.; Beaulac, R.; Gamelin, D. R., Electrochemically Controlled Auger Quenching of Mn2+ Photoluminescence in Doped Semiconductor Nanocrystals. *ACS Nano* **2011,** *5*, 4158–4168.
50. Allan, G.; Delerue, C., Fast relaxation of hot carriers by impact ionization in semiconductor nanocrystals: Role of defects. *Phys. Rev. B* **2009,** *79*, 195324.
51. Califano, M., Off-State Quantum Yields in the Presence of Surface Trap States in CdSe Nanocrystals: The Inadequacy of the Charging Model To Explain Blinking. *J. Phys. Chem. C* **2011,** *115*, 18051–18054.
52. Qu, L.; Peng, X., Control of Photoluminescence Properties of CdSe Nanocrystals in Growth. *J. Am. Chem. Soc.* **2002,** *124* (9), 2049-2055.
53. Ghosh, Y.; Mangum, B. D.; Casson, J. L.; Williams, D. J.; Htoon, H.; Hollingsworth, J. A., New Insights into the Complexities of Shell Growth and the Strong Influence of Particle Volume in Nonblinking "Giant" Core/Shell Nanocrystal Quantum Dots. *J. Am. Chem. Soc.* **2012,** *134* (23), 9634-9643.

Chapter 3: Copper's Role in the Photoluminescence of $Ag_{1-x}Cu_xInS_2$ Nanocrystals, from Copper-Doped $AgInS_2$ ($x \sim 0$) to $CuInS_2$ ($x = 1$)

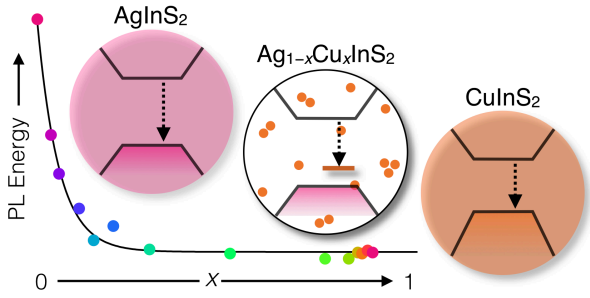

Adapted with permission from:

Hughes, K. E.; Ostheller, S. R.; Nelson, H. D.; Gamelin, D. R. *Nano Lett.* **2019**, *19*, 1318–1325.

3.1 Overview

A series of $Ag_{1-x}Cu_xInS_2$ nanocrystals (NCs) spanning from $0 \leq x \leq \sim 1$ was synthesized by partial cation exchange to identify copper's contributions to the electronic structure and spectroscopic properties of these NCs. Discrete mid-gap states appear above the valence band (VB) upon doping $AgInS_2$ NCs with Cu^+ (small x). Density function theory (DFT) calculations confirm that these mid-gap states are associated with the 3*d* valence orbitals of the Cu^+ impurities. With increasing x, these impurity *d* levels gradually evolve to become the VB edge of $CuInS_2$ NCs, but the highest-occupied orbital's description does not change significantly across the entire range of x. In contrast, with this gradual evolution, $Ag_{1-x}Cu_xInS_2$ NC photoluminescence shifts rapidly with initial additions of Cu^+ (small x) but then becomes independent of x beyond $x > \sim 0.20$, all the way up to $CuInS_2$ ($x = 1.00$). Data analysis indicates small but detectable hole delocalization in the luminescence excited state of $CuInS_2$ NCs, estimated by Monte Carlo simulations to involve at most about four copper ions. These results reinforce the description of $CuInS_2$ NCs as "heavily copper-doped NCs," in which photogenerated holes are rapidly localized in copper 3*d*-based orbitals, and they provide unique insights into the properties of self-trapped excitons in these materials.

3.2 Introduction

Ternary colloidal I-III-VI_2 nanocrystals (NCs) of copper and silver (*e.g.*, $CuInS_2$, $AgInS_2$, *etc*.) have attracted broad attention as Cd/Pb-free nanophosphors and have stimulated interest in new applications enabled by their solution processability, high photoluminescence quantum yields (PL QYs), and size-tunable band-gap energies, such as full-spectrum lighting, luminescent solar concentration, and quantum dot (QD) photovoltaics.[1-10] Despite high interest, the complex defect chemistries and structural disorder of I-III-VI_2 NCs still present major challenges to understanding and controlling their physical properties. In particular, the microscopic PL mechanisms active in these ternary NCs are still debated. Here, we report combined synthetic, spectroscopic, and computational studies aimed at addressing the unique photophysical properties of luminescent I-III-VI_2 NCs, focusing particularly on identifying the contributions of copper to the luminescence of $Ag_{1-x}Cu_xInS_2$ NCs in the range $\sim 0 \leq x \leq \sim 1$.

An interesting development in recent years has been the recognition that $CuInS_2$ and copper-doped II-VI or III-V semiconductor NCs share nearly identical spectroscopic properties,[11-12] suggesting closely related PL mechanisms. For copper-doped semiconductor NCs, a great deal of evidence now points to a photophysical sequence in which NC photoexcitation leads to rapid hole capture by Cu^+, followed by slow radiative recombination of this deeply trapped hole with the delocalized CB-like electron.[3] The electron in this scheme is subject to quantum confinement, affording tunability of this "free-to-bound" PL energy through NC size tuning or composition alloying. This mechanism in Cu^+-doped NCs has been demonstrated spectroscopically and by density functional theory (DFT),[12-15] and it also closely parallels the mechanism established in the classic G-Cu phosphor, Cu^+-doped ZnS (bulk).[3, 16-17] Photogenerated holes also localize around the Ag^+ impurity ions of Ag^+-doped II-VI NCs, yielding many of the same spectroscopic

characteristics found in analogous Cu^+-doped NCs, but the much larger second ionization energy of Ag^+ compared to Cu^+ results in inverted bonding and consequently hole wavefunctions that are dominated by silver-bound anion *p* orbitals rather than by the Ag(4*d*) orbitals themselves.[13]

For $CuInS_2$ and $AgInS_2$ NCs, the photoluminescence mechanisms are much less clear, and multiple plausible interpretations have been proposed.[1-3, 9] Most descriptions of $CuInS_2$ NC PL invoke the well-known Donor-Acceptor-Pair (DAP) recombination mechanism established for bulk $CuInS_2$. Various proposals describe carrier localization at lattice vacancies, anti-site defects, or rare point defects.[2, 9, 11, 18] Direct comparison[3] suggests that $CuInS_2$ NC PL actually has little in common with bulk $CuInS_2$ PL, however. Saturation of the band-edge TA bleach at relatively low excitation densities (only ~2 excitations/NC)[19-20] was interpreted as suggesting that at least one of the two charge carriers in the luminescent excited state occupies a delocalized quantized level, consistent with the size dependence of the PL energy. The small degeneracy of this quantized level points to electron delocalization, and the large Stokes shift then suggests deep hole trapping, with various specific hole-trapping point defects considered as possibilities.[2, 9, 11]

In an alternative mechanism, it has been suggested that holes rapidly localize at one or a few *lattice* Cu^+ ions in an exciton self-trapping process,[3, 12] driven by localization forces including *d*-band potential fluctuations and a positive feedback between hole contraction and nuclear reorganization. In this mechanism, PL derived from radiative "free-to-bound" recombination of a self-trapped hole with a delocalized CB electron is characterized by a large Stokes shift and vibronically broadened bandshape, directly analogous to the PL of Cu^+-doped semiconductor NCs and bulk Cu^+-doped phosphors.[12] DFT studies of $CuInS_2$ and related NCs have described a strong propensity for hole localization even in the ordered chalcopyrite lattice structure, associated with the combination of poor *d*-band electronic coupling and electrostatic fluctuations.[21] By analogy to

$CuInS_2$ NCs, the PL of $AgInS_2$ NCs is also frequently explained as DAP recombination,[22-24] and has also recently been proposed[25] to involve exciton self-trapping.

We hypothesized that careful examination of a well-controlled series of $Ag_{1-x}Cu_xInS_2$ ($0 \leq x \leq 1$) NCs would offer a unique opportunity to isolate the impact of just the monovalent cation (Ag^+ or Cu^+), thereby clarifying the specific role that this cation plays in the PL of such NCs. Given the structural similarity of $CuInS_2$ and $AgInS_2$ NCs, it should be possible to prepare alloyed $Ag_{1-x}Cu_xInS_2$ NCs at any value of x between 0.00 and 1.00 by direct chemical means. Indeed, solid solutions of bulk $Ag_{1-x}Cu_xInSe_2$ show essentially no segregation effects.[26-27] Furthermore, $Ag_{1-x}Cu_xInS_2$ NCs across this series should all possess many of the same native vacancy, interstitial, anti-site, or other point defects invoked when discussing the PL of $CuInS_2$ and $AgInS_2$ NCs, facilitating identification of the effects due specifically to copper. Micro- and nanocrystalline $Ag_{1-x}Cu_xInS_2$ have already been examined for solar photocatalysis and photovoltaics, where alloying with $CuInS_2$ has proven useful for narrowing the $AgInS_2$ energy gap to access more solar photons,[28-29] and several studies have also described red-shifted PL upon incorporation of Cu^+ into $AgInS_2$ NCs.[30-32] Prior studies of $Ag_{1-x}Cu_xInS_2$ NCs have primarily explored the dilute Cu^+ regime ($x < \sim 0.25$), however, and their goals did not require controlling for NC size or shape variations that can also shift absorption and PL energies.

In the present study, partial Ag^+-to-Cu^+ cation exchange was used to prepare a homologous series of alloyed $Ag_{1-x}Cu_xInS_2$ NCs that spans from $x = 0$ to $x \sim 1$, all derived from the same parent $AgInS_2$ NCs (Scheme 3.1, see Methods for experimental details). A hallmark of NC cation-exchange chemistry is its preservation of the anion sub-lattice, such that the NCs retain their general size and shape during the transformation.[33-37] A collection of optical spectroscopic methods was then used to probe the evolution of NC electronic structure across this composition

series. The experimental results are supplemented by DFT calculations that aid the data interpretation. Experimentally, the $Ag_{1-x}Cu_xInS_2$ NC PL energy is found to decrease rapidly upon addition of even small amounts of Cu^+ (small x), confirming direct participation of copper in the NC PL mechanism. DFT results show that dilute Cu^+ doping introduces discrete mid-gap Cu(3*d*) orbitals above the $AgInS_2$ NC valence band (VB) edge, similar to Cu^+-doped II-VI and III-V NCs, and consistent with hole trapping by copper in the luminescent excited states of these Cu^+-doped $AgInS_2$ NCs. Surprisingly, the $Ag_{1-x}Cu_xInS_2$ NC PL energy converges to the PL energy of $CuInS_2$ NCs at relatively small values of x (~0.20), remaining independent of x at larger values. This result is interpreted as reflecting detectable but very limited delocalization of photogenerated holes in the luminescent excited states of $Ag_{1-x}Cu_xInS_2$ NCs. Comparison of the data with Monte Carlo simulations suggests that photogenerated holes are trapped within small clusters of copper ions ($n \leq$ ~4) in $Ag_{1-x}Cu_xInS_2$ NCs, even in the limit of $x = 1.00$ ($CuInS_2$). These results establish copper's role as a deep hole trap in both Cu^+-doped and I-III-VI_2 NCs, and in particular support a self-trapped-exciton description of the luminescent excited state of $CuInS_2$ NCs.

3.3 Results, Analysis, and Discussion

Scheme 3.1. Synthesis of $AgInS_2$ NCs and Their Conversion to $Ag_{1-x}Cu_xInS_2$ NCs (~0 ≤ x ≤ ~1) by Partial Cation Exchange.

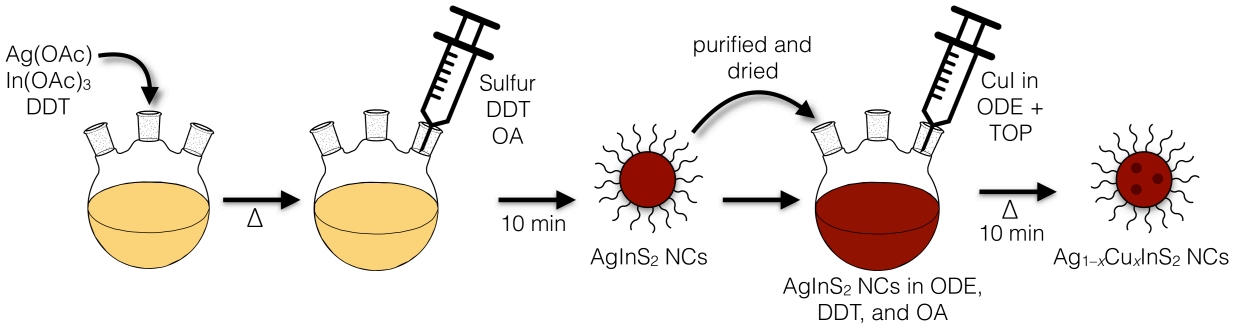

Figure 3.1A presents room-temperature absorption and continuous-wave (CW) PL spectra of representative $AgInS_2$ and $CuInS_2$ NCs with diameters of ~4 nm (synthesized independently, see Methods). Both NC samples show similar spectroscopic features: an absorption spectrum having a shoulder near its onset but lacking a clear maximum, and a broad, Stokes-shifted luminescence band. The absorption onset and PL maximum both occur at lower energies for the $CuInS_2$ NCs than for the $AgInS_2$ NCs. These results are consistent with analogous absorption and PL data reported previously for $CuInS_2$ and $AgInS_2$ NCs.[19, 22-23, 25, 38-39]

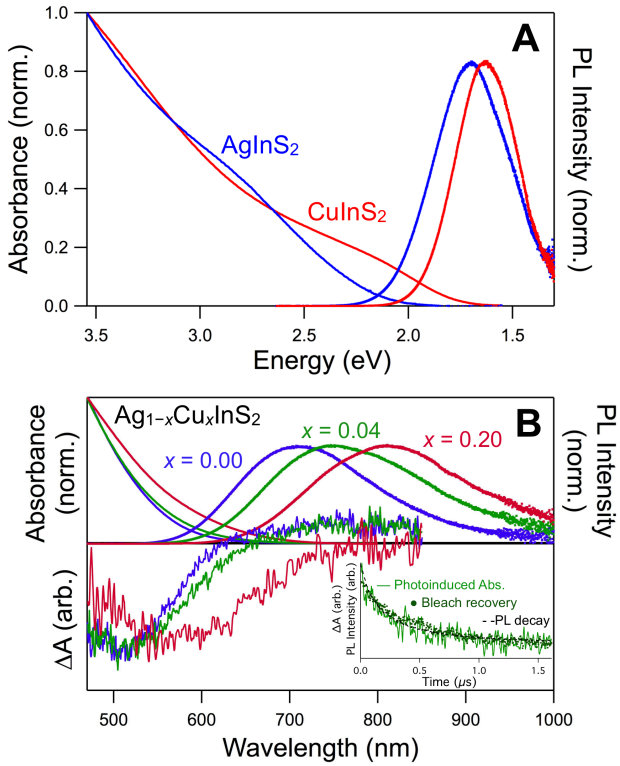

Figure 3.1. (A) Absorption and PL spectra of colloidal $AgInS_2$ NCs (blue) and $CuInS_2$ NCs (red) of similar sizes (d ~ 4 nm), suspended in toluene. **(B)** Absorption (top left), PL (top right), and TA (integrated between 0 and 300 ns, bottom) spectra of colloidal $Ag_{1-x}Cu_xInS_2$ NCs prepared by partial cation exchange from the same starting d = 3.9 nm $AgInS_2$ NCs. The blue traces show data for x = 0.00 (QY = 44%), the green traces show data for x ~0.04 (QY = 41%), and the red traces show data for x ~ 0.20 (QY = 32%). **Inset:** TA and PL decay dynamics associated with the x ~ 0.04 NCs shown in the main panel. The photoinduced absorption decay (green line, ~750 nm), the negative of the TA bleach recovery (dark green dots, ~500 nm), and the PL decay (dashed black line, 665-790 nm)

all show similar dynamics with a time constant of ~400 ns, consistent with all three measurements probing decay of the same luminescent excited state. All measurements were performed on NCs in toluene at room temperature.

Figure 3.1B summarizes absorption, PL, and transient-absorption (TA) spectroscopic results obtained for a series of $Ag_{1-x}Cu_xInS_2$ NCs with different x values ranging from 0.00 to 0.20, all prepared from the same starting d = 3.9 nm $AgInS_2$ NCs by partial cation exchange (Scheme 3.1). The PL quantum yields of these NCs are all similar, ranging from 32 to 44%. Like in Figure 3.1A ($AgInS_2$ and $CuInS_2$, or x = 0 and 1), increasing x decreases the absorption onset and PL energies. All three samples also show similar TA spectra featuring a broad bleach at the absorption edge and weak photoinduced absorption at lower energy, within the gap. As described above, the bleach is attributable to the presence of delocalized CB electrons, and recent TA studies[40-41] of Cu^+:CdSe/CdS and $CuInS_2$ NCs have attributed a similar mid-gap photoinduced absorption signal to electronic transitions involving filling of copper-localized photogenerated holes, consistent with experimental photoinduced absorption measurements in bulk Cu^+:ZnS crystals[16] and theoretical predictions for absorption in Cu^{2+}:CdSe QDs.[14] The PL involves decay of both the electron and the hole. We note that similar TA data have also been interpreted to suggest that the luminescence of $CuInS_2$/ZnS NCs results from deep electron trapping rather than deep hole trapping, based in part on the observation that the photoinduced absorption dynamics are insensitive to a low-energy "dump" pulse.[18] In the present data, however, both the TA bleach and the photoinduced absorption show the same dynamics as the PL decay (inset, $\tau \sim 400$ ns), consistent with all three of these observables probing the same luminescent excited state.

Figure 3.2 plots absorption (normalized) and differential-absorption spectra collected for a much larger series of $Ag_{1-x}Cu_xInS_2$ NCs with different values of x, again all obtained from the same $d = 3.9 \pm 0.4$ nm $AgInS_2$ NCs by partial cation exchange with Cu^+. The average size and the

size distribution remain essentially the same after copper incorporation (see Appendix B). Figure 3.2A also presents normalized room-temperature PL spectra of these NCs. The arrows in Figure 3.2A indicate the trends with increasing x. As x increases, there is an apparent redshift of the absorption onset, but the differential absorption spectra in Figure 3.2B suggest that this change is better described as growth of distinct new absorption at a fixed energy (~2.2 eV) within the original $AgInS_2$ NC absorption gap. The amplitude of this new absorption scales with x. Concomitantly, the PL band redshifts at small x, but appears to become independent of x at larger values of x.

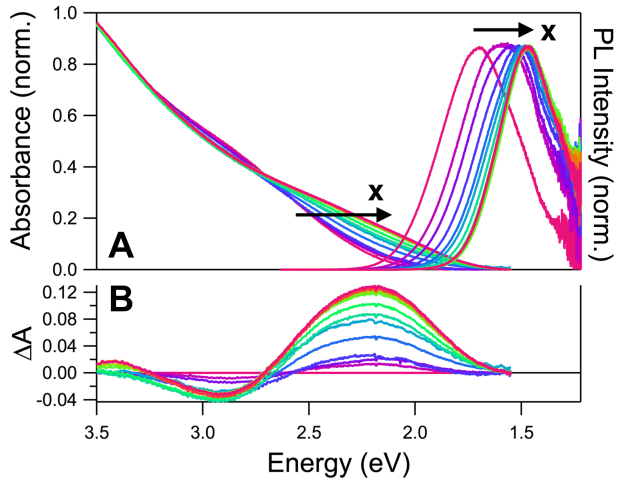

Figure 3.2. (A) Normalized absorption and PL spectra, and **(B)** differential absorption spectra of a series of $Ag_{1-x}Cu_xInS_2$ NCs with $0 \leq x \leq 0.9$. All data were collected at room temperature with the NCs in toluene. As x increases, new absorption grows in at ~2.2 eV, causing an apparent redshift of the absorption edge. The PL band maximum redshifts with increasing x. The absorption spectra are normalized at 3.54 eV.

The changes in the absorption spectrum with increasing x are attributed to introduction of discrete new mid-gap states upon incorporation of Cu^+ into the $AgInS_2$ NC lattice. This interpretation is supported by DFT calculations on model $AgInS_2$ NCs. Figure 3.3 presents the near-gap molecular-orbital (MO) energies computed for several 34-cation $Ag_{1-x}Cu_xInS_2$ NCs having values of $x = 0.00$, 0.18, 0.47, and 1.00. The CB edge is set to 0 eV for all NCs to facilitate comparison. When $x = 0.00$ ($AgInS_2$), the VB edge is defined by a highest-occupied MO (HOMO)

having ~66% $S^{2-}(3p)$-orbital character, with the remainder dominated by $Ag^{+}(4d)$-orbital character in an antibonding phase relationship with the $S^{2-}(3p)$ orbitals. The corresponding bonding combination of $Ag^{+}(4d)$ and $S^{2-}(3p)$ orbitals occurs much deeper in energy. The CB edge is defined by a lowest-unoccupied MO (LUMO) that has ~50% $In^{3+}(5s)$ character, with ~30% $Ag^{+}(5s)$ character and ~15% $S^{2-}(3p)$ character. These results agree well with those computed for bulk $AgInS_2$.[42-44]

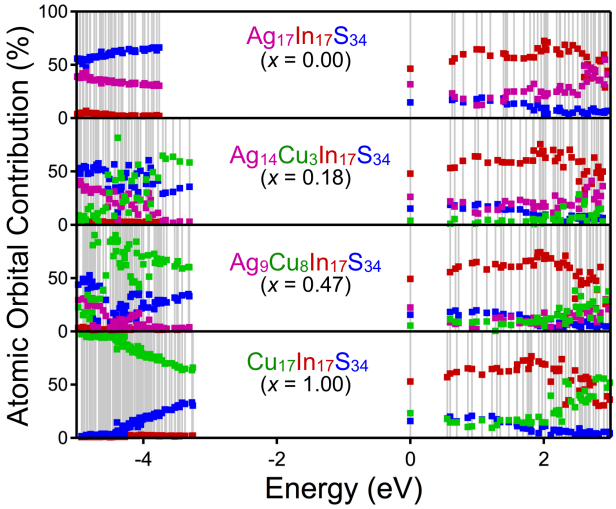

Figure 3.3. Molecular-orbital energies and atomic-orbital compositions of $Ag_{1-x}Cu_xInS_2$ NCs ($(Ag_{1-x}Cu_x)_{17}In_{17}S_{34}$, d ~1.6 nm, x = 0.00, 0.18, 0.47, 1.00) calculated by DFT. The specific clusters are indicated in each panel. Energies are referenced to the CB edge.

Substituting a few Cu^{+} ions into the $AgInS_2$ NC lattice introduces a discrete set of localized copper-centered orbitals just above the $AgInS_2$ VB edge. Increasing the copper content from x = 0.18 to 0.47 increases the number of these copper-based mid-gap orbitals but does not alter their energies substantially, consistent with the spectroscopic observation of growing mid-gap absorption with increasing x (Figure 3.2B). As x is increased toward 1.00, these mid-gap orbitals evolve to become the VB edge of $CuInS_2$ NCs. For all copper-containing compositions, the HOMO has ~50-60% $Cu^{+}(3d)$ character and substantial $S^{2-}(3p)$ covalency. Across this series of $Ag_{1-x}Cu_xInS_2$ NCs, there is negligible change in the In^{3+} and S^{2-} contributions to the CB edge, and

just the $Ag^+(5s)$ orbital contributions are replaced by $Cu^+(4s)$ contributions. Note that the mid-gap Cu^+ orbitals that appear in the dilute limit closely resemble the near-band-edge orbitals of the $CuInS_2$ NCs in both energy and composition, but simply occur with a much smaller density in the dilute-Cu^+ limit. Overall, these results demonstrate that the spectroscopically active orbitals of $CuInS_2$ NCs are almost identical to those of Cu^+-doped $AgInS_2$ NCs.

Although the experimental evolution of the absorption spectrum going from $AgInS_2$ to $CuInS_2$ NCs appears readily explained by these DFT results, the trend in the PL data for the same series is more complex. Figure 3.4 summarizes the PL data from Figure 3.2 by plotting the PL energy shift *vs x*. This plot shows that the PL energy decreases with addition of Cu^+ until $x \sim 0.20$, but then becomes independent of x between $x = \sim 0.20$ and 1.00. Increasing x in $Ag_{1-x}Cu_xInS_2$ NCs thus does not simply shift the PL to lower energies in proportion to x, as observed for example in $Cd_{1-x}Zn_xSe$ alloy NCs (with minor bowing), where delocalized excitons experience the average crystal composition. The PL data also do not follow the trend expected in the scenario of hole localization at individual Cu^+ ions, however. In this scenario, only very small values of x ($< \sim 0.03$) would be required to completely shift the PL to its new energy. Such a scenario is observed in Mn^{2+}-doped II-VI NCs, for example, where a single Mn^{2+} dopant is sufficient to completely shift the PL of a given NC to its new value, and increasing x has only a small additional effect. In contrast, the PL data in Figure 3.4A show that much larger values of x are required to reach the PL endpoint in the $Ag_{1-x}Cu_xInS_2$ NC series, despite the fact that the PL energy shifts rapidly even at very small x. At $x = 0.20$, where the PL energy becomes independent of x, the average NC possesses ~60 Cu^+ ions (see SI). We conclude that the PL characteristics of $CuInS_2$ NCs are already fully achieved at Cu^+ levels far below $x = 1.00$, but also that isolated Cu^+ impurity ions are not sufficient to make the PL of $Ag_{1-x}Cu_xInS_2$ NCs resemble that of $CuInS_2$ NCs.

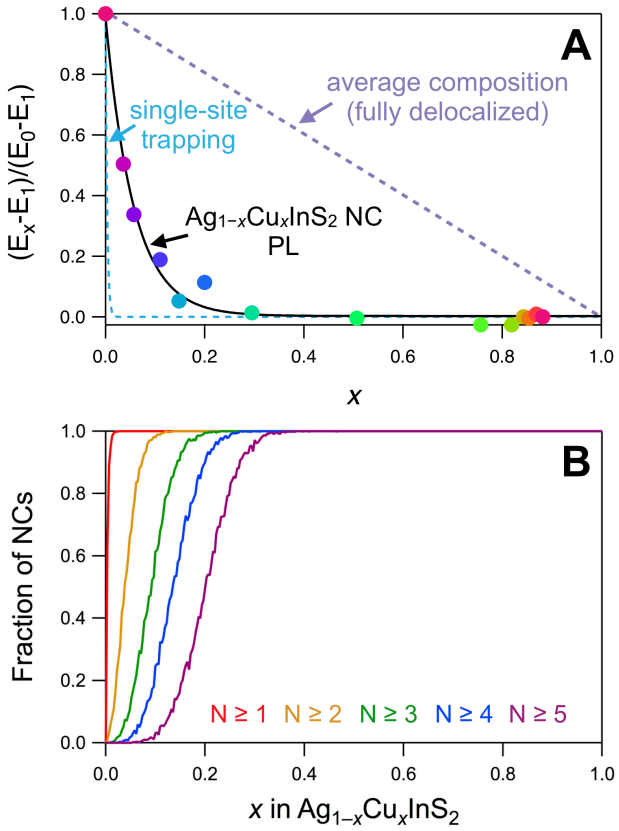

Figure 3.4. (A) Plot of PL energy shift (circles) *vs x* for the $Ag_{1-x}Cu_xInS_2$ NCs of Figure 3.2. The PL energy rapidly redshifts with small additions of copper until $x \sim 0.20$, beyond which it becomes independent of copper concentration. The black line is a guide to the eye. The blue dashed line shows the anticipated dependence of the PL energy on x for the scenario in which the hole in the luminescent excited state is completely localized on a single copper ion. The purple dashed line shows the anticipated dependence of the PL energy on x for the scenario in which the luminescent excited state is fully delocalized and experiences the average NC composition. **(B)** Statistics describing the probabilities of minimum Cu^+ cluster sizes in $Ag_{1-x}Cu_xInS_2$ NCs, computed by Monte Carlo methods for $d = 4.05$ nm NCs with ordered chalcopyrite lattice structures and plotted as a function of x. The curves illustrate the fraction of NCs possessing at least monomers ($N \geq 1$, red), nearest-neighbor dimers ($N \geq 2$, yellow), and clusters with 3 ($N \geq 3$, green), 4 ($N \geq 4$, blue), or 5 ($N \geq 5$, purple) of nearest-neighbor Cu^+ ions. At $x = 0.2$, nearly all NCs possess at least one cluster with N = 4 Cu^+ ions or larger.

It is conceivable that the results in Figure 3.4A could simply reflect the rare formation of some specific mid-gap trap state upon copper alloying, such as discussed in previous literature,[2, 9, 11] and that this trap is present in every NC above $x \sim 0.20$. This interpretation is excluded by the observation that the PL spectra at intermediate compositions (~0.10) are not describable as linear

combinations of the endpoint PL spectra (see SI). These data are thus inconsistent with the PL of $Ag_{1-x}Cu_xInS_2$ NCs coming from a specific rare defect.

Instead, we interpret the data in Figure 3.4A to suggest that holes localized at single copper dopants in the dilute Cu^+ limit ($x \sim 0$) can relax to lower energies by delocalizing over a larger number of copper impurity ions as x is increased, provided there exists sufficient inter-copper electronic coupling. Such electronic coupling involves the copper 3*d* valence orbitals and is limited to nearest-neighbor interactions, *i.e.*, hole delocalization requires nearest-neighbor copper ions. To analyze this scenario, the statistical distributions of Cu^+ ions within the $Ag_{1-x}Cu_xInS_2$ NCs of Figures 3.2 and 3.4A were analyzed as a function of x using Monte Carlo methods. Figure 3.4B plots the fraction of NCs possessing at least monomers ($N \geq 1$), nearest-neighbor dimers ($N \geq 2$), trimers ($N \geq 3$), tetramers ($N \geq 4$), and larger clusters ($N \geq 5$) of nearest-neighbor Cu^+ ions as a function of x, computed for model d = 4.05 nm NCs with ordered chalcopyrite lattice structures. From these results, the fraction of NCs possessing at least one Cu^+ dopant increases very rapidly at small x such that no undoped NCs remain beyond $x \sim 0.03$. Likewise, the fraction of NCs possessing at least one Cu^+-Cu^+ nearest-neighbor interaction grows very rapidly and reaches unity at $x \sim 0.12$. Both of these curves reach unity at values of x where the experimental PL energy still depends on x (Figure 3.4A), indicating that the PL energy is not determined by formation of either Cu^+ monomers or Cu^+-Cu^+ dimers within the NCs. Instead, the experimental NC PL energy only becomes independent of x at $x \geq \sim 0.20$, where the majority of NCs possess clusters of at least 3 and possibly at least 4 nearest-neighbor Cu^+ ions. It is impossible to identify any specific cluster that represents the limit of maximum hole delocalization, in part because multiple configurations exist for clusters of $N \geq 3$, but that complication does not preclude drawing the strong conclusion from this analysis that a small number of neighboring Cu^+ ions is necessary and sufficient to

maximally stabilize the luminescent excited state in $Ag_{1-x}Cu_xInS_2$ NCs. Because the PL spectrum is the same at x = 1.00 ($CuInS_2$) as it is at x = ~ 0.25, the data presented here also provide compelling support for hole localization within small clusters of lattice Cu^+ ions in $CuInS_2$ NCs. Hole localization over small copper clusters within $CuInS_2$ NCs has also recently been predicted by DFT studies of the VB electronic structures of $Zn_{2(1-x)}(Cu,In)_xS_2$ NCs,[21] where the combination of weak copper *d*-band electronic coupling, electrostatic fluctuations, and electron-nuclear coupling was proposed to cause hole self-trapping even in point-defect-free ordered chalcopyrite NCs.

We note that the analysis of Figure 3.4B assumes random alloying of Cu^+ and Ag^+ in these $Ag_{1-x}Cu_xInS_2$ NCs. It is conceivable that thermodynamic forces could cause some degree of Cu^+ and Ag^+ segregation within the NCs; in such a scenario, copper clusters would form more rapidly with x than plotted in Figure 3.4B, and slightly larger clusters would exist at any given x than predicted from the statistical analysis, but the same overall conclusion that holes delocalize over relatively small numbers of Cu^+ ions in $Ag_{1-x}Cu_xInS_2$ NCs would still be reached. Overall, these results and analysis reinforce the description of $CuInS_2$ NCs as "heavily copper-doped NCs," being more similar in electronic structure to dilutely Cu^+-doped NCs than to undoped II-VI or other semiconductor NCs that involve highly dispersive VBs.

3.4 Summary and Conclusions

In summary, the synthesis of a series of $Ag_{1-x}Cu_xInS_2$ NCs ($0 \leq x \leq 1$) by cation exchange starting from a single stock of $AgInS_2$ NCs has allowed the effects of copper on the absorption and PL spectroscopic properties of these NCs to be investigated systematically with minimal perturbation of other structural or compositional variables. These experiments reveal key aspects

of the electronic structures of $Ag_{1-x}Cu_xInS_2$, including $CuInS_2$ NCs. Specifically, the results presented here demonstrate that addition of Cu^+ into $AgInS_2$ NCs introduces discrete new mid-gap Cu(3*d*) orbitals just above the $Ag_{1-x}Cu_xInS_2$ VB edge. These new orbitals in the dilute Cu^+ limit ($x \sim 0.00$) are very similar to the orbitals at the VB edge of $CuInS_2$ NCs ($x = 1.00$). The NC PL energies show a striking trend of decreasing in energy with increasing x until ~0.20, beyond which they remain independent of x all the way up to $x = 1.00$. The absence of any x dependence of the PL energy between $x = 0.20$ and 1.00 indicates limited hole delocalization in such NCs, including in $CuInS_2$ NCs ($x = 1.00$), and this result in turn implies weak inter-Cu^+ electronic coupling relative to localization forces such as electron-nuclear coupling and electrostatic heterogeneity. Statistical modeling and analysis of the experimental data suggest hole delocalization over only around 3 or 4 copper ions in the luminescent excited state of $Ag_{1-x}Cu_xInS_2$ NCs with $x > \sim 0.20$, including $CuInS_2$ NCs, rather than over the entire NC volume. These findings are consistent with exciton self-trapping in $CuInS_2$ NCs.[3, 12, 21] The results and analysis presented here advance our fundamental understanding of the electronic structures and excited-state properties of luminescent copper-doped and copper-based semiconductor NCs and help to inform the development of future photonic or energy-conversion technologies that employ such materials.

3.5 Experimental Methods

3.5.1. Chemicals. Sulfur powder (99.98%), indium (III) acetate (99.99%), 1-dodecanethiol (DDT; ≤98%), copper (I) iodide (CuI; 98%), oleic acid (OA; 90%), and 1-octadecene (ODE; 90%) were purchased from Aldrich. Silver acetate (99%) and trioctylphosphine (TOP; 97%) were purchased from STREM. All chemicals were used as received.

3.5.2. Nanocrystal Synthesis and Partial Cation Exchange. Silver indium sulfide NCs were synthesized according to the following procedure, which was adapted from a previous literature

report.[22] To start, silver acetate (0.53 mmol), indium acetate (0.51 mmol), and DDT (83.3 mmol) were combined in a flask and stirred under nitrogen at 150 ºC for one hour. A separate, sulfur solution (sulfur (1.1 mmol), DDT (5.6 g), and OA (1.6 g)) was sonicated until all sulfur had dissolved (~30 min) and then purged with nitrogen for ~30 min. The sulfur precursor solution was then rapidly injected into the flask containing the silver, indium, and DDT precursors. The reaction was allowed to proceed for 10 minutes, at which point the flask was rapidly cooled. OA (~1 mL) was added to the flask at ~40 ºC, after which point the flask continued to cool to room temperature. The NCs were washed twice with ethanol, methanol, and acetone, and then resuspended in hexanes and OA. The NCs were washed a third time with methanol and resuspended in toluene.

All $Ag_{1-x}Cu_xInS_2$ NCs were synthesized based on a procedure adapted from a previous synthetic method,[45] and the concentration of copper and TOP in the copper precursor solution was varied to obtain NCs with different values of *x*. A representative synthesis is as follows: briefly, pre-formed $AgInS_2$ NCs were dried and resuspended (with sonication) in 1.2 mL DDT. 3.0 mL ODE and 0.1 mL OA were added to the NC solution. The flask was heated to 60 ºC, and three pump-purge cycles (20 min/cycle) were performed. A separate copper solution was also prepared for which 0.04 mmol CuI was dissolved in 12 mL ODE, and the solution was purged for ~30 min. 0.02 mL of TOP (0.045 mmol) was added, and the solution was sonicated for ~60 min. 0.55 mL of the copper precursor solution was then swiftly injected into the flask containing the $AgInS_2$ NCs, and the reaction was allowed to proceed for 10 minutes. The flask was then quickly cooled to room temperature. The NCs were washed twice with ethanol and methanol, resuspending in toluene in between. The final product was resuspended in toluene. Concentrations of silver and copper in the NCs were determined by analysis of dried NCs digested in ultrapure nitric acid (EMD

Chemicals) using inductively coupled plasma atomic emission spectrometry (ICP-AES; PerkinElmer).

3.5.3. Spectroscopic Measurements. Absorption spectra of the NCs were collected in toluene at room temperature using a Cary 5000 spectrophotometer (Varian). Continuous-wave (CW) photoluminescence (PL) spectra measurements were performed by exciting the colloidal NCs with a 405 nm laser diode and collecting the spectra using an OceanOptics 2000+ spectrometer. Transmission electron microscope (TEM) images were obtained using a FEI Tecnai G2 F20 operating at 200 kV, and size distribution analysis was performed on 115 individual NCs per sample. PL quantum yields were determined using an External Quantum Efficiency Measurement System with a Hamamatsu Integrating Sphere (C9920-12) and a Hamamatsu high-sensitivity photonic multichannel analyzer (C10027-01). Transient-absorption measurements were performed using an Ekspla Nd:YAG laser operating at a 25 Hz repetition rate. NCs were excited using the third harmonic of the 1064 nm fundamental with an excitation energy of ~100 μJ/pulse while stirring. A 150W CW Xe lamp was used as the white-light probe source. The pump and probe beams intersected at a 90° angle. The dynamics and spectra were collected using a monochromator and streak camera with an instrument response of ~20 ps.

3.5.4. Density Functional Theory Calculations. DFT calculations were performed using Gaussian 09[46] with the PBE0 hybrid DFT functional[47-48] and the Los Alamos double-ζ pseudocore potential and corresponding basis set, with explicit basis functions used to describe the S(3*s*, 3*p*), In(5*s*, 5*p*), Cu(3*d*, 4*s*, 4*p*) and Ag(4*d*, 5*s*, 5*p*) atomic orbitals.[49-50] This method has previously been applied to other doped NCs, including Cu^+:CdSe and Ag^+:CdSe NCs.[13, 51-52] Small, roughly spherical NCs with 34 total cations (Cu^+, Ag^+, and In^{3+}) and 34 anions were constructed in the ordered chalcopyrite crystal structure; all NC geometries were optimized before other electronic-

structure calculations were performed. Dangling bonds on uncompensated surface ions were passivated by pseudo-hydrogen atoms with fractional charges (+1.25 for In^{3+}, +1.75 for Cu^{+} and Ag^{+}, and +0.5 for S^{2-}).[53-54]

3.5.5. Monte Carlo Calculations. A spherical $AgInS_2$ NC (d = 4.05 nm, 310 Ag^{+} cations) was constructed from the bulk $AgInS_2$ crystal structure. For each possible Cu^{+} dopant concentration with Cu^{+} substituting for Ag^{+} (x = 0/310, 1/310, 2/310 ... 310/310), 1000 NCs were simulated. Because not all NCs in the experiment have identical numbers of dopants at a given ensemble dopant concentration, the actual number of dopants in each NC was selected from a Poissonian distribution around the average number of dopants at the given concentration. Dopants were randomly assigned to Ag^{+} cation sites, and the number and type of dopant clusters in each NC were determined. The data in Figure 3.4 represents the fraction of NCs (out of the 1000 simulated NCs) at each concentration that have at least one cluster of the specified size or larger.

3.6 References

1. Aldakov, D.; Léfrançois, A.; Reiss, P., Ternary and Quaternary Metal Chalcogenide Nanocrystals: Synthesis, Properties, and Applications. *J. Mater. Chem. C* **2013,** *1*, 3756-3776.
2. Leach, A. D. P.; Macdonald, J. E., The Optoelectronic Properties of $CuInS_2$ Nanocrystals and their Origin. *J. Phys. Chem. Lett.* **2016,** *7*, 572-583.
3. Knowles, K. E.; Hartstein, K. H.; Kilburn, T. B.; Marchioro, A.; Nelson, H. D.; Whitham, P. J.; Gamelin, D. R., Luminescent Colloidal Semiconductor Nanocrystals Containing Copper: Synthesis, Photophysics, and Applications. *Chem. Rev.* **2016,** *116* (18), 10820-10851.
4. Coughlan, C.; Ibáñez, M.; Dobrozhan, O.; Singh, A.; Cabot, A.; Ryan, K. M., Compound Copper Chalcogenide Nanocrystals. *Chem. Rev.* **2017,** *117*, 5865-6109.
5. Sandroni, M.; Wegner, K. D.; Aldakov, D.; Reiss, P., Prospects of Chalcopyrite-Type Nanocrystals for Energy Applications. *ACS Energy Lett.* **2017,** *2*, 1076-1088.
6. Li, L.; Daou, T. J.; Texier, I.; Chi, T. T. K.; Liem, N. Q.; Reiss, P., Highly Luminescent $CuInS_2$/ZnS Core/Shell Nanocrystals: Cadmium-Free Quantum Dots for In Vivo Imaging. *Chem. Mater.* **2009,** *21*, 2422-2429.

7. Knowles, K. E.; Kilburn, T. B.; Alzate, D.; McDowall, S.; Gamelin, D. R., Bright CuInS2/CdS Nanocrystal Phosphors for High-Gain Full-Spectrum Luminescent Solar Concentrators. *Chem. Commun.* **2015,** *51*, 9129–9132.
8. Meinardi, F.; McDaniel, H.; Carulli, F.; Colombo, A.; Velizhanin, K. A.; Makarov, N. S.; Simonutti, R.; Klimov, V. I.; Brovelli, S., Highly efficient large-area colourless luminescent solar concentrators using heavy-metal-free colloidal quantum dots. *Nat. Nanotech.* **2015,** *10*, 878–885.
9. Leach, A. D. P.; Shen, X.; Faust, A.; Cleveland, M. C.; La Croix, A. D.; Banin, U.; Pantelides, S. T.; Macdonald, J. E., Defect Luminescence from Wurtzite $CuInS_2$ Nanocrystals: Combined Experimental and Theoretical Analysis. *J. Phys. Chem. C* **2016,** *120*, 5207-5212.
10. Sumner, R.; Eiselt, S.; Kilburn, T. B.; Erickson, C.; Carlson, B.; Gamelin, D. R.; McDowall, S.; Patrick, D. L., Analysis of Optical Losses in High-Efficiency CuInS2-Based Nanocrystal Luminescent Solar Concentrators: Balancing Absorption vs Scattering. *J. Phys. Chem. C* **2017,** *121*, 3252–3260.
11. Rice, W. D.; McDaniel, H.; Klimov, V. I.; Crooker, S. A., Magneto-Optical Properties of CuInS2 Nanocrystals. *J. Phys. Chem. Lett.* **2014,** *5* (23), 4105-4109.
12. Knowles, K. E.; Nelson, H. D.; Kilburn, T. B.; Gamelin, D. R., Singlet–Triplet Splittings in the Luminescent Excited States of Colloidal Cu+:CdSe, Cu+:InP, and CuInS2 Nanocrystals: Charge-Transfer Configurations and Self-Trapped Excitons. *J. Am. Chem. Soc.* **2015,** *137* (40), 13138-13147.
13. Nelson, H. D.; Hinterding, S. O. M.; Fainblat, R.; Creutz, S. E.; Li, X.; Gamelin, D. R., Mid-Gap States and Normal vs Inverted Bonding in Luminescent Cu+- and Ag+-Doped CdSe Nanocrystals. *J. Am. Chem. Soc.* **2017,** *139*, 6411–6421.
14. Nelson, H. D.; Li, X.; Gamelin, D. R., Computational Studies of the Electronic Structures of Copper-Doped CdSe Nanocrystals: Oxidation States, Singlet-Triplet Splittings, Jahn-Teller Distortions, and Vibronic Bandshapes. *J. Phys. Chem. C* **2016,** *120*, 5714–5723.
15. Hassan, A.; Zhang, X.; Liu, X.; Rowland, C. E.; Jawaid, A. M.; Chattopadhyay, S.; Gulec, A.; Shamirian, A.; Zuo, X.; Klie, R. F.; Schaller, R. D.; Snee, P. T., Charge Carriers Modulate the Bonding of Semiconductor Nanoparticle Dopants As Revealed by Time-Resolved X-ray Spectroscopy. *ACS Nano* **2017,** *11*, 10070-10076.
16. Suzuki, A.; Shionoya, S., Mechanism of the Green-Copper Luminescence in ZnS Crystals. I. Direct Evidence for the Pair Emission Mechanism. *J. Phys. Soc. Jpn.* **1971,** *31*, 1455-1461.
17. Yen, W. M.; Shionoya, S.; Yamamoto, H., *Phosphor Handbook*. Second ed.; CRC Press: New York, 2007.
18. Kraatz, I. T.; Booth, M.; Whitaker, B. J.; Nix, M. G. D.; Critchley, K., Sub-Bandgap Emission and Intraband Defect-Related Excited-State Dynamics in Colloidal CuInS2/ZnS Quantum Dots Revealed by Femtosecond Pump−Dump−Probe Spectroscopy. *J. Phys. Chem. C* **2014,** *118*, 24102−24109.
19. Li, L.; Pandey, A.; Werder, D. J.; Khanal, B. P.; Pietryga, J. M.; Klimov, V. I., Efficient Synthesis of Highly Luminescent Copper Indium Sulfide-Based Core/Shell Nanocrystals with Surprisingly Long-Lived Emission. *J. Am. Chem. Soc.* **2011,** *133* (5), 1176-1179.
20. Sun, J.; Zhu, D.; Zhao, J.; Ikezawa, M.; Wang, X.; Masumoto, Y., Ultrafast Carrier Dynamics in $CuInS_2$ Quantum Dots. *Appl. Phys. Lett.* **2014,** *104*, 023118.

21. Nelson, H. D.; Gamelin, D. R., Valence-Band Electronic Structures of Cu+-Doped ZnS, Alloyed Cu−In−Zn−S, and Ternary CuInS2 Nanocrystals: A Unified Description of Photoluminescence across Compositions. *J. Phys. Chem. C* **2018,** *122*, 18124–18133.
22. Hamanaka, Y.; Ogawa, T.; Tsuzuki, M.; Kuzuya, T., Photoluminescence Properties and Its Origin of AgInS2 Quantum Dots with Chalcopyrite Structure. *J. Phys. Chem. C* **2011,** *115* (5), 1786-1792.
23. Hamanaka, Y.; Ozawa, K.; Kuzuya, T., Enhancement of Donor–Acceptor Pair Emissions in Colloidal AgInS2 Quantum Dots with High Concentrations of Defects. *J. Phys. Chem. C* **2014,** *118* (26), 14562-14568.
24. Mao, B.; Chuang, C.-H.; Wang, J.; Burda, C., Synthesis and Photophysical Properties of Ternary I–III–VI AgInS2 Nanocrystals: Intrinsic versus Surface States. *J. Phys. Chem. C* **2011,** *115* (18), 8945-8954.
25. Stroyuk, O.; Raevskaya, A.; Spranger, F.; Selyshchev, O.; Dzhagan, V.; Schulze, S.; Zahn, D. R. T.; Eychmüller, A., Origin and Dynamics of Highly Efficient Broadband Photoluminescence of Aqueous Glutathione-Capped Size-Selected Ag–In–S Quantum Dots. *J. Phys. Chem. C* **2018,** *122*, 13648–13658.
26. Ciszek, T. F., Melt Growth and some Properties of CuxAg1-xInSe2 and CuInyGa1-ySe2 Chalcopyrite Solid Solution Crystals. *J. Cryst. Growth* **1986,** *79*, 689-694.
27. Albornoz, J. G.; Serna, R.; León, M., Optical Properties and Electronic Structure of Polycrystalline Ag1−xCuxInSe2 Alloys. *J. Appl. Phys.* **2005,** *97*, 103515.
28. Tsuji, I.; Kato, H.; Kudo, A., Photocatalytic Hydrogen Evolution on ZnS−CuInS2−AgInS2 Solid Solution Photocatalysts with Wide Visible Light Absorption Bands. *Chem. Mater.* **2006,** *18*, 1969–1975.
29. Saha, S. K.; Guchhait, A.; Pal, A. J., Hybrid pn-junction solar cells based on layers of inorganic nanocrystals and organic semiconductors: optimization of layer thickness by considering the width of the depletion region. *Phys. Chem. Chem. Phys.* **2014,** *16* (9), 4193-4201.
30. Guchhait, A.; Pal, A. J., Copper-Diffused AgInS2 Ternary Nanocrystals in Hybrid Bulk-Heterojunction Solar Cells: Near-Infrared Active Nanophotovoltaics. *ACS Appl. Mater. Inter.* **2013,** *5* (10), 4181-4189.
31. Chen, S.; Demillo, V.; Lu, M.; Zhu, X., Preparation of photoluminescence tunable Cu-doped AgInS2 and AgInS2/ZnS nanocrystals and their application as cellular imaging probes. *RSC Adv.* **2016,** *6* (56), 51161-51170.
32. Raevskaya, A.; Rozovik, O.; Novikova, A.; Selyshchev, O.; Stroyuk, O.; Dzhagan, V.; Goryacheva, I.; Gaponik, N.; Zahn, D. R. T.; Eychmüller, A., Luminescence and photoelectrochemical properties of size-selected aqueous copper-doped Ag–In–S quantum dots. *RSC Adv.* **2018,** *8* (14), 7550-7557.
33. Son, D. H.; Hughes, S. M.; Yin, Y.; Alivisatos, A. P., Cation Exchange Reactions in Ionic Nanocrystals. *Science* **2004,** *306*, 1009-1012.
34. Jain, P. K.; Amirav, L.; Aloni, S.; Alivisatos, A. P., Nanoheterostructure Cation Exchange: Anionic Framework Conservation. *J. Am. Chem. Soc* **2010,** *132*, 9997-9999.
35. Groeneveld, E.; Witteman, L.; Lefferts, M.; Ke, X.; Bals, S.; Van Tendeloo, G.; de Mello Donega, C., Tailoring ZnSe–CdSe Colloidal Quantum Dots via Cation Exchange: From Core/Shell to Alloy Nanocrystals. *ACS Nano* **2013,** *7* (9), 7913-7930.
36. Gupta, S.; Kershaw, S. V.; Rogach, A. L., 25th Anniversary Article: Ion Exchange in Colloidal Nanocrystals. *Adv. Mater.* **2013,** *25*, 6923-6944.

37. De Trizio, L.; Manna, L., Forging Colloidal Nanostructures via Cation Exchange Reactions. *Chem. Rev.* **2016,** *116*, 10852–10887.
38. Knowles, K. E.; Kilburn, T. B.; Alzate, D. G.; McDowall, S.; Gamelin, D. R., Bright CuInS2/CdS nanocrystal phosphors for high-gain full-spectrum luminescent solar concentrators. *Chemical Communications* **2015,** *51* (44), 9129-9132.
39. Cheng, K.-C.; Law, W.-C.; Yong, K.-T.; Nevins, J. S.; Watson, D. F.; Ho, H.-P.; Prasad, P. N., Synthesis of near-infrared silver-indium-sulfide (AgInS2) quantum dots as heavy-metal free photosensitizer for solar cell applications. *Chem. Phys. Lett.* **2011,** *515* (4), 254-257.
40. Hughes, K. E.; Hartstein, K. H.; Gamelin, D. R., Photodoping and Transient Spectroscopies of Copper-Doped CdSe/CdS Nanocrystals. *ACS Nano* **2018,** *12* (1), 718-728.
41. Berends, A. C.; Rabouw, F. T.; Spoor, F. C. M.; Bladt, E.; Grozema, F. C.; Houtepen, A. J.; Siebbeles, L. D. A.; de Mello Donegá, C., Radiative and Nonradiative Recombination in CuInS2 Nanocrystals and CuInS2-Based Core/Shell Nanocrystals. *J. Phys. Chem. Lett.* **2016,** *7* (17), 3503-3509.
42. Liu, J.; Hua, E., Electronic structure and absolute band edge position of tetragonal AgInS2 photocatalyst: A hybrid density functional study. *Mater. Sci. Semicond. Process.* **2015,** *40*, 446-452.
43. Huang, D.; Persson, C., Photocatalyst AgInS2 for active overall water-splitting: A first-principles study. *Chem. Phys. Lett.* **2014,** *591*, 189-192.
44. Sharma, S.; Verma, A. S.; Jindal, V. K., First principles studies of structural, electronic, optical, elastic and thermal properties of Ag-chalcopyrites (AgInX2: X=S, Se). *Phys. B: Cond. Matter* **2014,** *438*, 97-108.
45. Yang, L.; Knowles, K. E.; Gopalan, A.; Hughes, K. E.; James, M. C.; Gamelin, D. R., One-Pot Synthesis of Monodisperse Colloidal Copper-Doped CdSe Nanocrystals Mediated by Ligand–Copper Interactions. *Chem. Mater.* **2016,** *28* (20), 7375-7384.
46. Frisch, M. J.; Trucks, G. W.; Schlegel, H. B.; Scuseria, G. E.; Robb, M. A.; Cheeseman, J. R.; Scalmani, G.; Barone, V.; Mennucci, B.; Petersson, G. A.; Nakatsuji, H.; Caricato, M.; Li, X.; Hratchian, H. P.; Izmaylov, A. F.; Bloino, J.; Zheng, G.; Sonnenberg, J. L.; Hada, M.; Ehara, M.; Toyota, K.; Fukuda, R.; Hasegawa, J.; Ishida, M.; Nakajima, T.; Honda, Y.; Kitao, O.; Nakai, H.; Vreven, T.; Montgomery Jr., J. A.; Peralta, J. E.; Ogliaro, F.; Bearpark, M. J.; Heyd, J.; Brothers, E. N.; Kudin, K. N.; Staroverov, V. N.; Kobayashi, R.; Normand, J.; Raghavachari, K.; Rendell, A. P.; Burant, J. C.; Iyengar, S. S.; Tomasi, J.; Cossi, M.; Rega, N.; Millam, N. J.; Klene, M.; Knox, J. E.; Cross, J. B.; Bakken, V.; Adamo, C.; Jaramillo, J.; Gomperts, R.; Stratmann, R. E.; Yazyev, O.; Austin, A. J.; Cammi, R.; Pomelli, C.; Ochterski, J. W.; Martin, R. L.; Morokuma, K.; Zakrzewski, V. G.; Voth, G. A.; Salvador, P.; Dannenberg, J. J.; Dapprich, S.; Daniels, A. D.; Farkas, Ö.; Foresman, J. B.; Ortiz, J. V.; Cioslowski, J.; Fox, D. J. *Gaussian 09*, Gaussian, Inc.: Wallingford, CT, USA, 2009.
47. Perdew, J. P.; Burke, K.; Ernzerhof, M., Generalized Gradient Approximation Made Simple. *Phys. Rev. Lett.* **1996,** *77*, 3865-3868.
48. Adamo, C.; Barone, V., Toward Reliable Density Functional Methods without Adjustable Parameters: The PBE0 Model. *J. Chem. Phys.* **1999,** *110*, 6158-6170.

49. Hay, P. J.; Wadt, W. R., Ab initio effective core potentials for molecular calculations. Potentials for K to Au including the outermost core orbitals. *J. Chem. Phys.* **1985,** *82* (1), 299-310.
50. Wadt, W. R.; Hay, P. J., Ab initio effective core potentials for molecular calculations. Potentials for main group elements Na to Bi. *J. Chem. Phys.* **1985,** *82* (1), 284-298.
51. Badaeva, E.; Feng, Y.; Gamelin, D. R.; Li, X., Investigation of Pure and Co^{2+}-Doped ZnO Quantum Dot Electronic Structures Using the Density Functional Theory: Choosing the Right Functional. *New J. Phys.* **2008,** *10*, 055013.
52. Nelson, H. D.; Li, X.; Gamelin, D. R., Computational Studies of the Electronic Structures of Copper-Doped CdSe Nanocrystals: Oxidation States, Jahn−Teller Distortions, Vibronic Bandshapes, and Singlet−Triplet Splittings. *J. Phys. Chem. C* **2016,** *120*, 5714-5723.
53. Huang, X.; Lindgren, E.; Chelikowsky, J. R., Surface Passivation Method for Semiconductor Nanostructures. *Phys. Rev. B* **2005,** *71*, 165328.
54. Wang, L.-W.; Li, J., First-Principles Thousand-Atom Quantum Dot Calculations. *Phys. Rev. B* **2004,** *69*, 153302.

Chapter 4: **Effects of Surface Chemistry on the Photophysics of Colloidal InP Nanocrystals**

Adapted from:

Hughes, K. E.; Stein, J. L.; Friedfeld, M. R.; Cossairt, B. M.; Gamelin, D. R. *In Preparation.*

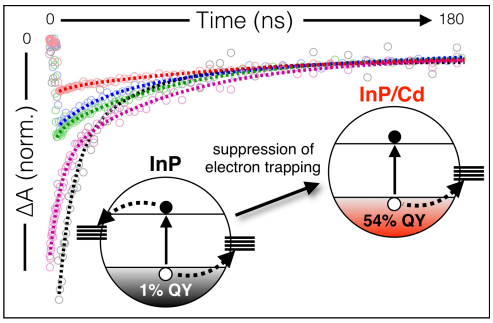

4.1 Overview

Indium Phosphide (InP) semiconductor nanocrystals (NCs) provide a promising alternative to traditional heavy-metal-based materials, and implementation of InP NCs into consumer products is rapidly increasing. However, as-synthesized InP NCs have very low photoluminescence quantum yields (PLQY). While empirical methods have led to NCs with near-unity PLQYs, a fundamental understanding of how specific synthetic and post-synthetic protocols alter the electronic landscape of InP NCs is lacking. Using a combination of room temperature and low temperature time-resolved spectroscopies, we studied a series of homologous InP NCs prepared from InP clusters to elucidate how specific charge-carrier trapping processes are affected when different surface treatments are performed. From the data we observe signatures of bright-dark excitonic splitting in our samples with only sub-monolayer coverage of select additives (divalent Lewis acids and fluoride)—a phenomenon that has only been previously demonstrated with thick-shelled samples. We also conclude that the PLQY increases observed for our samples occur through elimination of surface traps that specifically localize photoexcited electrons. However, hole trapping still exists. Together, these synthetic and spectroscopic results help move us one step closer to understanding how the experiments we perform in the wet lab directly affect the photophysical mechanisms of our materials so as to engineer targeted synthetic strategies to obtain InP NCs with the highest possible PLQYs.

4.2 Introduction

Colloidal semiconductor nanocrystals (NCs) are the subject of intense research for application in a variety of technologies including solar energy conversion, biological imaging, and solid-state lighting.[1] A hallmark of colloidal NCs is the tunability of absorption and photoluminescence (PL) energies as well as their ability to emit with narrow PL linewidths—both of which make such NCs attractive as downconversion phosphors for wide-color-gamut displays.[2] As incorporation of these materials into consumer products increases, however, environmental concerns over heavy-metal-based NCs have refocused research toward less toxic materials. Indium phosphide (InP) NCs are a proven alternative to traditional cadmium- and lead-based chalcogenide NCs. InP NCs are less toxic than traditional cadmium selenide (CdSe) NCs,[3-4] reducing environmental and health concerns. Their larger Bohr radius compared to CdSe also allows absorption and PL energies to be tuned across a wider spectral window,[5] which is of interest for display technologies. Despite these advantages, chemical issues still persist that must be addressed before InP becomes the material of choice for widespread industrial phosphor applications. In particular, as-synthesized InP NCs generally exhibit low (~1%) photoluminescence quantum yields (PLQYs), broad PL linewidths, and substantial trap luminescence because of numerous surface defects that introduce deep charge-carrier trap states.[6] Furthermore, even with substantial modification of the NC cores, they cover the desired color gamut less effectively and with lower internal quantum efficiencies than more-toxic CdSe NC emitters.

To improve the performance of colloidal InP NCs, it is necessary to develop synthetic procedures that can control their photophysics and suppress undesired carrier trapping. Unfortunately, little is known about the microscopic identities of carrier traps in InP NCs.[7-10] There is even little consensus about the relative importance of electron *vs* hole trapping in determining

the PLQYs of InP NCs; low PLQYs have been attributed to electron trapping at under-coordinated indium sites (*a.k.a.*, phosphorus vacancies),[7, 9] but also to hole trapping at under-coordinated phosphorus sites.[6, 11] High PLQYs have mainly been obtained by growing thick or gradient shells onto InP NC surfaces.[12-14] For example, a 95% PLQY was recently reported for InP/ZnSe/ZnS NCs.[13] Some reports have described increased InP NC PLQYs after etching with HF to remove surface traps.[15-18] From ultrafast spectroscopic studies of as-synthesized, HF-treated, and ZnS-shelled InP NCs, one study noted a lack of correlation between PLQY and transient absorption (TA) bleach recovery, pointing to a lack of electron trapping.[10] The presence of a rapid PL decay component (on a ~600 ps window) that was absent from the TA dynamics indicated rapid hole trapping, and growth of a ZnS shell was shown to eliminate this hole trapping.[10] Electron trapping at under-coordinated indium sites was concluded from optically detected magnetic resonance (ODMR) data showing a resonance broadened by hyperfine interactions with indium nuclei.[9] Clearly, a deeper fundamental understanding of the influence of surface chemistry on the PL of colloidal InP NCs will help to improve the quality and reliability of these materials for next-generation display and spectral-conversion technologies.

Here, we describe spectroscopic studies of a series of five homologous InP NC samples that collectively allow a systematic investigation into the effects of different surface chemistries on charge-carrier trapping, and hence on InP NC PLQYs. As-synthesized InP NCs made from InP clusters have indium-rich surfaces[19] and show low (~1%) PLQYs, consistent with under-coordinated surface indium ions acting as electron traps. Post-synthetic reaction with metal-carboxylates induces surface cation exchange[19] and vastly increases the PLQY (up to ~50%). Synthesizing the InP NCs in the presence of fluorinated ionic liquids yields surface In–F bonds[17] and increases the PLQY up to 20%, successfully replicating the results of HF etching.[20] Shell

growth also increases the PLQY.[12-14, 21] Variable-temperature (VT) PL and TA measurements reveal that the PLQY increases observed across this series of NC samples stems primarily from elimination of surface electron traps. Even with essentially complete suppression of electron trapping, the PLQY reaches only ~50%, and hole trapping is still observed. These results demonstrate that the PLQYs of these InP NCs depend quite substantially on both electron and hole trapping. Notably, VTPL measurements of InP NCs with sub-monolayer chemical modifications reveal clear signatures of exciton fine-structure splittings that in the past have only been observed after high-quality shell growth, highlighting the efficacy of such targeted surface modifications for reducing nonradiative carrier recombination losses in InP NCs. These findings advance our understanding of surface traps in colloidal InP NCs and contribute to the development of well-defined chemical tools for suppressing carrier trapping in these technologically important materials.

4.3 Methods

4.3.1. General Considerations. All glassware was dried in a 160 °C oven overnight prior to use. All reactions, unless otherwise noted, were performed under an inert atmosphere of nitrogen using a glovebox or using standard Schlenk techniques. Myristic acid (≥99%), indium acetate (99.99%), anhydrous acetonitrile, anhydrous ethanol, zinc stearate, sulfur powder (99.5% sublimed), and selenium powder (99.99%) were purchased from Sigma-Aldrich Chemical Co. and used without further purification. Diethyl zinc (95%) and dimethyl cadmium (97%) were purchased from Strem Chemicals and stored in a nitrogen atmosphere glovebox. Toluene purchased from Sigma-Aldrich Chemical Co. was collected from a solvent still and stored over activated 3 Å molecular sieves in a glovebox. 1-Octadecene (1-ODE, 90%) and trioctylphosphine

(TOP, 97%) were purchased from Sigma-Aldrich Chemical Co. and dried by being stirred overnight with CaH_2, distilled, and stored over activated 3 Å molecular sieves in a nitrogen atmosphere glovebox. Bio-Beads S-X1 for gel permeation chromatography were purchased from Bio-Rad Laboratories and dried under vacuum before being stored in a glovebox. Cadmium oleate was prepared from dimethyl cadmium and oleic acid using a literature procedure.[22] Zinc myristate was prepared from diethyl zinc and myristic acid using a modified literature procedure.[19]

4.3.2. Synthesis of InP NCs. First, myristate-capped InP clusters were synthesized following a modified preparation and stored as a solid in a nitrogen atmosphere glovebox.[23-24] InP clusters (180 mg) were dissolved in 2 mL of 1-ODE and loaded into a septum-capped syringe. In a 50 mL 3-neck round-bottom (RB) flask, 34 mL of 1-ODE was heated to 300 °C under a nitrogen atmosphere on a Schlenk line. While stirring vigorously, the cluster solution was removed from the glovebox and rapidly injected into the flask. Upon injection, the solution turned dark red and larger particle growth was monitored at 285 °C by UV-Vis spectroscopy until the absorbance maximum no longer red-shifted (approx. 12 min). The solution flask was cooled down by placing it in an oil bath. The 1-ODE was removed through distillation under reduced pressure. The resulting NC paste was transferred into a glovebox for purification and re-dissolved in a minimal amount of toluene. To remove residual 1-ODE, a single precipitation cycle was performed with acetonitrile as the non-solvent and centrifuge settings at 7000 rpm for 10 min. After removing the clear supernatant, the red pellet was dissolved in a minimal amount of toluene and purified by gel permeation chromatography. The resulting InP NC solution, free of excess ligand, was stored as a stock solution in toluene in the glovebox.

4.3.3. Preparation of InP/M NCs. InP/M NC samples were prepared following a modified procedure.[19] Using the InP NC stock solution, estimated to be 0.08 M In^{3+}, 1 mL (0.08 mmol In^{3+})

of solution was dried down and re-suspended in 1-ODE. To produce InP/Zn, zinc myristate (64 mg, 0.12 mmol Zn^{2+}) was suspended in 4 mL of 1-ODE and heated to 80 °C while stirring in a 15 mL 3-neck RB flask on the Schlenk line. The 1 mL solution of InP NCs was injected and heated to 200 °C. The reaction was halted after 2 hours following no further changes in the absorbance or photoluminescence features. Particle purification was performed in the same fashion as the InP NCs. To produce InP/Cd, the same steps were followed with cadmium oleate (28 mg, 0.04 mmol) instead of zinc myristate.

4.3.4. Preparations of InP/ZnSeS NCs. InP NCs were coated with a ZnSeS shell following a modified literature procedure as described by Lee et al.[21] First, TOP-Se and TOP-S 1 M solutions were prepared in the glovebox by dissolving selenium or sulfur powder in distilled TOP. Similar to the InP NC stock synthesis, a solution of InP NCs was prepared by injecting a solution of the myristate-capped InP clusters (20 mg, 0.045 mmol In^{3+}, dissolved in 1 mL 1-ODE) into 5 mL of 1-ODE at 300 °C. Particle growth was monitored at 285 °C and cooled down to 220 °C following no further changes by UV-Vis. Zinc stearate (285 mg, 0.45 mmol) was injected as a suspension in 1-ODE (2 mL) and held at 220 °C for 15 min. Then, a solution containing TOP-S (45 uL, 0.045 mmol) and TOP-Se (405 uL, 0.405 mmol) was injected and the temperature was raised to 300 °C and held for 60 minutes while monitoring the photoluminescence. After cooling down to room temperature, the solution was transferred into the glovebox and filtered with syringe filters (PTFE) and then the 1-ODE was removed by vacuum distillation. The resulting NC paste was purified with multiple precipitation cycles using toluene and ethanol as the solvent and non-solvent, respectively.

4.3.5. Synthesis of InP NCs Treated with Fluoride-Containing Ionic Liquid. Under a nitrogen atmosphere, 10 mL of 1-octadecene was added and the flask was heated to 290 °C. In a

glovebox, 0.068 g (0.004 mmol) of InP clusters and 0.382 g (1.503 mmol) of 1-hexyl-3-methylimidazolium tetrafluoroborate (hmim BF_4) was suspended in 2 mL of 1-octadecene. Note: the ionic liquid is immiscible in 1-octadecene at room temperature. The biphasic mixture was loaded into a plastic syringe and rapidly injected into the flask at 290 °C. The reaction vessel was stirred for 25 minutes after which the vessel was cooled to room temperature. The 1-octadecene was removed via vacuum distillation and the orange solid was dissolved in 5 mL toluene and precipitated by addition of acetonitrile (approximately 10 mL). The supernatant was removed via centrifugation and this process was repeated. The resulting solid was further purified via size-exclusion chromatography.[25]

4.3.6. Spectroscopic Measurements. Absorption and continuous-wave (CW) photoluminescence (PL) measurements of NC samples were conducted at room temperature in toluene. Absorption spectra were collected on a Cary 60 spectrophotometer (Varian). CW PL measurements were performed by exciting the colloidal NCs with a 405 nm laser diode and collecting the spectra using an OceanOptics 2000+ spectrometer. Transmission electron microscope (TEM) images were collected using a FEI Tecnai G2 F20 operating at 200 kV, and size distribution analysis was performed on 200–300 individual NCs per sample. PL quantum yield (PLQY) values were measured using an External Quantum Efficiency Measurement System with a Hamamatsu Integrating Sphere (C9920-12) and a Hamamatsu high-sensitivity photonic multichannel analyzer (C10027-01). Transient absorption (TA) measurements were performed using an EOS unit from Ultrafast Systems at University of Washington's Molecular Analysis Facility. The 800 nm output from a Coherent Libra amplified Ti:Sapphire laser (1 kHz repetition rate) was frequency-doubled using an OPA to excite the colloidal NCs in a 2 mm air-free cuvette with an average excitation power of ~5 μW measured through a 200 μm pinhole. The NCs were

stirred during the entirety of the experiment. The probe white-light was generated using an external q-switched Nd:YAG laser with an electronic delay. The collinear pump and probe beams overlapped at the sample. Room-temperature time-resolved photoluminescence measurements (TRPL) were performed by exciting the colloidal NCs with the frequency-doubled output of a Ti:Sapphire laser (400 nm, 150 fs pulse, power either 300 μW or ~30 μW, repetition rate either 1000 or 150 kHz). PL decay curves were recorded using a monochromator and streak camera (instrument response: ~25 ps). Variable-temperature (VT) TRPL measurements were performed on NC films fabricated by drop-casting colloidal NC solutions onto quartz discs, which were then placed in a closed-cooling Displex cryostat. NC films were excited using the third harmonic of the 1064 nm fundamental output from an Ekspla Nd:YAG laser with a 50 Hz repetition rate and an excitation energy of 1.3 μJ. The VT-TRPL dynamics and spectra were collected using a monochromator and streak camera (instrument response: ~20 ps).

4.4 Results and Analysis

4.3.1. Sample Preparation and General Characterization. Figure 4.1 presents TEM images of InP NCs (d = 2.7 ± 0.4 nm), InP/F NCs (d = 2.4 ± 0.3 nm), InP/Zn NCs (d = 2.7 ± 0.3 nm), and InP/Cd NCs (d = 2.7 ± 0.3 nm), all synthesized from carboxylate-ligated InP clusters. All of these NCs have quasi-spherical shapes and similar sizes, except the InP/F NCs, whose average NC diameter is slightly smaller than those of the others (2.4 *vs* 2.7 nm).

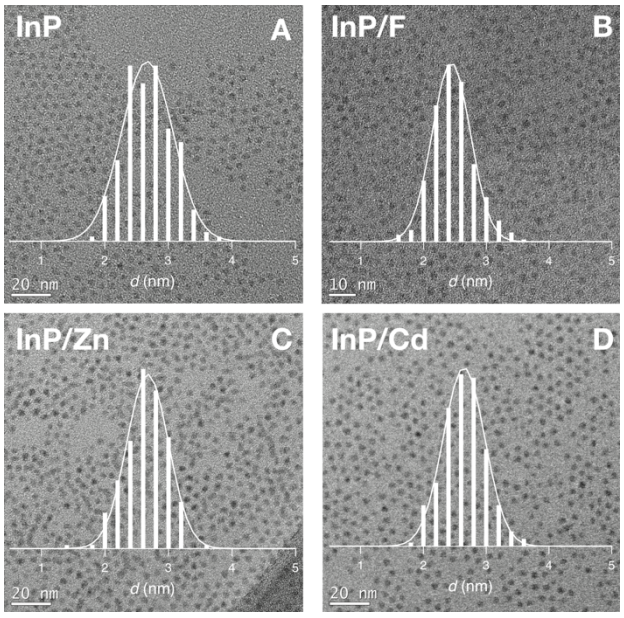

Figure 4.1. TEM images of selected InP NC samples. **(A)** InP NCs, $d = 2.7 \pm 0.4$ nm, **(B)** InP/F NCs, $d = 2.4 \pm 0.3$ nm, **(C)** InP/Zn NCs, $d = 2.7 \pm 0.3$ nm, and **(D)** InP/Cd NCs, $d = 2.7 \pm 0.3$ nm.

Figure 4.2 summarizes the absorption and continuous wave (CW) PL of the same series of NC samples shown in Figure 4.1, plus an additional InP/ZnSeS NC sample. The spectra are shown in order of increasing PLQY. The untreated InP NC sample shows a first excitonic absorption maximum at 2.24 eV and exhibits a low (< 1%) excitonic PLQY accompanied by broad trap emission to lower energy. Synthesis of the NCs in the presence of fluorinated ionic liquids (InP/F, see experimental section) increases the PLQY to 20%. The first excitonic absorption maximum is blue-shifted by ~180 meV to ~2.24 eV, and the trap PL is reduced relative to the excitonic PL. Annealing the as-prepared InP NCs in the presence of Zn-carboxylates forms InP/Zn NCs, which show a slight blue-shift of 60 meV, moving the first excitonic absorption maximum to ~2.3 eV. These NCs show an excitonic PLQY of 21%, and the low-energy trap PL is nearly indistinguishable from the baseline. Growth of a thin (~1.2 nm) ZnSeS shell on the as-prepared InP NCs broadens the first excitonic absorption maximum (centered at ~2.25 eV) and excitonic PL and increases the PLQY to 50%. Lastly, InP/Cd NCs synthesized by annealing InP NCs in the

presence of Cd-carboxylate show a first excitonic maximum that is red-shifted from that of the as-prepared InP NCs by ~120 meV (to 2.12 eV), and have a PLQY of 54%. The PL band appears to have an asymmetric shape, tailing to lower energies. These results demonstrate that InP NC surface modifications can dramatically increase PLQYs (<1% to 54%) and shift band-edge absorption by nearly 200 meV without significantly changing the NC size.

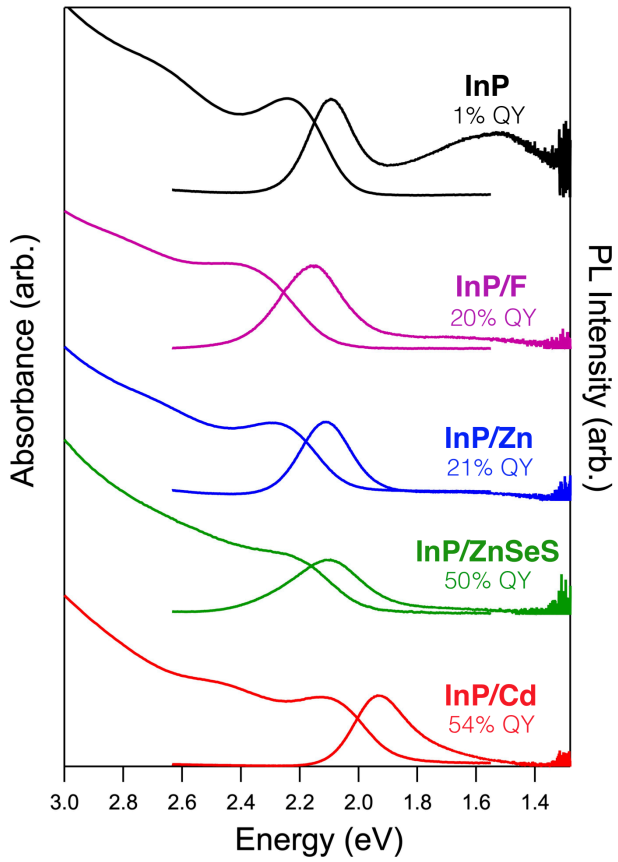

Figure 4.2. Absorption (left) and CW PL (right) of the InP NCs (black, 1% PLQY), InP/F NCs (fuchsia, 20% PLQY), InP/Zn NCs (blue, 21% PLQY), InP/ZnSeS NCs (green, 50% PLQY), and InP/Cd NCs (red, 54% PLQY) that were used in this study. All samples shown were made starting with InP clusters and were measured colloidally in toluene at room temperature. The NC size stays roughly the same, despite shifts of the first excitonic transition across the sample series.

4.3.2. Variable-Temperature Photoluminescence. Figure 4.3 shows variable-temperature (VT) PL data of InP NCs (Figure 4.3A, D), InP/F NCs (Figure 4.3B, E), and InP/Cd NCs (Figure 4.3C, F). Across the series of samples, the ratio of excitonic-to-trap PL intensities increases with

increasing sample PLQY. For all three samples, the excitonic PL shifts to lower energy and decreases in intensity with increasing temperature, as reported previously.[8, 26-28] The time-averaged PL intensities of all three samples also decrease with increasing temperature. Figures 4.3D, E, and F show excitonic PL decay dynamics measured as a function of temperature for the same series of NC samples. All three samples show multi-exponential (quasi-biexponential) decay at all temperatures. For each sample, the PL decay curves appear to converge to a similar slow decay time at all temperatures. At short times (0–3 ns), however, the InP/F and InP/Cd NCs (Figure 4.3E, F) both show fast decay components whose amplitudes *increase* with increasing temperature. This temperature dependence contrasts with that of the InP NCs (Figure 4.3D), whose excitonic PL intensity merely decreases with increasing temperature on all time scales. To the best of our knowledge, this trend at short times has not been noted previously. An increase in time-integrated excitonic PL intensity with increasing temperature has been reported for InP/ZnS core/shell NCs,[29] but this trend was not commented upon. The observation of increasing short-time excitonic PL intensities with increasing temperature is significant because it suggests that *radiative* recombination is accelerated at higher temperatures.

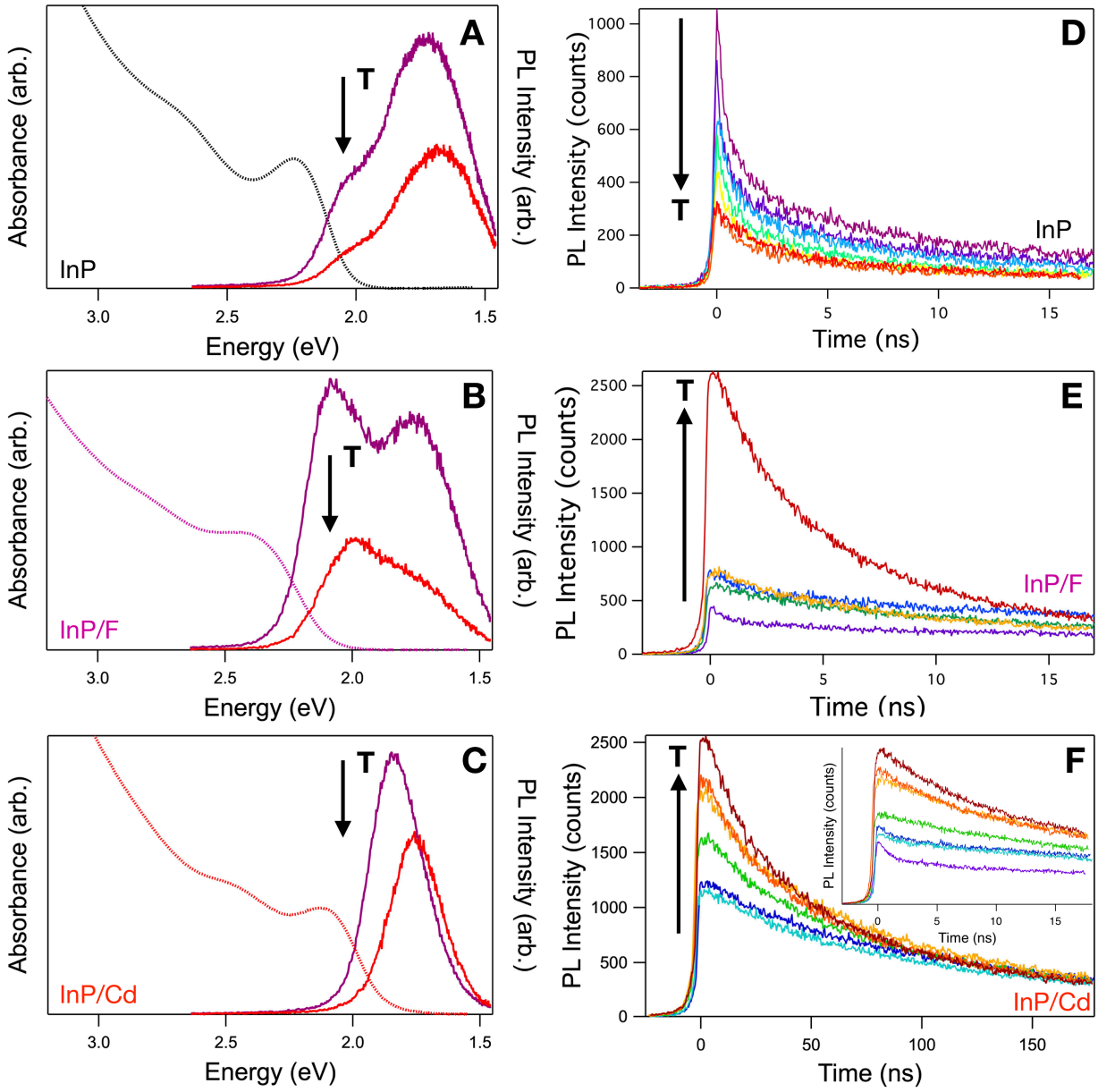

Figure 4.3. (A, B, C) Room-temperature absorption spectra (dotted), variable-temperature photoluminescence spectra (solid), and **(D, E, F)** variable-temperature excitonic PL decay dynamics measured for various InP NCs. Data were collected at temperatures between 24 and 300 K for **(A, D)** as-prepared InP NCs, **(B, E)** InP/F NCs, and **(C, F)** InP/Cd NCs. PL spectra were obtained by integrating streak-camera data over 1 μs. PL decay curves were obtained by integrating between ~2.15 eV and 2.00 eV for the InP NCs, between ~2.20 eV and 2.00 eV for the InP/F NCs, and between ~1.95 eV and 1.75 eV for the InP/Cd NCs.

To explore the anomalous temperature dependence observed in Figure 4.3, Figure 4.4A plots the integrated short-time (0–3 ns) excitonic PL intensities of each sample *versus* temperature. Whereas the InP PL intensity decreases with increasing temperature, the short-time excitonic PL

intensities of the InP/Cd and InP/F NCs both continue to increase with increasing temperature all the way up to room temperature. Figure 4.4B plots the weighted-average excitonic PL decay times for these three samples as a function of temperature (see SI for fitting). For the InP NCs, the average PL decay time increases slightly from ~5.5 ns at 25 K to ~8.0 ns at 240 K, but for the InP/F NCs the average PL decay time *decreases* from 80 ns at 33 K to ~20 ns at 300 K, and for the InP/Cd NCs it also decreases, from ~165 ns at 40 K to ~70 ns at 300 K. The decreasing PL decay times in Figure 4.4B combined with the increasing short-time PL intensities in Figure 4.4A support the conclusion that radiative recombination at short times accelerates with increasing temperature in these NCs. In the as-prepared InP NCs, this behavior is obscured by rapid nonradiative decay (PLQY < 1%), but in the InP/Cd and InP/F NCs where the PLQYs are greater, this trend in radiative decay rates becomes evident.

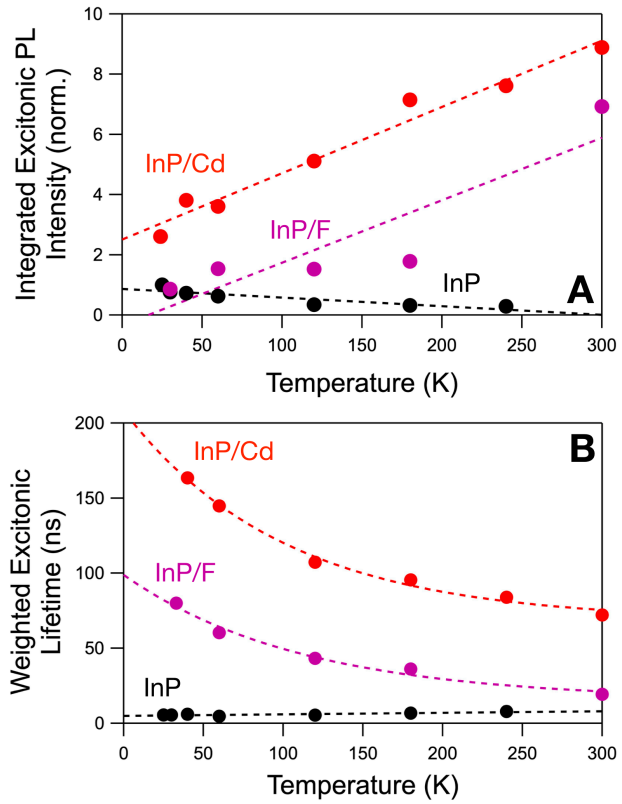

Figure 4.4. (A) Excitonic PL intensities integrated over short times (0–3 ns), plotted as a function of temperature for the InP NCs (black), InP/F NCs (fuchsia), and InP/Cd NCs (red) described by Figure 4.3. **(B)** Weighted average excitonic PL decay times plotted as a

function of temperature for the same three NC samples. The excitonic PL decay of the InP NCs slows slightly with increasing temperature, but the excitonic PL decay of the InP/F and InP/Cd NCs accelerates with increasing temperature. The dashed lines are guides to the eye.

4.3.3. Electron vs Hole Trapping. Figure 4.5 presents room-temperature TA bleach-recovery dynamics measured at the bleach maximum (see Figure 4.5 inset for TA spectra) and normalized at $t = 0$ for each of the NCs described by Figure C.3 (see Appendix C). For comparison, Figure 4.5 also plots excitonic and mid-gap trap-state PL decay dynamics for each sample (see Figure 4.3). The TA bleach-recovery curves have been inverted for comparison with the other dynamics data. The samples are presented in order of increasing PLQY to illustrate a general trend of slower dynamics within the first ~50 ns associated with higher PLQYs. Normalization at $t = 0$ also highlights a rough trend of increasing divergence between TA and excitonic TRPL decay curves at long times with increasing PLQY.

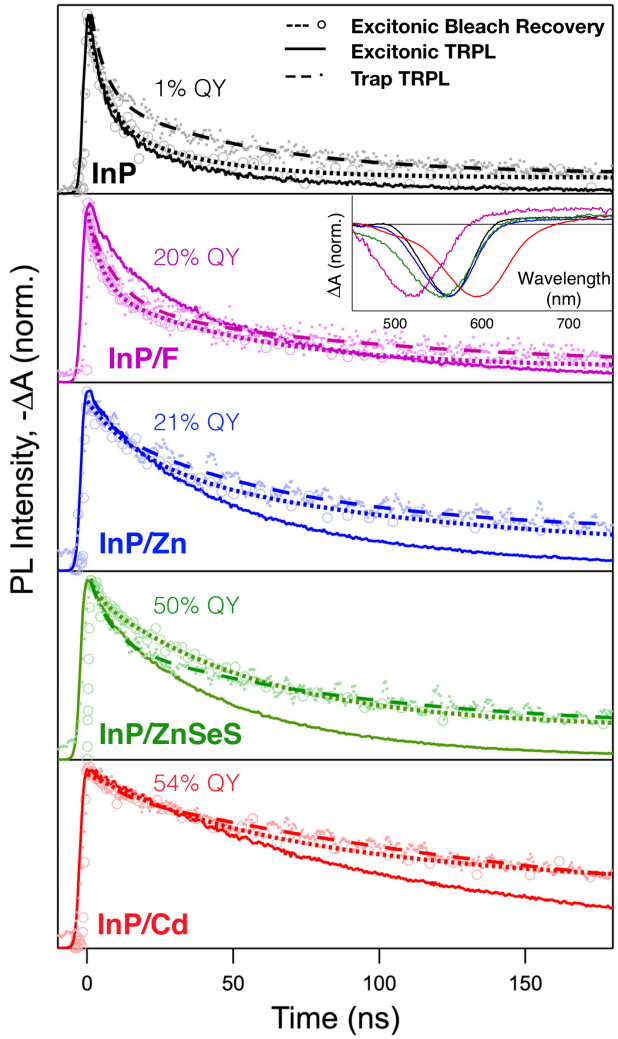

Figure 4.5. Normalized room-temperature excitonic TA bleach recovery (circles and short-dashed lines), excitonic TRPL decay (solid lines), and trap TRPL decay (dots and long-dashed lines) for all five InP NC samples, presented in order of increasing PLQY. All data were collected at room temperature on NCs suspended in toluene. The untreated InP NCs (black) show the fastest decay in all three measurements, as well as the lowest PLQY. The excitonic TRPL decays most quickly, with the greatest difference at long times seen for NCs with the highest PLQYs. Inset: normalized TA spectra for all five samples, following the same color scheme.

To interpret the trends in Figure 4.5, we take advantage of the different sensitivities of the TA and PL measurements to different types of charge carriers, as established previously[30-33] and summarized in Scheme 4.1: whereas excitonic TRPL reports on the dynamics of pairs of conduction-band (CB) electrons and valence-band (VB) holes (Scheme 4.1A), band-edge TA bleach-recovery dynamics are dominated by contributions from the CB electron population

(Scheme 4.1E, F), with the VB hole contributing less to the bleach amplitude because of the greater VB degeneracy.[30-31, 34] Trap-state PL dynamics can reflect either the CB electron or VB hole dynamics depending on the specific configuration of the luminescent excited state (Scheme 4.1J or K), or they can reflect neither in the scenario where both carriers are localized (Scheme 4.1L). Given these considerations, it is possible to deduce information about the photogenerated excited states from the comparison of TA and TRPL dynamics.

Scheme 4.1. Illustration of Charge-Carrier Processes Probed by Band-Edge TA, Excitonic TRPL, and Trap-State TRPL Measurements.

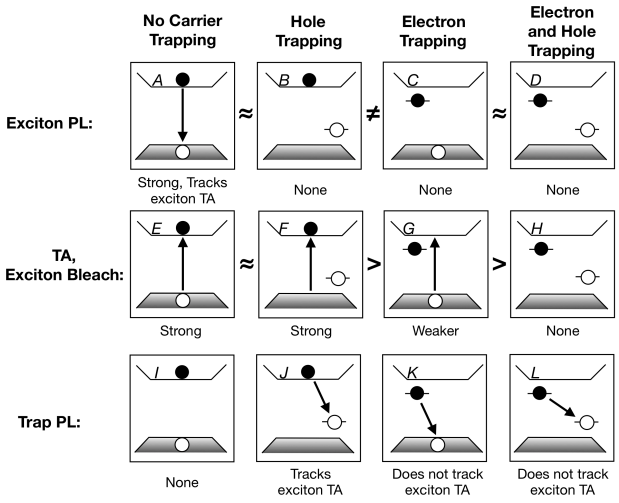

For the as-prepared InP NCs, the TA and excitonic TRPL signals in Figure 4.5 both decay with the same dominant time constant of $\tau \sim 7$ ns, and the trap-state PL follows much the same dynamics. From Scheme 4.1, we interpret this $\tau \sim 7$ ns process as trapping of CB electrons. The observation that the trap-state PL decays with the same $\tau \sim 7$ ns time constant supports assignment of this trap-state PL as involving recombination of a CB electron with a deeply trapped hole, and it further indicates that some extent of hole trapping occurs on timescales faster than our measurement window. This latter conclusion is consistent with previous reports of sub-nanosecond hole trapping in InP NCs.[10] The exciton PL decays to nearly zero with this $\tau \sim 7$ ns time constant, consistent with the low excitonic PLQY of these NCs being in part attributable to electron trapping,

but the TA bleach and the trap-state PL both show significant amplitudes (rel.) at long times, which also suggests a population of CB electrons that decays slowly *via* radiative recombination with deeply trapped holes (*i.e.*, by trap-state PL).

Moving down the NC series toward higher excitonic PLQYs, the key trends are (*i*) elimination of the $\tau \sim 7$ ns component in the exciton TA bleach and PL dynamics, and (*ii*) more prominent differences between excitonic PL and TA (or trap-state PL) amplitudes *at long times*. In the InP/Cd NCs, which have the highest excitonic PLQYs, the $\tau \sim 7$ ns decay component is almost completely absent, suggesting almost complete elimination of CB electron trapping. This trend suggests a correlation between the $\tau \sim 7$ ns process and the NC PLQY, and hence supports the conclusion that InP NC PLQYs are at least in part determined by CB electron-trapping dynamics.

To underscore this result, the TA bleach-recovery curves from Figure 4.5 are replotted in Figure 4.6A normalized at long times ($t > 120$ ns). The inset shows the same data normalized at $t = 0$. This representation of the data reveals a clear correlation between the TA amplitude at short times and the PLQY. To quantify this relationship, Figure 4.6B plots excitonic PLQY *vs* the normalized integrated intensity of the fast TA component for each sample, obtained by fitting each TA trace to a biexponential function and then integrating just the fast component (see SI for numerical results). Figure 4.6B reveals an inverse correlation between PLQY and the amount of fast TA bleach recovery. A qualitatively similar conclusion is reached without any fitting, by just plotting the *y* intercept of the data in Figure 4.6B *vs* PLQY (see SI). This correlation provides strong evidence that the surface modifications performed here help to increase NC PLQYs by suppressing CB electron trapping on the ~7 ns timescale. Interestingly, the best-fit line describing the InP, InP/F, InP/Zn, and InP/Cd NCs does not intercept the *y* axis at PLQY = 100%, but instead

it intercepts at PLQY ~ 50%. This observation suggests that elimination of electron traps alone in this series of NC samples can only increase their PLQYs to ~50% (± 4%). The remaining ~50% nonradiative decay is presumably attributable to hole trapping. These results suggest that it is possible to eliminate electron trapping almost entirely by simple surface modification with Cd^{2+}. To achieve unity PLQY, however, the remaining hole trapping must also be eliminated, but the Cd^{2+}, Zn^{2+}, and F^- surface modifications described here appear to have little influence on such trapping. All three modifications affect the surface cations but not surface anions (i.e., P^{3-}), either by reducing the number of surface In^{3+} or by formation of surface In-F bonds. Among the samples investigated here, only the InP/ZnSeS NCs also involve modification of the surface anions, burying surface phosphides to leave only sulfide and selenide at the surfaces. As such, it is tempting to interpret the comparison between InP/Zn and InP/ZnSeS NCs as attributable to additional suppression of hole trapping; both samples show similar PL losses to electron trapping, as gauged by their similar integrated fast TA decay, but the PLQY of the InP/ZnSeS NCs is more than double that of the InP/Zn NCs.

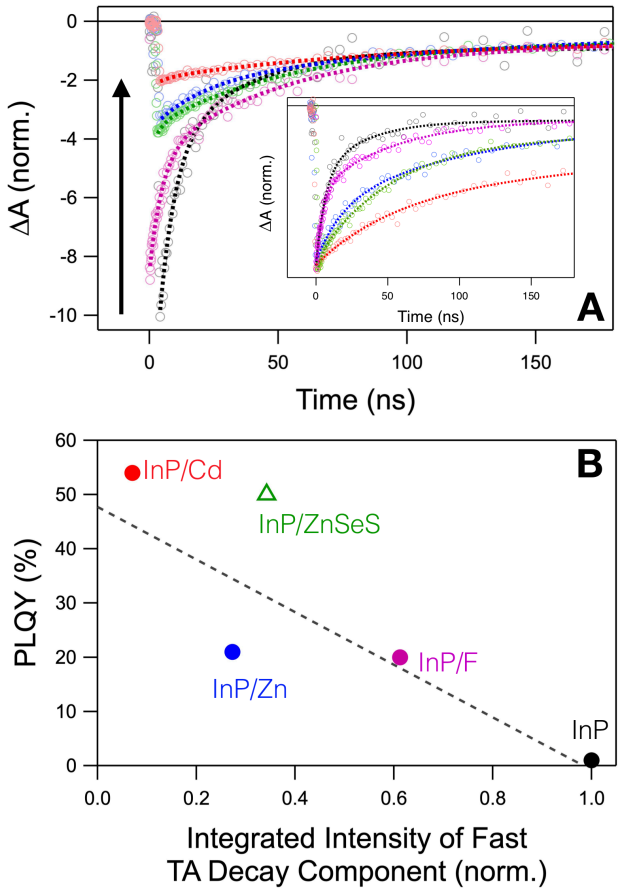

Figure 4.6. (A) Room-temperature TA exciton bleach-recovery dynamics normalized at *t* = 120 ns for all of the InP NC samples from Figure 4.5. The InP NCs (1% PLQY) show the most (rel.) bleach recovery at early times, and the InP/Cd NCs (54% PLQY) show the least. Inset: The same curves normalized at *t* = 0 ns. **(B)** Exciton PLQYs for InP, InP/F, InP/Zn, InP/Cd NCs (circles), and InP/ZnSeS NCs (open triangle), plotted as a function of the normalized integrated fast TA bleach recovery. *x*-axis values were obtained by fitting the TA bleach-recovery dynamics normalized at 120 ns to a bi-exponential function on a 200 ns time window and integrating the fast-decay component. The dashed line shows a best-fit line to the circular data points.

4.5 Discussion

For nearly two decades, intense research has been dedicated to the development of bright InP NCs with narrow PL linewidths and high PLQYs,[12-13, 17, 19-20, 35-37] largely motivated by the prospect of using such low-toxicity materials as spectral-conversion phosphors in current- and next-generation lighting and display technologies. Like many semiconductor NCs, InP NC surfaces are identified as the source of many non-radiative recombination losses. In most cases,

however, it has not been easy to connect synthetic improvements in NC PLQY with specific surface moieties or trapping processes, and consequently the major source(s) of nonradiative recombination remain poorly understood. Time-resolved spectroscopic evidence has pointed specifically to hole trapping as the primary limitation to high PLQYs in InP NCs,[10] but ODMR data suggests predominant electron trapping in such samples.[9] A recent study analyzed a combination of TA and TRPL dynamics from InP NCs.[10] This combination of probes can be used to disentangle the individual contributions from electron and hole trapping because of their different selectivity for the two carrier types. Based on the observation of rapid TRPL decay (~600 ps time-scale) without any corresponding excitonic TA bleach recovery, and the absence of any correlation between sample PLQY and TA decay rate over tens of nanoseconds, the authors concluded that hole trapping is solely responsible for the low PLQYs of InP NCs.

In the present study, we have sought to understand the effects of specific surface chemistries on carrier trapping in colloidal InP NCs. Using a series of closely related samples all prepared from InP clusters, we have demonstrated substantial increases in PLQY when the NC surfaces are modified not just by growth of ZnSeS shells, but also by simple binding of Cd^{2+}, Zn^{2+}, and F^{-} ions. With this series of related NCs in hand, TA and TRPL spectroscopies were then used to investigate specifically which carrier-recombination processes are affected by these surface modifications. The data from these experiments suggest that *both* electron and hole trapping contribute significantly to nonradiative decay in the parent InP NCs prior to surface modification. The data further show that electron trapping can be selectively suppressed and almost completely eliminated by simple surface modifications involving addition of Cd^{2+}, Zn^{2+}, or F^{-}. Elimination of electron trapping increases the NC PLQYs only up to ~50%, however, indicating that hole trapping is approximately equally substantial in the initial InP NCs. ZnSeS shell growth appears to partially

eliminate hole trapping as described previously,[10] but it does not eliminate electron-trapping sites as effectively as Cd^{2+} modification alone.

These trends are explained by the observation that all of the sample modifications examined here directly affect the NC surface cations; Cd^{2+} and Zn^{2+} replace surface-terminating In^{3+}, and the F^- modification leads to strong In-F bonds at the NC surfaces. All three modifications suppress electron trapping, consistent with such trapping involving surface In^{3+} cations. Shelling the NCs with ZnSeS appears to have all of the advantages of replacing surface In^{3+} with Zn^{2+}, and additionally partially suppresses hole trapping. The observation that Se/S anion termination of InP NC surfaces reduces hole trapping is consistent with such trapping involving surface phosphide moieties. These trends across the entire series of NC samples investigated here are summarized in Scheme 4.2.

Scheme 4.2. Illustration Depicting the Effect of Different Surface Chemistries on the Reduction of Electron Trapping in InP NCs

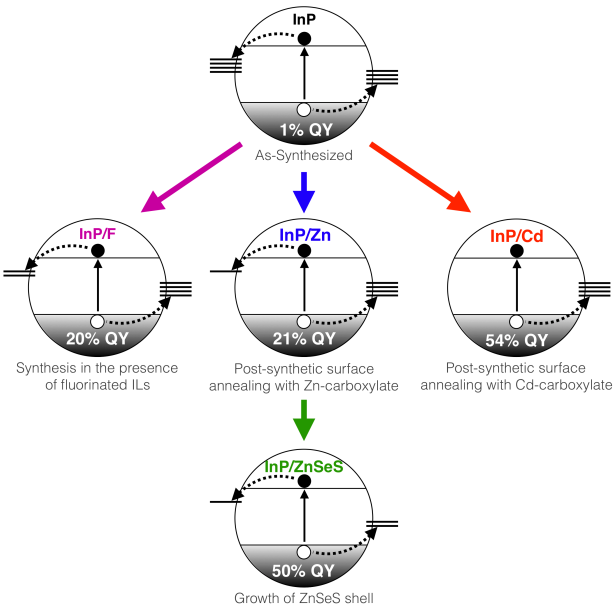

An interesting observation is that InP NC surfaces terminated by F^- are less prone to electron trapping than those terminated by ^-O_2CR. This observation suggests specifically that

undercoordinated In^{3+} serves as an electron-trapping site; F^- binds In^{3+} more strongly than carboxylates do while occupying only a single coordination site, reducing the probability of undercoordinated surface In^{3+}. This conclusion is consistent with the observation that addition of Cd^{2+} to the surfaces of InP NCs almost completely eliminates electron trapping, whereas parallel chemistry with Zn^{2+} is somewhat less effective, and both show far less electron trapping than the native InP NC surfaces. This trend can be understood by recognizing that each surface In^{3+} requires three anions for complete charge compensation. When one or two of these charge-compensating anions is a surface carboxylate, a high density of surface ligands is required to avoid undercoordinated In^{3+}, but such densities generate high steric pressures[38-39] that favor partial ligand dissociation. We hypothesize that this steric pressure is partially relieved when some surface carboxylates are replaced with much smaller F^- anions, but also when surface In^{3+} cations are replaced with divalent Cd^{2+} or Zn^{2+} cations that only require two anionic ligands for charge compensation. Relief of steric pressure allows better surface anion coordination and hence fewer electron-trapping sites. The difference between Cd^{2+} and Zn^{2+} is also intriguing. Cd^{2+} completely eliminates surface electron trapping, but Zn^{2+} does not. We have previously shown that Cd^{2+} binds the InP NC surface more strongly than Zn^{2+},[19, 25] and this difference may account for the greater ability of Cd^{2+} to eliminate surface electron traps.

Beyond their effect on PLQYs, the surface modifications described here also have interesting effects on other aspects of InP NC PL. For example, the data show that the energy of the NC's first excitonic transition can be tuned in either direction by post-synthetic surface annealing with divalent cations, as detailed previously.[19, 40] Less obvious is the observation that such sub-monolayer surface modification manifests itself in distinctive variable-temperature PL characteristics previously only associated with InP/ZnS[36, 41] and InP/ZnSe[42] core/shell NCs

involving relatively thick passivating shells. Specifically, the InP/Cd and InP/F NCs show the unusual combination of decreasing PL decay times but *increasing* short-time PL intensities with increasing temperature, a signature of thermal dark-bright exciton population equilibration. At low temperatures, the fast PL decay is due to emission from a higher-energy brighter state prior to relaxation into the lower-energy dark state, followed by slower emission from the forbidden dark state.[42] As the temperature is increased, the fast decay disappears and the lifetime of the slow component decreases due to thermal population of the bright state. This behavior is not observed in our InP NCs, most likely due to the dominance of fast non-radiative decay, and to our knowledge such behavior has not been observed previously in any unshelled InP NCs. It is noteworthy that this transformation with surface modification is only apparent from VTPL data collected in the time domain. CW VTPL data for the InP, InP/F, and InP/Cd NCs all show decreasing intensities with increasing temperature, consistent with the presence of thermally activated nonradiative decay in all three samples. Similar CW data have been reported elsewhere for unshelled InP NCs,[28] and in fact most VTPL studies have focused on time-averaged data of shelled InP NC samples,[13, 28-29, 33, 36, 41-44] but it is not possible to deduce any information about bright state population from such CW data. It is remarkable that the simple surface modifications described here can eliminate non-radiative recombination to a sufficient extent that these NCs behave photophysically similar to InP/ZnS and InP/ZnSe core/shell NCs.

4.6 Summary and Conclusions

In summary, we have synthesized a homologous series of NCs originating from InP clusters with which to study the effects of surface chemistry on charge-carrier trapping processes in InP NCs. When the surface cations are manipulated through cation exchange or termination with fluoride, our data indicate that PLQY increases occur as a result of specifically eliminating electron traps, but that both electron and hole trapping are roughly equally important in determining the sample PLQY. Both cation binding strength, which dictates surface coverage, and valency, which dictates obligate ligand density, are implicated as playing prominent roles in the efficacy of electron trap suppression. Elimination of electron trapping allows us to observe signatures of bright-dark excitonic splitting in samples with only sub-monolayer surface coverage, something that has never been reported before for un-shelled samples. A combination of TA and TRPL spectroscopy allows us to determine that there is still hole trapping in our samples, and it is likely that there is a theoretical PLQY maximum attainable by only addressing electron trapping (~50%). In order to achieve the highest possible PLQY, both electron and hole traps must be eliminated. Overall, the results presented here move us one step closer to fully addressing charge-carrier trapping in InP NCs by improving our fundamental knowledge, and therefore ability to create targeted synthetic strategies with which to deterministically obtain 100% PLQY InP NCs.

4.7 References

1. Talapin, D. V.; Lee, J.-S.; Kovalenko, M. V.; Shevchenko, E. V., Prospects of Colloidal Nanocrystals for Electronic and Optoelectronic Applications. *Chem. Rev.* **2010,** *110* (1), 389-458.
2. Shirasaki, Y.; Supran, G. J.; Bawendi, M. G.; Bulović, V., Emergence of colloidal quantum-dot light-emitting technologies. *Nat. Photonics* **2012,** *7*, 13.
3. Tarantini, A.; Wegner, K. D.; Dussert, F.; Sarret, G.; Beal, D.; Mattera, L.; Lincheneau, C.; Proux, O.; Truffier-Boutry, D.; Moriscot, C.; Gallet, B.; Jouneau, P. H.; Reiss, P.;

Carrière, M., Physicochemical alterations and toxicity of InP alloyed quantum dots aged in environmental conditions: A safer by design evaluation. *NanoImpact* **2019,** *14*, 100168.
4. Wegner, K. D.; Dussert, F.; Truffier-Boutry, D.; Benayad, A.; Beal, D.; Mattera, L.; Ling, W. L.; Carrière, M.; Reiss, P., Influence of the Core/Shell Structure of Indium Phosphide Based Quantum Dots on Their Photostability and Cytotoxicity. *Front. Chem.* **2019,** *7* (466).
5. Tamang, S.; Lincheneau, C.; Hermans, Y.; Jeong, S.; Reiss, P., Chemistry of InP Nanocrystal Syntheses. *Chem. Mater.* **2016,** *28* (8), 2491-2506.
6. Fu, H.; Zunger, A., InP quantum dots: Electronic structure, surface effects, and the redshifted emission. *Phys. Rev. B* **1997,** *56* (3), 1496-1508.
7. Mićić, O. I.; Nozik, A. J.; Lifshitz, E.; Rajh, T.; Poluektov, O. G.; Thurnauer, M. C., Electron and Hole Adducts Formed in Illuminated InP Colloidal Quantum Dots Studied by Electron Paramagnetic Resonance. *J.Phys.Chem. B* **2002,** *106* (17), 4390-4395.
8. Kim, S. H.; Wolters, R. H.; Heath, J. R., Photophysics of size-selected InP nanocrystals: Exciton recombination kinetics. *J. Chem. Phys.* **1996,** *105* (18), 7957-7963.
9. Langof, L.; Ehrenfreund, E.; Lifshitz, E.; Micic, O. I.; Nozik, A. J., Continuous-Wave and Time-Resolved Optically Detected Magnetic Resonance Studies of Nonetched/Etched InP Nanocrystals. *J. Phys. Chem. B* **2002,** *106* (7), 1606-1612.
10. Janke, E. M.; Williams, N. E.; She, C.; Zherebetskyy, D.; Hudson, M. H.; Wang, L.; Gosztola, D. J.; Schaller, R. D.; Lee, B.; Sun, C.; Engel, G. S.; Talapin, D. V., Origin of Broad Emission Spectra in InP Quantum Dots: Contributions from Structural and Electronic Disorder. *J. Am. Chem. Soc.* **2018,** *140* (46), 15791-15803.
11. Blackburn, J. L.; Ellingson, R. J.; Mićić, O. I.; Nozik, A. J., Electron Relaxation in Colloidal InP Quantum Dots with Photogenerated Excitons or Chemically Injected Electrons. *J. Phys. Chem. B* **2003,** *107* (1), 102-109.
12. Hahm, D.; Chang, J. H.; Jeong, B. G.; Park, P.; Kim, J.; Lee, S.; Choi, J.; Kim, W. D.; Rhee, S.; Lim, J.; Lee, D. C.; Lee, C.; Char, K.; Bae, W. K., Design Principle for Bright, Robust, and Color-Pure InP/ZnSexS1–x/ZnS Heterostructures. *Chem. Mater.* **2019**.
13. Kim, Y.; Ham, S.; Jang, H.; Min, J. H.; Chung, H.; Lee, J.; Kim, D.; Jang, E., Bright and Uniform Green Light Emitting InP/ZnSe/ZnS Quantum Dots for Wide Color Gamut Displays. *ACS Appl. Nano Mater.* **2019,** *2* (3), 1496-1504.
14. Kim, S.; Kim, T.; Kang, M.; Kwak, S. K.; Yoo, T. W.; Park, L. S.; Yang, I.; Hwang, S.; Lee, J. E.; Kim, S. K.; Kim, S.-W., Highly Luminescent InP/GaP/ZnS Nanocrystals and Their Application to White Light-Emitting Diodes. *J. Am. Chem. Soc.* **2012,** *134* (8), 3804-3809.
15. Mićić, O. I.; Cheong, H. M.; Fu, H.; Zunger, A.; Sprague, J. R.; Mascarenhas, A.; Nozik, A. J., Size-Dependent Spectroscopy of InP Quantum Dots. *J. Phys. Chem. B* **1997,** *101* (25), 4904-4912.
16. Talapin, D. V.; Gaponik, N.; Borchert, H.; Rogach, A. L.; Haase, M.; Weller, H., Etching of Colloidal InP Nanocrystals with Fluorides: Photochemical Nature of the Process Resulting in High Photoluminescence Efficiency. *J. Phys. Chem. B* **2002,** *106* (49), 12659-12663.
17. Kim, T.-G.; Zherebetskyy, D.; Bekenstein, Y.; Oh, M. H.; Wang, L.-W.; Jang, E.; Alivisatos, A. P., Trap Passivation in Indium-Based Quantum Dots through Surface Fluorination: Mechanism and Applications. *ACS Nano* **2018,** *12* (11), 11529-11540.
18. Mićić, O. I.; Sprague, J.; Lu, Z.; Nozik, A. J., Highly efficient band-edge emission from InP quantum dots. *Appl. Phys. Lett.* **1996,** *68* (22), 3150-3152.

19. Stein, J. L.; Mader, E. A.; Cossairt, B. M., Luminescent InP Quantum Dots with Tunable Emission by Post-Synthetic Modification with Lewis Acids. *J. Phys. Chem. Lett.* **2016,** *7* (7), 1315-1320.
20. Siramdas, R.; McLaurin, E. J., InP Nanocrystals with Color-Tunable Luminescence by Microwave-Assisted Ionic-Liquid Etching. *Chem. Mater.* **2017,** *29* (5), 2101-2109.
21. Lim, J.; Bae, W. K.; Lee, D.; Nam, M. K.; Jung, J.; Lee, C.; Char, K.; Lee, S., InP@ZnSeS, Core@Composition Gradient Shell Quantum Dots with Enhanced Stability. *Chem. Mater.* **2011,** *23* (20), 4459-4463.
22. Stein, J. L.; Steimle, M. I.; Terban, M. W.; Petrone, A.; Billinge, S. J. L.; Li, X.; Cossairt, B. M., Cation Exchange Induced Transformation of InP Magic-Sized Clusters. *Chem. Mater.* **2017,** *29* (18), 7984-7992.
23. Gary, D. C.; Terban, M. W.; Billinge, S. J. L.; Cossairt, B. M., Two-Step Nucleation and Growth of InP Quantum Dots via Magic-Sized Cluster Intermediates. *Chem. Mater.* **2015,** *27* (4), 1432-1441.
24. Park, N.; Monahan, M.; Ritchhart, A.; Friedfeld, M. R.; Cossairt, B. M., Synthesis of In37P20(O2CR)51 Clusters and Their Conversion to InP Quantum Dots. *J. Vis. Exp.* **2019,** (147), e59425.
25. Roberge, A.; Stein, J. L.; Shen, Y.; Cossairt, B. M.; Greytak, A. B., Purification and In Situ Ligand Exchange of Metal-Carboxylate-Treated Fluorescent InP Quantum Dots via Gel Permeation Chromatography. *J. Phys. Chem. Lett.* **2017,** *8* (17), 4055-4060.
26. Jing, P.; Zheng, J.; Ikezawa, M.; Liu, X.; Lv, S.; Kong, X.; Zhao, J.; Masumoto, Y., Temperature-Dependent Photoluminescence of CdSe-Core CdS/CdZnS/ZnS-Multishell Quantum Dots. *J. Phys. Chem. C* **2009,** *113* (31), 13545-13550.
27. Cho, E.; Kim, T.; Choi, S.-m.; Jang, H.; Min, K.; Jang, E., Optical Characteristics of the Surface Defects in InP Colloidal Quantum Dots for Highly Efficient Light-Emitting Applications. *ACS Appl. Nano Mater.* **2018,** *1* (12), 7106-7114.
28. Savchenko, S. S.; Vokhmintsev, A. S.; Weinstein, I. A., Effect of temperature on the spectral properties of InP/ZnS nanocrystals. *Journal of Physics: Conference Series* **2018,** *961*, 012003.
29. Narayanaswamy, A.; Feiner, L. F.; Meijerink, A.; van der Zaag, P. J., The Effect of Temperature and Dot Size on the Spectral Properties of Colloidal InP/ZnS Core−Shell Quantum Dots. *ACS Nano* **2009,** *3* (9), 2539-2546.
30. Ellingson, R. J.; Blackburn, J. L.; Yu, P.; Rumbles, G.; Mićić, O. I.; Nozik, A. J., Excitation Energy Dependent Efficiency of Charge Carrier Relaxation and Photoluminescence in Colloidal InP Quantum Dots. *J. Phys Chem. B* **2002,** *106* (32), 7758-7765.
31. Thomas, A.; Sandeep, K.; Somasundaran, S. M.; Thomas, K. G., How Trap States Affect Charge Carrier Dynamics of CdSe and InP Quantum Dots: Visualization through Complexation with Viologen. *ACS Energy Lett.* **2018,** *3* (10), 2368-2375.
32. Hunsche, S.; Dekorsy, T.; Klimov, V.; Kurz, H., Ultrafast dynamics of carrier-induced absorption changes in highly-excited CdSe nanocrystals. *Appl. Phys. B* **1996,** *62* (1), 3-10.
33. Rowland, C. E.; Liu, W.; Hannah, D. C.; Chan, M. K. Y.; Talapin, D. V.; Schaller, R. D., Thermal Stability of Colloidal InP Nanocrystals: Small Inorganic Ligands Boost High-Temperature Photoluminescence. *ACS Nano* **2014,** *8* (1), 977-985.
34. Klimov, V. I.; McBranch, D. W.; Leatherdale, C. A.; Bawendi, M. G., Electron and hole relaxation pathways in semiconductor quantum dots. *Phys. Rev. B* **1999,** *60* (19), 13740-13749.

35. Dennis, A. M.; Mangum, B. D.; Piryatinski, A.; Park, Y.-S.; Hannah, D. C.; Casson, J. L.; Williams, D. J.; Schaller, R. D.; Htoon, H.; Hollingsworth, J. A., Suppressed Blinking and Auger Recombination in Near-Infrared Type-II InP/CdS Nanocrystal Quantum Dots. *Nano Lett.* **2012,** *12* (11), 5545-5551.
36. Biadala, L.; Siebers, B.; Beyazit, Y.; Tessier, M. D.; Dupont, D.; Hens, Z.; Yakovlev, D. R.; Bayer, M., Band-Edge Exciton Fine Structure and Recombination Dynamics in InP/ZnS Colloidal Nanocrystals. *ACS Nano* **2016,** *10* (3), 3356-3364.
37. Chandrasekaran, V.; Tessier, M. D.; Dupont, D.; Geiregat, P.; Hens, Z.; Brainis, E., Nearly Blinking-Free, High-Purity Single-Photon Emission by Colloidal InP/ZnSe Quantum Dots. *Nano Lett.* **2017,** *17* (10), 6104-6109.
38. Gary, D. C.; Flowers, S. E.; Kaminsky, W.; Petrone, A.; Li, X.; Cossairt, B. M., Single-Crystal and Electronic Structure of a 1.3 nm Indium Phosphide Nanocluster. *J. Am. Chem. Soc.* **2016,** *138* (5), 1510-1513.
39. Cossairt, B. M., Shining Light on Indium Phosphide Quantum Dots: Understanding the Interplay among Precursor Conversion, Nucleation, and Growth. *Chem. Mater.* **2016,** *28* (20), 7181-7189.
40. Kirkwood, N.; Monchen, J. O. V.; Crisp, R. W.; Grimaldi, G.; Bergstein, H. A. C.; du Fossé, I.; van der Stam, W.; Infante, I.; Houtepen, A. J., Finding and Fixing Traps in II–VI and III–V Colloidal Quantum Dots: The Importance of Z-Type Ligand Passivation. *J. Am. Chem. Soc.* **2018,** *140* (46), 15712-15723.
41. Shirazi, R.; Kopylov, O.; Kovacs, A.; Kardynał, B. E., Temperature dependent recombination dynamics in InP/ZnS colloidal nanocrystals. *Appl. Phys. Lett.* **2012,** *101* (9), 091910.
42. Brodu, A.; Ballottin, M. V.; Buhot, J.; van Harten, E. J.; Dupont, D.; La Porta, A.; Prins, P. T.; Tessier, M. D.; Versteegh, M. A. M.; Zwiller, V.; Bals, S.; Hens, Z.; Rabouw, F. T.; Christianen, P. C. M.; de Mello Donega, C.; Vanmaekelbergh, D., Exciton Fine Structure and Lattice Dynamics in InP/ZnSe Core/Shell Quantum Dots. *ACS Photonics* **2018,** *5* (8), 3353-3362.
43. Pham, T. T.; Chi Tran, T. K.; Nguyen, Q. L., Temperature-dependent photoluminescence study of InP/ZnS quantum dots. *Advances in Natural Sciences: Nanoscience and Nanotechnology* **2011,** *2* (2), 025001.
44. Narayanaswamy, A.; Feiner, L. F.; van der Zaag, P. J., Temperature Dependence of the Photoluminescence of InP/ZnS Quantum Dots. *J. Phys. Chem. C* **2008,** *112* (17), 6775-6780.

Appendix A: ***Supplementary Information for Chapter 2***
Photodoping and Transient Spectroscopies of Copper-Doped CdSe/CdS Nanocrystals

Reprinted with permission from:
Hughes, K. E.; Hartstein, K. H., Gamelin, D. R. *ACS Nano* **2018**, *12*, 718–728.

A.1 Chemicals

Cadmium Oxide (CdO; 99.5%), oleic acid (OA; 90%), 1-octadecene (ODE; 90%), hexadecylamine (HDA; 90%), trioctylphosphine oxide (TOPO; 99%), selenium (99.99%), 1-octanethiol (≥98.5%), and copper iodide (CuI; 98%) were purchased from Aldrich. Trioctylphosphine (TOP; 97%) was purchased from STREM. All chemicals were used as received.

A.2 Continuous-Wave Absorption and Photoluminescence Measurements

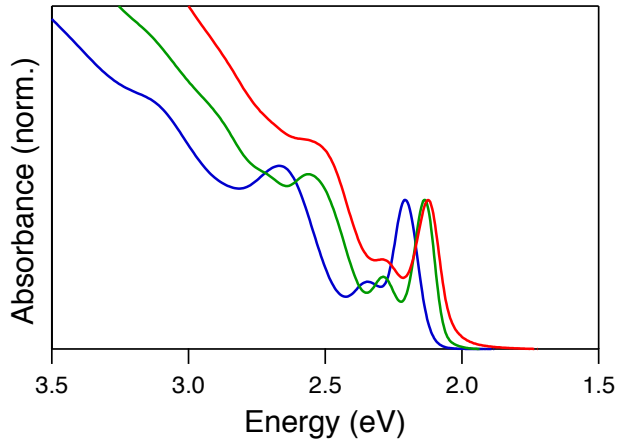

Figure A.1. Absorption spectra of CdSe (blue), CdSe/CdS core/shell (green), and Cu^{+}:CdSe/CdS (red) NCs in toluene.

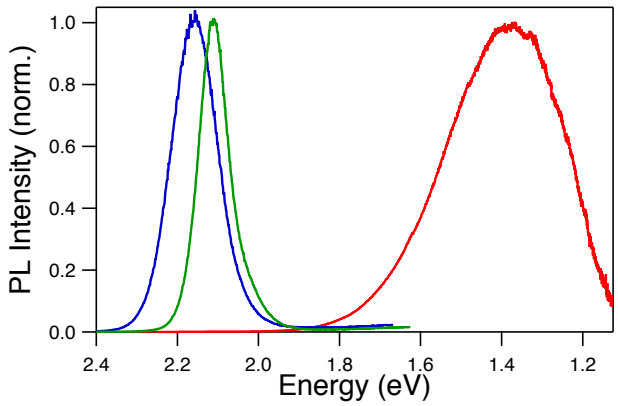

Figure A.2. Room-temperature PL spectra of CdSe (blue), CdSe/CdS (green), and Cu^{+}:CdSe/CdS (red) NCs show the large effective Stokes shift of the PL when copper is added to the NC lattice.

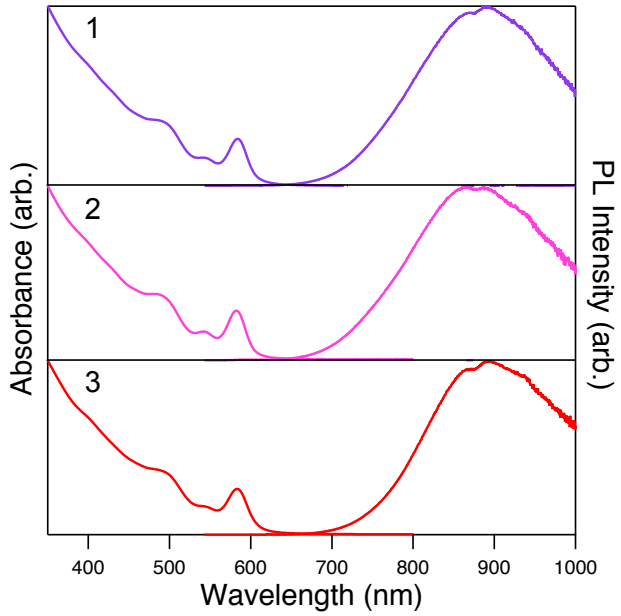

Figure A.3. Electronic absorption spectra of the three different samples of Cu^{+}:CdSe/CdS NCs used in the experiments presented here. The absorption and PL spectra of sample 1 are shown in Figure 2.2 of the main text. The same spectroscopic features were observed for all copper-doped core/shell NC samples.

A.3 TEM Characterization

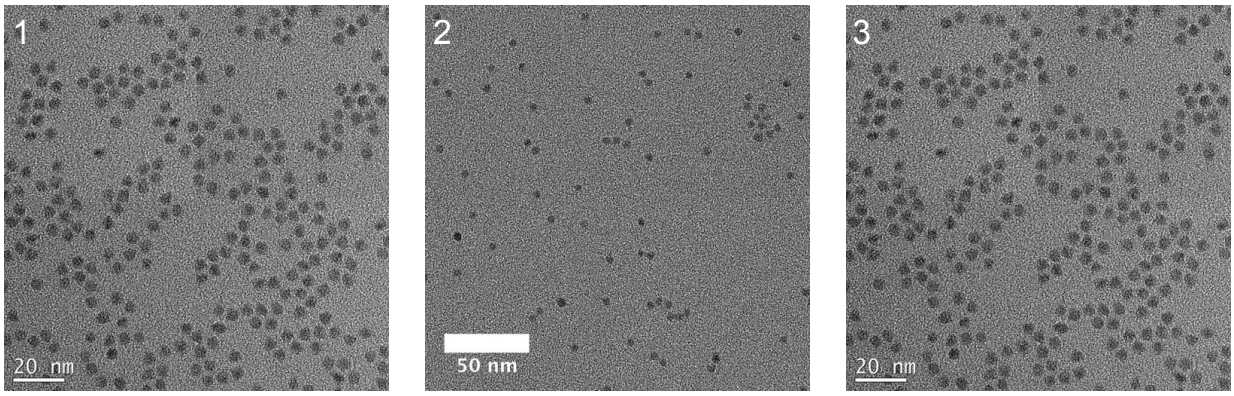

Figure A.4. TEM images of the same three Cu^{+}:CdSe/CdS NC samples described in Figure A3. The NCs have average diameters of (1) 5.3 nm ± 0.4 nm, (2) 5.5 ± 0.3 nm, and (3) 5.0 nm ± 0.3 nm. The TEM image of sample 1 is the one shown in the main text.

A.4 Transient Absorption and Time-Resolved Photoluminescence Measurements

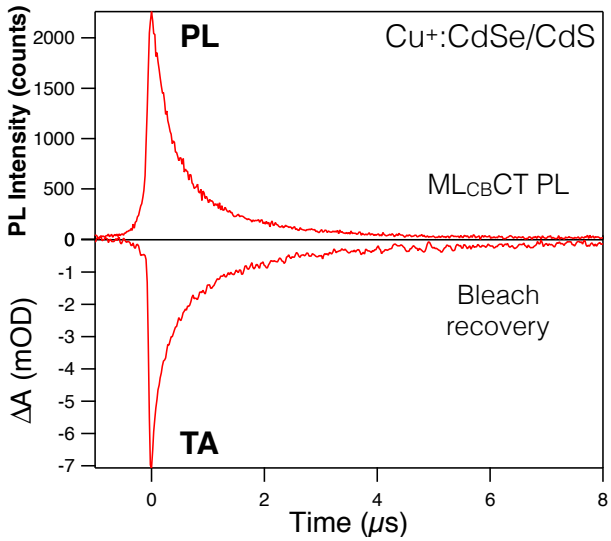

Figure A.5. TRPL decay (top, integrated between 740 and 830 nm) and TA bleach-recovery (bottom, integrated between 570 and 580 nm) dynamics for sample 2 of the Cu^{+}:CdSe/CdS NCs from Figure A3. Both curves show similar decay times of ~675 ns.

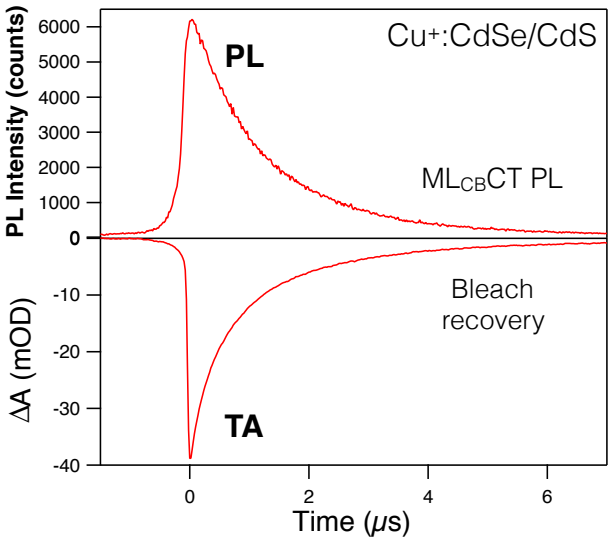

Figure A.6. TRPL decay (top, integrated between 700 and 870 nm) and TA bleach recovery (bottom, integrated between 580 and 585 nm) dynamics for sample 3 of the Cu^{+}:CdSe/CdS NCs from Figure A3. Both curves show similar time constants of ~1.25 µs.

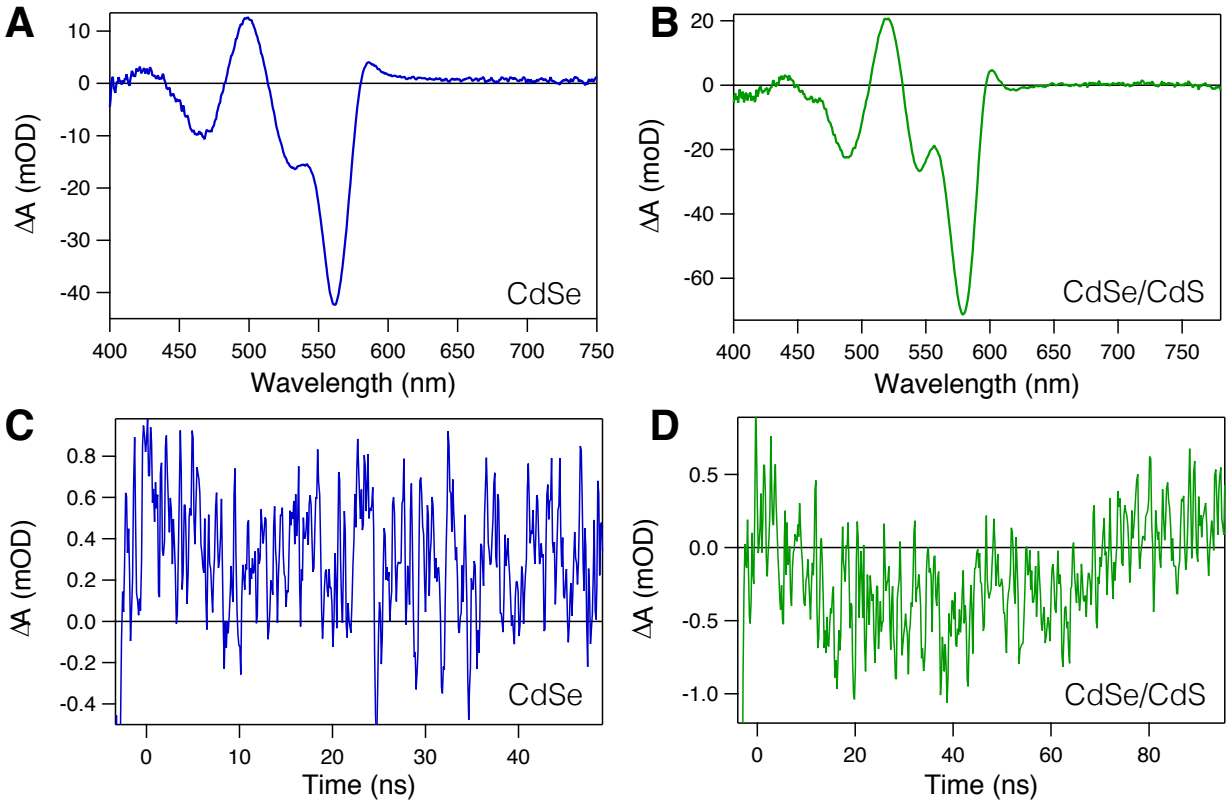

Figure A.7. Transient-absorption data for CdSe and CdSe/CdS NCs. **(A)** TA spectrum of CdSe NCs. **(B)** TA spectrum of CdSe/CdS NCs. **(C)** TA dynamics for CdSe NCs integrated between 700 and 750 nm, showing the absence of a time-dependent signal in this region. **(D)** TA dynamics for CdSe/CdS NCs integrated between 700 and 750 nm, showing the absence of a time-dependent signal. These limits of integration were chosen to allow comparison with the TA dynamics collected for the Cu^{+}:CdSe/CdS NCs described in the main text, where a photoinduced TA signal is observed.

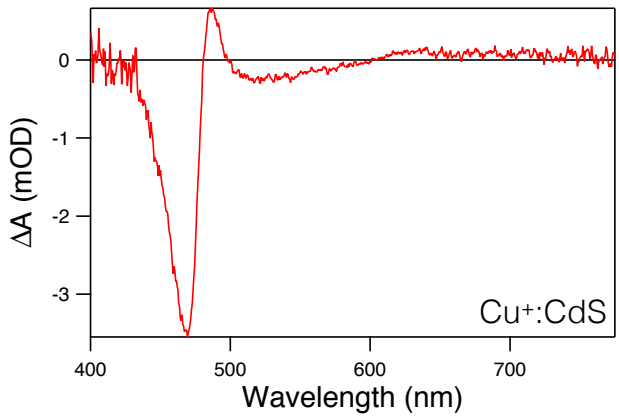

Figure A.8. Transient absorption spectrum collected for Cu^{+}:CdS NCs. The spectrum is similar to those observed for Cu^{+}:CdSe/CdS NCs, but here the positive intensity at the red edge of the first-exciton's bleach is clearly evident.

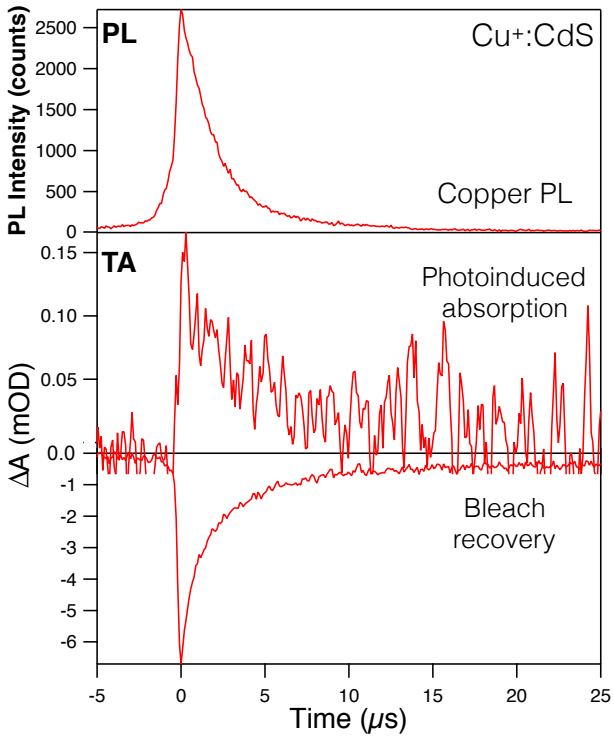

Figure A.9. TRPL decay (top, integrated between 630 and 715 nm) and TA dynamics (middle, integrated between 630 and 715 nm, and bottom, integrated between 460 and 475 nm) for the Cu^{+}:CdS NCs of Figure A8. All three curves show similar time constants of ~2.3 µs.

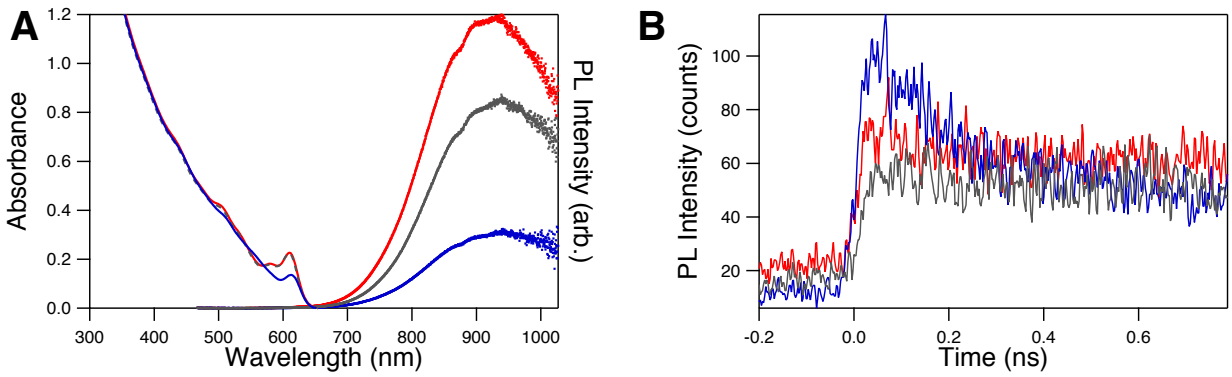

Figure A.10. (A) Absorption (left) and PL (right) spectra of Cu^{+}:CdSe/CdS NCs collected before (red) and after (blue) photodoping to an average of $\langle n \rangle = 0.8$, as seen by the bleach in the absorption of the first excitonic maximum and the decrease in $ML_{CB}CT$ PL intensity (see main text, Figure 2.8). The grey trace shows the absorption and PL after the photodoped NCs are reoxidized in air. The absorption spectrum recovers completely upon reoxidation but the PL intensity is smaller, attributed to surface modifications during the photodoping/reoxidation cycle. **(B)** TRPL dynamics measured on a 1 ns window for the samples in panel (A). The change in PL intensity between the initial and reoxidized data is attributed to surface modifications during the photodoping/reoxidation cycle.

Appendix B: ***Supplementary Information for Chapter 3***
Copper's Role in the Photoluminescence of $Ag_{1-x}Cu_xInS_2$ Nanocrystals, from Copper-Doped $AgInS_2$ ($x \sim 0$) to $CuInS_2$ ($x = 1$)

Reprinted with permission from:
Hughes, K. E.; Ostheller, S. R.; Nelson, H. D.; Gamelin, D. R. *Nano Lett.* **2019**, *19*, 1318–1325.

B.1. TEM Characterization

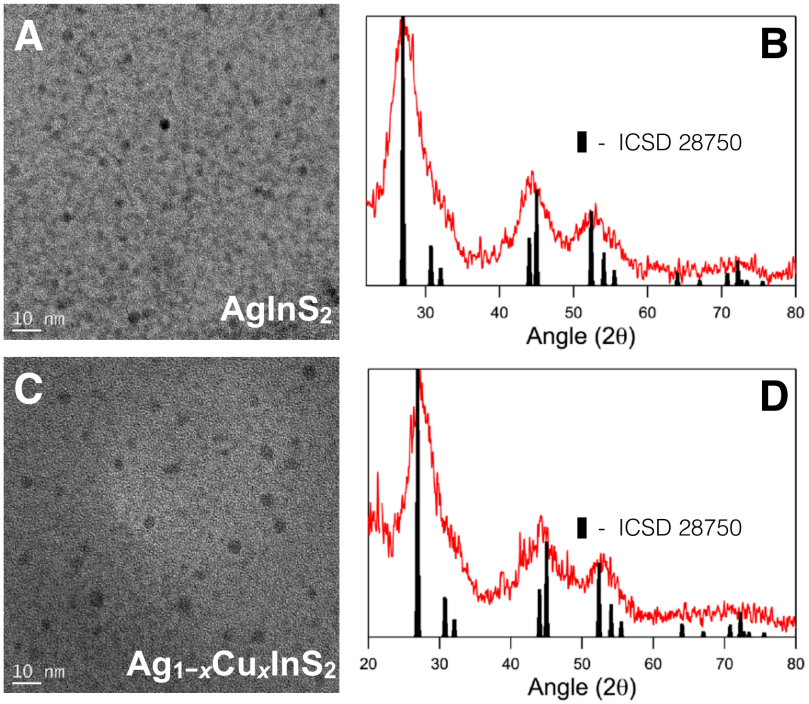

Figure B.1. (A) TEM image of representative $AgInS_2$ NCs. The average diameter of these NCs is $d = 3.9 \pm 0.4$ nm. **(B)** X-ray diffraction data collected for the same $AgInS_2$ NCs shown in panel A. **(C)** TEM image of the same NCs shown in panel A after partial cation exchange with copper to form $Ag_{1-x}Cu_xInS_2$ NCs ($x = 0.04$, $d = 3.9 \pm 0.5$ nm). **(D)** X-ray diffraction pattern of the same $Ag_{1-x}Cu_xInS_2$ NCs as shown in C. For reference, the black lines in B and D show the X-ray diffraction pattern for the $AgInS_2$ chalcopyrite crystal structure.

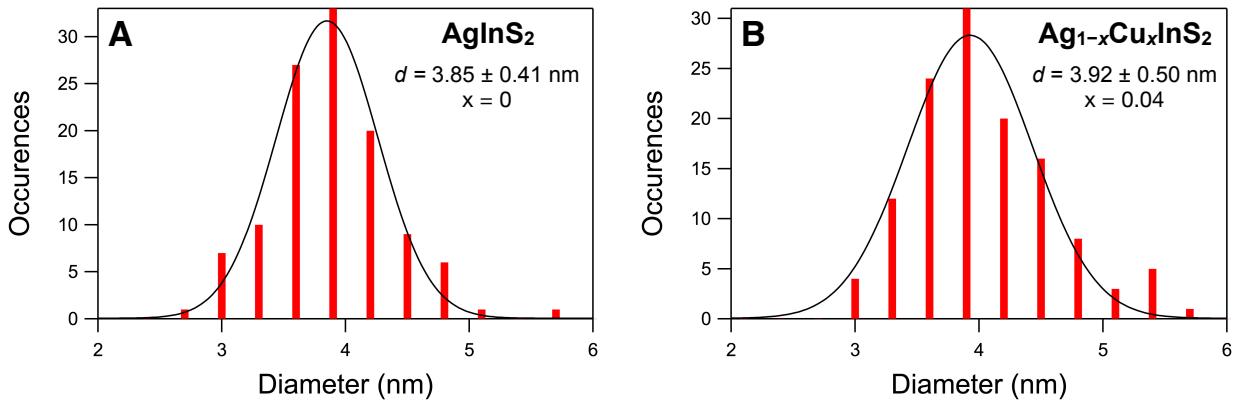

Figure B.2. TEM size histograms for the **(A)** $AgInS_2$ NCs and **(B)** $Ag_{1-x}Cu_xInS_2$ NCs (x = 0.04) from Figure B1. TEM size distribution analysis was performed on ~115 NCs for each sample.

B.2 Monte Carlo Simulations

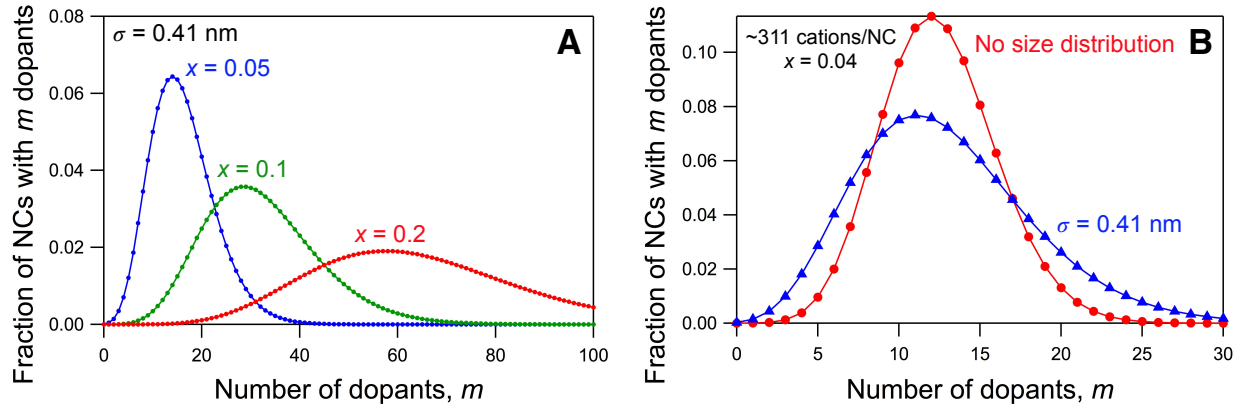

Figure B.3. Poissonian statistics calculated for $Ag_{1-x}Cu_xInS_2$ NCs (d = 3.85 nm, ~311 cations/NC).[1] **(A)** Statistical distribution showing the fraction of $Ag_{1-x}Cu_xInS_2$ NCs with m dopants where x = 0.05 (blue), x = 0.1 (green), and x = 0.2 (red). Calculations include the size distribution determined from TEM (σ = 0.41 nm). **(B)** Statistical distribution showing the fraction of $Ag_{0.96}Cu_{0.04}InS_2$ NCs with m dopants without (red) and with (blue) the size distribution from TEM. The two calculations give similar results.

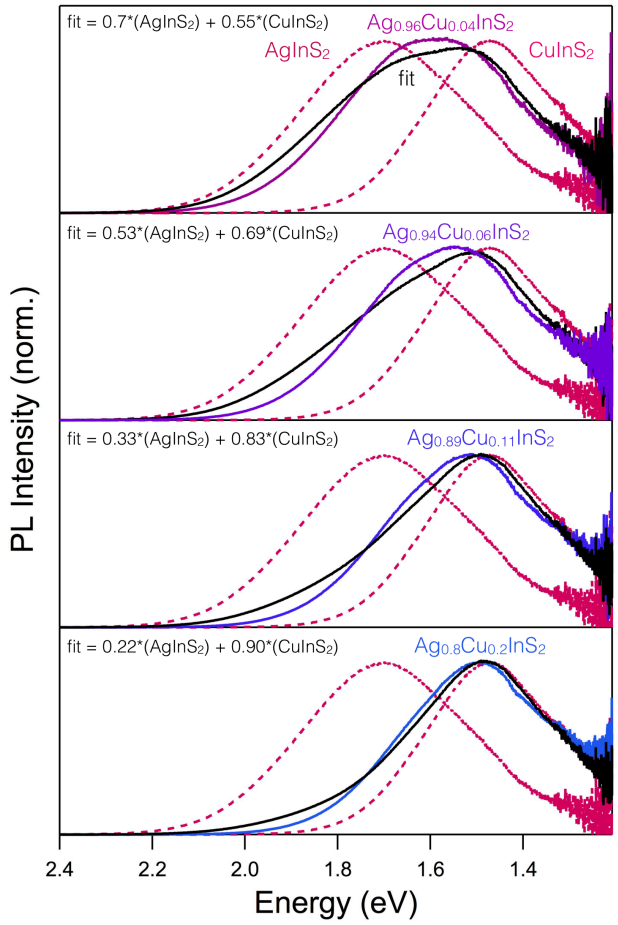

Figure B.4. Simulations of experimental $Ag_{1-x}Cu_xInS_2$ NC PL spectra from Figure 3.2 of the main text, showing that the experimental $Ag_{1-x}Cu_xInS_2$ NC PL spectra are not described well simply as linear combinations of the two endpoint spectra. Each experimental spectrum is simulated as a least-squares fitted linear combination of $x = 0$ ($AgInS_2$, left) and $x = 0.88$ (~$CuInS_2$, right) spectra, also from Figure 3.2. The dashed traces show the end-point spectra (the same in all panels), the colored solid curves show the experimental $Ag_{1-x}Cu_xInS_2$ NC PL spectra, and the black solid curves show the least-squares linear-combination fits. The best-fit amplitudes are shown in each panel. These simulations all show poor reproduction of the experimental PL spectra at high energies and near the PL maxima.

B.3 References

1. Bradshaw, L. R.; May, J. W.; Dempsey, J. L.; Li, X.; Gamelin, D. R., Ferromagnetic Excited-State Mn2+ Dimers in Zn1-xMnxSe Quantum Dots Observed by Time-Resolved Magnetophotoluminescence. *Phys. Rev. B* **2014,** *89* (11), 115312.

Appendix C: ***Supplementary Information for Chapter 4***
Effects of Surface Chemistry on the Photophysics of Colloidal InP Nanocrystals

Reprinted with permission from:
Hughes, K. E.; Stein, J. L.; Friedfeld, M. R.; Cossairt, B. M.; Gamelin, D. R. *In Preparation.*

C.1 Variable-Temperature Time-Resolved Spectra and Dynamics Measurements

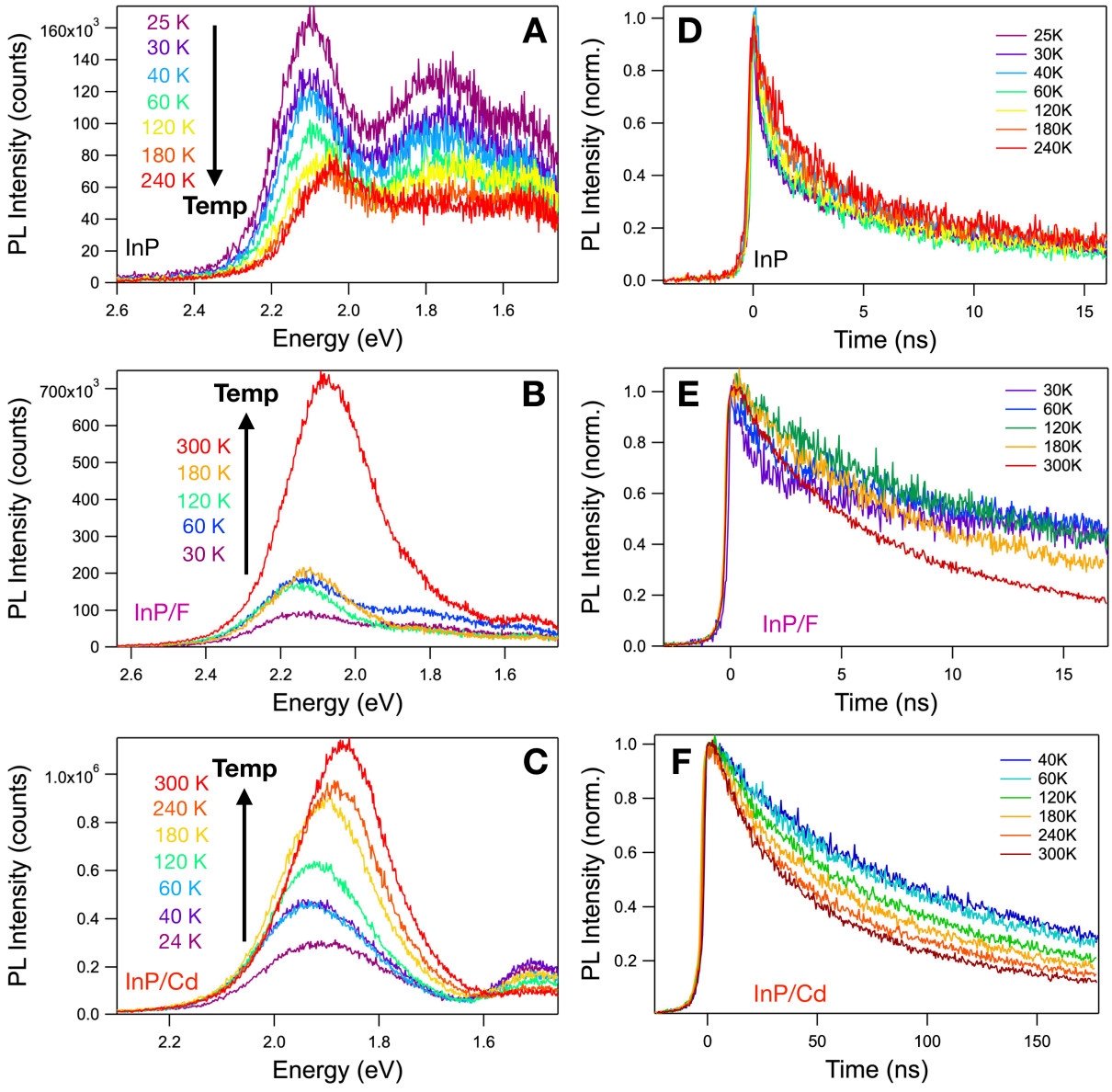

Figure C.1. (A, B, C) Variable-temperature time-resolved photoluminescence spectra at short times (0–3 ns) and **(D, E, F)** normalized PL decay dynamics of various InP NCs measured at different temperatures between 24 and 300 K. **(A, D)** As-prepared InP NCs, **(B, E)**, InP/F NCs,

(C, F) InP/Cd NCs. Data were collected on NC samples deposited as dilute films. The PL decay curves are the same data shown in the main text (Figure 4.3 D-F) and were obtained by integrating between ~2.15 eV and 2.00 eV for InP NCs, between 2.20 eV and ~2.00 eV for the InP/F NCs, and between ~1.95 eV and ~1.75 eV for the InP/Cd NCs.

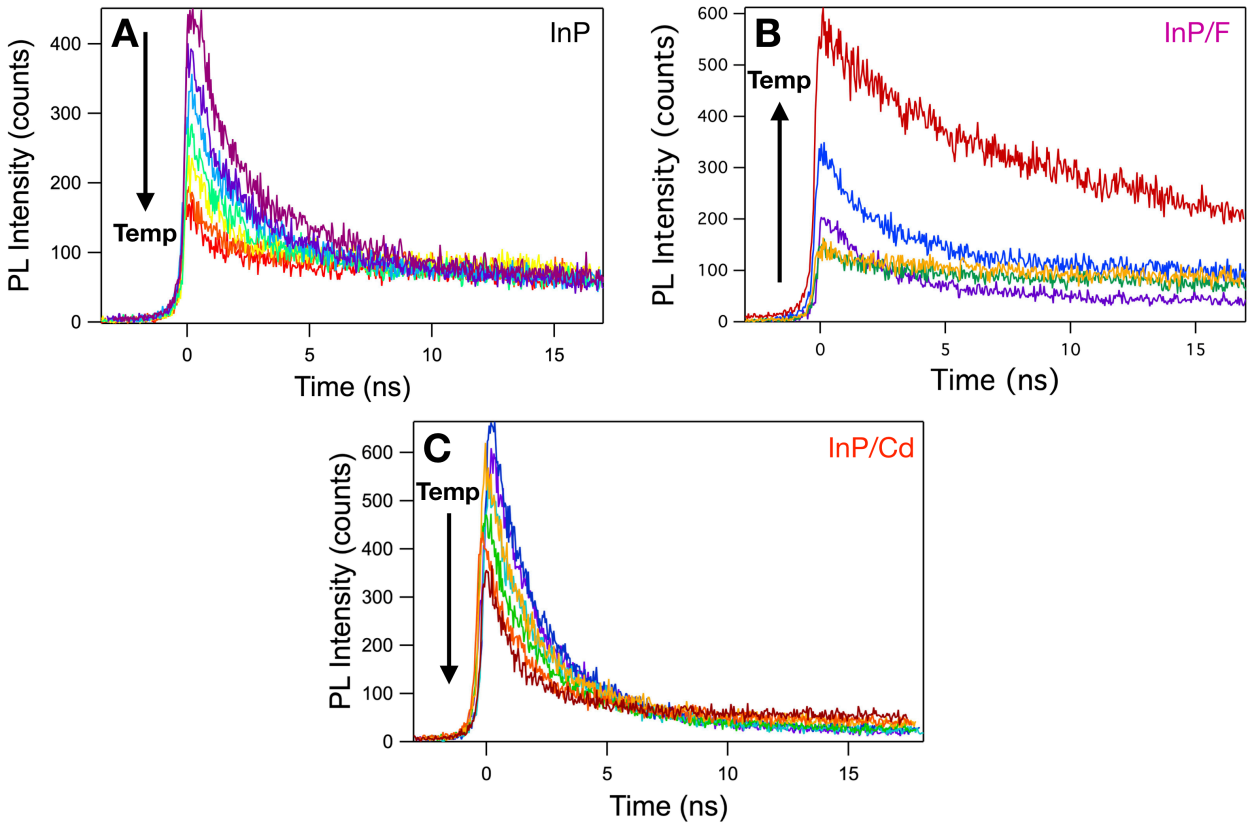

Figure C.2. Trap PL decay dynamics of InP **(A)**, InP/F **(B)**, and InP/Cd **(C)** NCs measured at temperatures between 24 and 300 K. The trace colors correlate with the colors in Figure C.1. Dynamics for the InP NCs were obtained by integrating between ~1.7 and 1.9 eV, between 1.8 and 1.9 eV for the InP/F NCs, and between 1.5 and 1.6 eV for the InP/Cd NCs.

C.2 Data Fitting Parameters for VTPL and TA Measurements

All decay traces were fit to the biexponential eq C.1.

$$y = y_0 + A_1 * \exp[-invTau_1 * x] + A_2 * \exp[-invTau_2 * x] \qquad \text{(Eq C.1.)}$$

Weighted lifetimes were calculated using eq C.2.

$$\tau_{weighted} = \frac{[(A_1 * \tau_1) + (A_2 * \tau_2)]}{A_1 + A_2} \qquad \text{(Eq C.2.)}$$

Table C.1. Fitting parameters for VTPL excitonic decay dynamics (Figure 4.4 of the main text).

Sample	Temp (K)	A_1	τ_1 (ns)	A_2	τ_2 (ns)	Weighted τ (ns)
InP	25	0.58	0.6	0.37	13.4	6
(20 ns fitting window)	30	0.51	0.6	0.377	12.1	6
	40	0.53	0.8	0.44	12.2	6
	60	0.56	0.7	0.39	10.4	5
	120	0.58	0.9	0.38	12.3	5
	180	0.51	1.1	0.42	13.6	7
	240	0.51	1.7	0.41	15.4	8
InP/F	33	0.42	25	0.56	120	80
(200 ns fitting window)	60	0.54	24	0.47	102	60
	120	0.62	18	0.38	84	43
	180	0.67	16	0.34	75	36
	300	0.86	12	0.2	53	19
InP/Cd	40	0.47	60	0.54	253	164
(200 ns fitting window)	60	0.46	56	0.56	217	145
	120	0.35	32	0.68	146	107
	180	0.39	28	0.64	137	96
	240	0.46	25	0.56	132	84
	300	0.55	25	0.5	124	72

Table C.2. Fitting parameters for TA bleach-recovery dynamics.

Sample	y_0	A_1	Decay constant (1), $invTau_1$ (ns)	A_2	Decay constant (2), $invTau_2$ (ns)
InP	0	-0.6798	128.51	-0.2874	10
InP/F	0	-0.51243	158.29	-0.44177	10
InP/Zn	0	-0.18402	127.42	-0.77727	10
InP/ZnSeS	0	-0.20074	110.88	-0.82649	10
InP/Cd	-0.29896	-0.080993	217.89	-0.62696	10

C.3 Data Analysis for TA Measurements

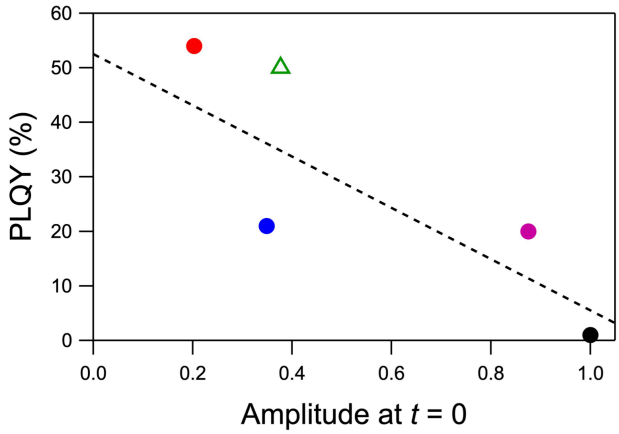

Figure C.3. PLQY of all five InP samples (InP (black), InP/F (fuchsia), InP/Zn (blue), InP/ZnSeS (green), and InP/Cd (red)) as a function of the amplitude of the TA bleach recovery at $t = 0$, corresponding to the data shown in Figure 4.6A of the main text.

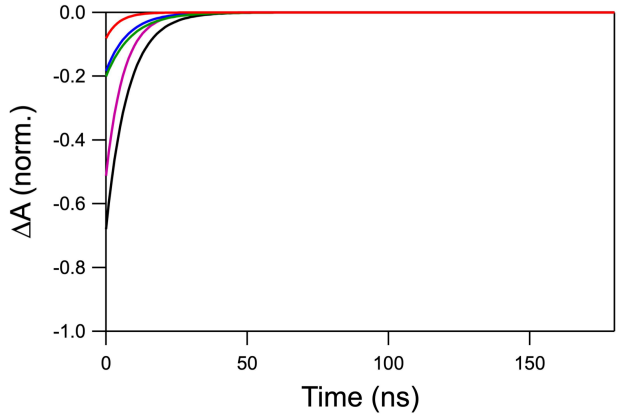

Figure C.4. Fast-decay components of biexponential fits to TA bleach-recovery dynamics for InP (black), InP/F (fuchsia), InP/Zn (blue), InP/ZnSeS (green), and InP/Cd (red) NCs. These curves were integrated to obtain the data points shown in Figure 4.6B of the main text.

Bibliography

Adam, S.; Talapin, D. V.; Borchert, H.; Lobo, A.; McGinley, C.; Castro, A. R. B. d.; Haase, M.; Weller, H.; Möller, T., The effect of nanocrystal surface structure on the luminescence properties: Photoemission study of HF-etched InP nanocrystals. *J. Chem. Phys.* **2005,** *123* (8), 084706.

Adamo, C.; Barone, V., Toward Reliable Density Functional Methods without Adjustable Parameters: The PBE0 Model. *J. Chem. Phys.* **1999,** *110*, 6158-6170.

Albornoz, J. G.; Serna, R.; León, M., Optical Properties and Electronic Structure of Polycrystalline Ag1−xCuxInSe2 Alloys. *J. Appl. Phys.* **2005,** *97*, 103515.

Aldakov, D.; Léfrançois, A.; Reiss, P., Ternary and Quaternary Metal Chalcogenide Nanocrystals: Synthesis, Properties, and Applications. *J. Mater. Chem. C* **2013,** *1*, 3756-3776.

Allan, G.; Delerue, C., Fast relaxation of hot carriers by impact ionization in semiconductor nanocrystals: Role of defects. *Phys. Rev. B* **2009,** *79*, 195324.

Badaeva, E.; Feng, Y.; Gamelin, D. R.; Li, X., Investigation of Pure and Co^{2+}-Doped ZnO Quantum Dot Electronic Structures Using the Density Functional Theory: Choosing the Right Functional. *New J. Phys.* **2008,** *10*, 055013.

Baghbanzadeh, M.; Carbone, L.; Cozzoli, P. D.; Kappe, C. O., Microwave-Assisted Synthesis of Colloidal Inorganic Nanocrystals. *Angew. Chem., Int. Ed.* **2011,** *50* (48), 11312-11359.

Berends, A. C.; Rabouw, F. T.; Spoor, F. C. M.; Bladt, E.; Grozema, F. C.; Houtepen, A. J.; Siebbeles, L. D. A.; de Mello Donegá, C., Radiative and Nonradiative Recombination in CuInS2 Nanocrystals and CuInS2-Based Core/Shell Nanocrystals. *J. Phys. Chem. Lett.* **2016,** *7* (17), 3503-3509.

Biadala, L.; Siebers, B.; Beyazit, Y.; Tessier, M. D.; Dupont, D.; Hens, Z.; Yakovlev, D. R.; Bayer, M., Band-Edge Exciton Fine Structure and Recombination Dynamics in InP/ZnS Colloidal Nanocrystals. *ACS Nano* **2016,** *10* (3), 3356-3364.

Blackburn, J. L.; Ellingson, R. J.; Mićić, O. I.; Nozik, A. J., Electron Relaxation in Colloidal InP Quantum Dots with Photogenerated Excitons or Chemically Injected Electrons. *J. Phys. Chem. B* **2003,** *107* (1), 102-109.

Boles, M. A.; Ling, D.; Hyeon, T.; Talapin, D. V., The surface science of nanocrystals. *Nat. Mater.* **2016,** *15*, 141.

Bradshaw, L. R.; Knowles, K. E.; McDowall, S.; Gamelin, D. R., Nanocrystals for Luminescent Solar Concentrators. *Nano Lett.* **2015,** *15* (2), 1315-1323.

Bradshaw, L. R.; May, J. W.; Dempsey, J. L.; Li, X.; Gamelin, D. R., Ferromagnetic Excited-State Mn2+ Dimers in Zn1-xMnxSe Quantum Dots Observed by Time-Resolved Magnetophotoluminescence. *Phys. Rev. B* **2014,** *89* (11), 115312.

Brodu, A.; Ballottin, M. V.; Buhot, J.; van Harten, E. J.; Dupont, D.; La Porta, A.; Prins, P. T.; Tessier, M. D.; Versteegh, M. A. M.; Zwiller, V.; Bals, S.; Hens, Z.; Rabouw, F. T.; Christianen, P. C. M.; de Mello Donega, C.; Vanmaekelbergh, D., Exciton Fine Structure and Lattice Dynamics in InP/ZnSe Core/Shell Quantum Dots. *ACS Photonics* **2018,** *5* (8), 3353-3362.

Brovelli, S.; Galland, C.; Viswanatha, R.; Klimov, V. I., Tuning Radiative Recombination in Cu-doped Nanocrystals via Electrochemical Control of Surface Trapping. *Nano Lett.* **2012,** *12* (8), 4372-4379.

Bruchez, M.; Moronne, M.; Gin, P.; Weiss, S.; Alivisatos, A. P., Semiconductor Nanocrystals as Fluorescent Biological Labels. *Science* **1998,** *281* (5385), 2013.

Califano, M., Off-State Quantum Yields in the Presence of Surface Trap States in CdSe Nanocrystals: The Inadequacy of the Charging Model To Explain Blinking. *J. Phys. Chem. C* **2011,** *115*, 18051–18054.

Carroll, G. M.; Tsui, E. Y.; Brozek, C. K.; Gamelin, D. R., Spectroelectrochemical Measurement of Surface Electrostatic Contributions to Colloidal CdSe Nanocrystal Redox Potentials. *Chem. Mater.* **2016,** *28*, 7912–7918.

Chadi, D. J., Atomic and Electronic Structures of Reconstructed Si(100) Surfaces. *Phys. Rev. Lett.* **1979,** *43* (1), 43-47.

Chandrasekaran, V.; Tessier, M. D.; Dupont, D.; Geiregat, P.; Hens, Z.; Brainis, E., Nearly Blinking-Free, High-Purity Single-Photon Emission by Colloidal InP/ZnSe Quantum Dots. *Nano Lett.* **2017,** *17* (10), 6104-6109.

Chen, S.; Demillo, V.; Lu, M.; Zhu, X., Preparation of photoluminescence tunable Cu-doped AgInS2 and AgInS2/ZnS nanocrystals and their application as cellular imaging probes. *RSC Adv.* **2016,** *6* (56), 51161-51170.

Cheng, K.-C.; Law, W.-C.; Yong, K.-T.; Nevins, J. S.; Watson, D. F.; Ho, H.-P.; Prasad, P. N., Synthesis of near-infrared silver-indium-sulfide (AgInS2) quantum dots as heavy-metal free photosensitizer for solar cell applications. *Chem. Phys. Lett.* **2011,** *515* (4), 254-257.

Cho, E.; Kim, T.; Choi, S.-m.; Jang, H.; Min, K.; Jang, E., Optical Characteristics of the Surface Defects in InP Colloidal Quantum Dots for Highly Efficient Light-Emitting Applications. *ACS Appl. Nano Mater.* **2018,** *1* (12), 7106-7114.

Ciszek, T. F., Melt Growth and some Properties of CuxAg1-xInSe2 and CuInyGa1-ySe2 Chalcopyrite Solid Solution Crystals. *J. Cryst. Growth* **1986,** *79*, 689-694.

Cohn, A. W.; Rinehart, J. D.; Schimpf, A. M.; Weaver, A. L.; Gamelin, D. R., Size Dependence of Negative Trion Auger Recombination in Photodoped CdSe Nanocrystals. *Nano Letters* **2014,** *14* (1), 353-358.

Cohn, A. W.; Schimpf, A. M.; Gunthardt, C. E.; Gamelin, D. R., Size-Dependent Trap-Assisted Auger Recombination in Semiconductor Nanocrystals. *Nano Lett.* **2013,** *13* (4), 1810-1815.

Cooper, J. K.; Gul, S.; Lindley, S. A.; Yano, J.; Zhang, J. Z., Tunable Photoluminescent Core/Shell Cu+-Doped ZnSe/ZnS Quantum Dots Codoped with Al3+, Ga3+, or In3+. *ACS Appl. Mater. Interfaces* **2015,** *7* (18), 10055-10066.

Cossairt, B. M., Shining Light on Indium Phosphide Quantum Dots: Understanding the Interplay among Precursor Conversion, Nucleation, and Growth. *Chem. Mat.* **2016,** *28* (20), 7181-7189.

Coughlan, C.; Ibáñez, M.; Dobrozhan, O.; Singh, A.; Cabot, A.; Ryan, K. M., Compound Copper Chalcogenide Nanocrystals. *Chem. Rev.* **2017,** *117*, 5865-6109.

Debnath, T.; Maiti, S.; Maity, P.; Ghosh, H. N., Subpicosecond Exciton Dynamics and Biexcitonic Feature in Colloidal CuInS2 Nanocrystals: Role of In–Cu Antisite Defects. *J. Phys. Chem. Lett.* **2015,** *6* (17), 3458-3465.

Dennis, A. M.; Mangum, B. D.; Piryatinski, A.; Park, Y.-S.; Hannah, D. C.; Casson, J. L.; Williams, D. J.; Schaller, R. D.; Htoon, H.; Hollingsworth, J. A., Suppressed Blinking and Auger Recombination in Near-Infrared Type-II InP/CdS Nanocrystal Quantum Dots. *Nano Lett.* **2012,** *12* (11), 5545-5551.

Ekimov, A. I.; Efros, A. L.; Onushchenko, A. A., Quantum size effect in semiconductor microcrystals. *Solid State Commun.* **1985,** *56* (11), 921-924.

Ellingson, R. J.; Blackburn, J. L.; Yu, P.; Rumbles, G.; Mićić, O. I.; Nozik, A. J., Excitation Energy Dependent Efficiency of Charge Carrier Relaxation and Photoluminescence in Colloidal InP Quantum Dots. *J. Phys. Chem. B* **2002,** *106* (32), 7758-7765.

Erickson, C. S.; Bradshaw, L. R.; McDowall, S.; Gilbertson, J. D.; Gamelin, D. R.; Patrick, D. L., Zero-Reabsorption Doped-Nanocrystal Luminescent Solar Concentrators. *ACS Nano* **2014,** *8* (4), 3461-3467.

Franceschetti, A.; Zunger, A., Optical transitions in charged CdSe quantum dots. *Phys. Rev. B* **2000,** *62*, R16287-R16290.

Frisch, M. J.; Trucks, G. W.; Schlegel, H. B.; Scuseria, G. E.; Robb, M. A.; Cheeseman, J. R.; Scalmani, G.; Barone, V.; Mennucci, B.; Petersson, G. A.; Nakatsuji, H.; Caricato, M.; Li, X.; Hratchian, H. P.; Izmaylov, A. F.; Bloino, J.; Zheng, G.; Sonnenberg, J. L.; Hada, M.; Ehara, M.; Toyota, K.; Fukuda, R.; Hasegawa, J.; Ishida, M.; Nakajima, T.; Honda, Y.; Kitao, O.; Nakai, H.; Vreven, T.; Montgomery Jr., J. A.; Peralta, J. E.; Ogliaro, F.; Bearpark, M. J.; Heyd, J.; Brothers, E. N.; Kudin, K. N.; Staroverov, V. N.; Kobayashi, R.; Normand, J.; Raghavachari, K.; Rendell,

A. P.; Burant, J. C.; Iyengar, S. S.; Tomasi, J.; Cossi, M.; Rega, N.; Millam, N. J.; Klene, M.; Knox, J. E.; Cross, J. B.; Bakken, V.; Adamo, C.; Jaramillo, J.; Gomperts, R.; Stratmann, R. E.; Yazyev, O.; Austin, A. J.; Cammi, R.; Pomelli, C.; Ochterski, J. W.; Martin, R. L.; Morokuma, K.; Zakrzewski, V. G.; Voth, G. A.; Salvador, P.; Dannenberg, J. J.; Dapprich, S.; Daniels, A. D.; Farkas, Ö.; Foresman, J. B.; Ortiz, J. V.; Cioslowski, J.; Fox, D. J. *Gaussian 09*, Gaussian, Inc.: Wallingford, CT, USA, 2009.

Fu, H.; Zunger, A., InP quantum dots: Electronic structure, surface effects, and the redshifted emission. *Phys. Rev. B* **1997,** *56* (3), 1496-1508.

Gary, D. C.; Flowers, S. E.; Kaminsky, W.; Petrone, A.; Li, X.; Cossairt, B. M., Single-Crystal and Electronic Structure of a 1.3 nm Indium Phosphide Nanocluster. *J. Am. Chem. Soc.* **2016,** *138* (5), 1510-1513.

Gary, D. C.; Terban, M. W.; Billinge, S. J. L.; Cossairt, B. M., Two-Step Nucleation and Growth of InP Quantum Dots via Magic-Sized Cluster Intermediates. *Chem. Mater.* **2015,** *27* (4), 1432-1441.

Ghosh, Y.; Mangum, B. D.; Casson, J. L.; Williams, D. J.; Htoon, H.; Hollingsworth, J. A., New Insights into the Complexities of Shell Growth and the Strong Influence of Particle Volume in Nonblinking "Giant" Core/Shell Nanocrystal Quantum Dots. *J. Am. Chem. Soc.* **2012,** *134* (23), 9634-9643.

Gopal, M. B., Ag and Cu doped colloidal CdSe nanocrystals: partial cation exchange and luminescence. *Mater. Res. Express* **2015,** *2*, 085004.

Grandhi, G. K.; Tomar, R.; Viswanatha, R., Study of Surface and Bulk Electronic Structure of II–VI Semiconductor Nanocrystals Using Cu as a Nanosensor. *ACS Nano* **2012,** *6* (11), 9751-9763.

Grandhi, G. K.; Viswanatha, R., Tunable Infrared Phosphors Using Cu Doping in Semiconductor Nanocrystals: Surface Electronic Structure Evaluation. *J. Phys. Chem. Lett.* **2013,** *4* (3), 409-415.

Groeneveld, E.; Witteman, L.; Lefferts, M.; Ke, X.; Bals, S.; Van Tendeloo, G.; de Mello Donega, C., Tailoring ZnSe–CdSe Colloidal Quantum Dots via Cation Exchange: From Core/Shell to Alloy Nanocrystals. *ACS Nano* **2013,** *7* (9), 7913-7930.

Guchhait, A.; Pal, A. J., Copper-Diffused AgInS2 Ternary Nanocrystals in Hybrid Bulk-Heterojunction Solar Cells: Near-Infrared Active Nanophotovoltaics. *ACS Appl. Mater. Inter.* **2013,** *5* (10), 4181-4189.

Gupta, S.; Kershaw, S. V.; Rogach, A. L., 25th Anniversary Article: Ion Exchange in Colloidal Nanocrystals. *Adv. Mater.* **2013,** *25*, 6923-6944.

Hahm, D.; Chang, J. H.; Jeong, B. G.; Park, P.; Kim, J.; Lee, S.; Choi, J.; Kim, W. D.; Rhee, S.; Lim, J.; Lee, D. C.; Lee, C.; Char, K.; Bae, W. K., Design Principle for Bright, Robust, and Color-Pure InP/ZnSexS1–x/ZnS Heterostructures. *Chem. Mat.* **2019**.

Hamanaka, Y.; Ozawa, K.; Kuzuya, T., Enhancement of Donor–Acceptor Pair Emissions in Colloidal AgInS2 Quantum Dots with High Concentrations of Defects. *J. Phys. Chem. C* **2014,** *118* (26), 14562-14568.

Hamanaka, Y.; Ogawa, T.; Tsuzuki, M.; Kuzuya, T., Photoluminescence Properties and Its Origin of AgInS2 Quantum Dots with Chalcopyrite Structure. *J. Phys. Chem. C* **2011,** *115* (5), 1786-1792.

Hartstein, K. H.; Erickson, C. S.; Tsui, E. Y.; Marchioro, A.; Gamelin, D. R., Electron Stability and Negative-Tetron Luminescence in Free-Standing Colloidal n-Type CdSe/CdS Quantum Dots. *ACS Nano* **2017,** *11* (10), 10430-10438.

Harvey, E. N., *A History of Luminescence: From the Earliest Times Until 1900*. CreateSpace Independent Publishing Platform: 2015.

Hassan, A.; Zhang, X.; Liu, X.; Rowland, C. E.; Jawaid, A. M.; Chattopadhyay, S.; Gulec, A.; Shamirian, A.; Zuo, X.; Klie, R. F.; Schaller, R. D.; Snee, P. T., Charge Carriers Modulate the Bonding of Semiconductor Nanoparticle Dopants As Revealed by Time-Resolved X-ray Spectroscopy. *ACS Nano* **2017,** *11*, 10070-10076.

Hay, P. J.; Wadt, W. R., Ab initio effective core potentials for molecular calculations. Potentials for K to Au including the outermost core orbitals. *J. Chem. Phys.* **1985,** *82* (1), 299-310.

Huang, D.; Persson, C., Photocatalyst AgInS2 for active overall water-splitting: A first-principles study. *Chem. Phys. Lett.* **2014,** *591*, 189-192.

Huang, J.; Yang, Y.; Xue, S.; Yang, B.; Liu, S.; Shen, J., Photoluminescence and electroluminescence of ZnS:Cu nanocrystals in polymeric networks. *Appl. Phys. Lett.* **1997,** *70* (18), 2335-2337.

Huang, X.; Lindgren, E.; Chelikowsky, J. R., Surface Passivation Method for Semiconductor Nanostructures. *Phys. Rev. B* **2005,** *71*, 165328.

Hughes, K. E.; Hartstein, K. H.; Gamelin, D. R., Photodoping and Transient Spectroscopies of Copper-Doped CdSe/CdS Nanocrystals. *ACS Nano* **2018,** *12* (1), 718-728.

Hunsche, S.; Dekorsy, T.; Klimov, V.; Kurz, H., Ultrafast dynamics of carrier-induced absorption changes in highly-excited CdSe nanocrystals. *Appl. Phys. B* **1996,** *62* (1), 3-10.

Jain, P. K.; Amirav, L.; Aloni, S.; Alivisatos, A. P., Nanoheterostructure Cation Exchange: Anionic Framework Conservation. *J. Am. Chem. Soc* **2010,** *132*, 9997-9999.

Jana, S.; Srivastava, B. B.; Acharya, S.; Santra, P. K.; Jana, N. R.; Sarma, D. D.; Pradhan, N., Prevention of photooxidation in blue-green emitting Cu doped ZnSe nanocrystals. *Chem. Commun.* **2010,** *46* (16), 2853-2855.

Janke, E. M.; Williams, N. E.; She, C.; Zherebetskyy, D.; Hudson, M. H.; Wang, L.; Gosztola, D. J.; Schaller, R. D.; Lee, B.; Sun, C.; Engel, G. S.; Talapin, D. V., Origin of Broad Emission Spectra in InP Quantum Dots: Contributions from Structural and Electronic Disorder. *J. Am. Chem. Soc.* **2018,** *140* (46), 15791-15803.

Jara, D. H.; Stamplecoskie, K. G.; Kamat, P. V., Two Distinct Transitions in CuxInS2 Quantum Dots. Bandgap versus Sub-Bandgap Excitations in Copper-Deficient Structures. *J. Phys. Chem. Lett.* **2016,** *7* (8), 1452-1459.

Jha, P. P.; Guyot-Sionnest, P., Trion Decay in Colloidal Quantum Dots. *ACS Nano* **2009,** *3*, 1011–1015.

Jiang, T.; Song, J.; Wang, H.; Ye, X.; Wang, H.; Zhang, W.; Yang, M.; Xia, R.; Zhu, L.; Xu, X., Aqueous synthesis of color tunable Cu doped Zn-In-S/ZnS nanoparticles in the whole visible region for cellular imaging. *J. Mater. Chem. B* **2015,** *3* (11), 2402-2410.

Jing, P.; Zheng, J.; Ikezawa, M.; Liu, X.; Lv, S.; Kong, X.; Zhao, J.; Masumoto, Y., Temperature-Dependent Photoluminescence of CdSe-Core CdS/CdZnS/ZnS-Multishell Quantum Dots. *J. Phys. Chem. C* **2009,** *113* (31), 13545-13550.

Kim, Y.; Ham, S.; Jang, H.; Min, J. H.; Chung, H.; Lee, J.; Kim, D.; Jang, E., Bright and Uniform Green Light Emitting InP/ZnSe/ZnS Quantum Dots for Wide Color Gamut Displays. *ACS Appl. Nano Mater.* **2019,** *2* (3), 1496-1504.

Kim, S.; Kim, T.; Kang, M.; Kwak, S. K.; Yoo, T. W.; Park, L. S.; Yang, I.; Hwang, S.; Lee, J. E.; Kim, S. K.; Kim, S.-W., Highly Luminescent InP/GaP/ZnS Nanocrystals and Their Application to White Light-Emitting Diodes. *J. Am. Chem. Soc.* **2012,** *134* (8), 3804-3809.

Kim, S. H.; Wolters, R. H.; Heath, J. R., Photophysics of size-selected InP nanocrystals: Exciton recombination kinetics. *J. Chem. Phys.* **1996,** *105* (18), 7957-7963.

Kim, T.-G.; Zherebetskyy, D.; Bekenstein, Y.; Oh, M. H.; Wang, L.-W.; Jang, E.; Alivisatos, A. P., Trap Passivation in Indium-Based Quantum Dots through Surface Fluorination: Mechanism and Applications. *ACS Nano* **2018,** *12* (11), 11529-11540.

Kirkwood, N.; Monchen, J. O. V.; Crisp, R. W.; Grimaldi, G.; Bergstein, H. A. C.; du Fossé, I.; van der Stam, W.; Infante, I.; Houtepen, A. J., Finding and Fixing Traps in II–VI and III–V Colloidal Quantum Dots: The Importance of Z-Type Ligand Passivation. *J. Am. Chem. Soc.* **2018,** *140* (46), 15712-15723.

Klimov, V. I., Optical Nonlinearities and Ultrafast Carrier Dynamics in Semiconductor Nanocrystals. *J. Phys. Chem. B* **2000,** *104* (26), 6112-6123.

Klimov, V. I.; McBranch, D. W.; Leatherdale, C. A.; Bawendi, M. G., Electron and hole relaxation pathways in semiconductor quantum dots. *Phys. Rev. B* **1999,** *60*, 13740-13749.

Knowles, K. E.; Frederick, M. T.; Tice, D. B.; Morris-Cohen, A. J.; Weiss, E. A., Colloidal Quantum Dots: Think Outside the (Particle-in-a-)Box. *J. Phys. Chem. Lett.* **2012,** *3*, 18-26.

Knowles, K. E.; Hartstein, K. H.; Kilburn, T. B.; Marchioro, A.; Nelson, H. D.; Whitham, P. J.; Gamelin, D. R., Luminescent Colloidal Semiconductor Nanocrystals Containing Copper: Synthesis, Photophysics, and Applications. *Chem. Rev.* **2016,** *116* (18), 10820-10851.

Knowles, K. E.; Kilburn, T. B.; Alzate, D. G.; McDowall, S.; Gamelin, D. R., Bright CuInS2/CdS nanocrystal phosphors for high-gain full-spectrum luminescent solar concentrators. *Chem. Commun.* **2015,** *51* (44), 9129-9132.

Knowles, K. E.; Nelson, H. D.; Kilburn, T. B.; Gamelin, D. R., Singlet–Triplet Splittings in the Luminescent Excited States of Colloidal Cu+:CdSe, Cu+:InP, and CuInS2 Nanocrystals: Charge-Transfer Configurations and Self-Trapped Excitons. *J. Am. Chem. Soc.* **2015,** *137* (40), 13138-13147.

Kraatz, I. T.; Booth, M.; Whitaker, B. J.; Nix, M. G. D.; Critchley, K., Sub-Bandgap Emission and Intraband Defect-Related Excited-State Dynamics in Colloidal CuInS2/ZnS Quantum Dots Revealed by Femtosecond Pump−Dump−Probe Spectroscopy. *J. Phys. Chem. C* **2014,** *118*, 24102−24109.

Langof, L.; Ehrenfreund, E.; Lifshitz, E.; Micic, O. I.; Nozik, A. J., Continuous-Wave and Time-Resolved Optically Detected Magnetic Resonance Studies of Nonetched/Etched InP Nanocrystals. *J. Phys. Chem. B* **2002,** *106* (7), 1606-1612.

Leach, A. D. P.; Macdonald, J. E., The Optoelectronic Properties of $CuInS_2$ Nanocrystals and their Origin. *J. Phys. Chem. Lett.* **2016,** *7*, 572-583.

Leach, A. D. P.; Shen, X.; Faust, A.; Cleveland, M. C.; La Croix, A. D.; Banin, U.; Pantelides, S. T.; Macdonald, J. E., Defect Luminescence from Wurtzite $CuInS_2$ Nanocrystals: Combined Experimental and Theoretical Analysis. *J. Phys. Chem. C* **2016,** *120*, 5207-5212.

Li, L.; Daou, T. J.; Texier, I.; Chi, T. T. K.; Liem, N. Q.; Reiss, P., Highly Luminescent $CuInS_2$/ZnS Core/Shell Nanocrystals: Cadmium-Free Quantum Dots for In Vivo Imaging. *Chem. Mater.* **2009,** *21*, 2422-2429.

Li, L.; Pandey, A.; Werder, D. J.; Khanal, B. P.; Pietryga, J. M.; Klimov, V. I., Efficient Synthesis of Highly Luminescent Copper Indium Sulfide-Based Core/Shell Nanocrystals with Surprisingly Long-Lived Emission. *J. Am. Chem. Soc.* **2011,** *133* (5), 1176-1179.

Lim, J.; Bae, W. K.; Lee, D.; Nam, M. K.; Jung, J.; Lee, C.; Char, K.; Lee, S., InP@ZnSeS, Core@Composition Gradient Shell Quantum Dots with Enhanced Stability. *Chem. Mater.* **2011,** *23* (20), 4459-4463.

Liu, J.; Hua, E., Electronic structure and absolute band edge position of tetragonal AgInS2 photocatalyst: A hybrid density functional study. *Mater. Sci. Semicond. Process.* **2015,** *40*, 446-452.

Maiti, S.; Dana, J.; Jadhav, Y.; Debnath, T.; Haram, S. K.; Ghosh, H. N., Electrochemical Evaluation of Dopant Energetics and the Modulation of Ultrafast Carrier Dynamics in Cu-Doped CdSe Nanocrystals. *J. Phys. Chem. C* **2017,** *121*, 27233-27240.

Mao, B.; Chuang, C.-H.; Wang, J.; Burda, C., Synthesis and Photophysical Properties of Ternary I–III–VI AgInS2 Nanocrystals: Intrinsic versus Surface States. *J. Phys. Chem. C* **2011,** *115* (18), 8945-8954.

McArthur, E. A.; Morris-Cohen, A. J.; Knowles, K. E.; Weiss, E. A., Charge Carrier Resolved Relaxation of the First Excitonic State in CdSe Quantum Dots Probed with Near-Infrared Transient Absorption Spectroscopy. *J. Phys. Chem. B* **2010,** *114* (45), 14514-14520.

Meinardi, F.; McDaniel, H.; Carulli, F.; Colombo, A.; Velizhanin, K. A.; Makarov, N. S.; Simonutti, R.; Klimov, V. I.; Brovelli, S., Highly efficient large-area colourless luminescent solar concentrators using heavy-metal-free colloidal quantum dots. *Nat. Nanotech.* **2015,** *10*, 878–885.

Mićić, O. I.; Cheong, H. M.; Fu, H.; Zunger, A.; Sprague, J. R.; Mascarenhas, A.; Nozik, A. J., Size-Dependent Spectroscopy of InP Quantum Dots. *J. Phys. Chem. B* **1997,** *101* (25), 4904-4912.

Mićić, O. I.; Nozik, A. J.; Lifshitz, E.; Rajh, T.; Poluektov, O. G.; Thurnauer, M. C., Electron and Hole Adducts Formed in Illuminated InP Colloidal Quantum Dots Studied by Electron Paramagnetic Resonance. *J.Phys.Chem. B* **2002,** *106* (17), 4390-4395.

Mićić, O. I.; Sprague, J.; Lu, Z.; Nozik, A. J., Highly efficient band-edge emission from InP quantum dots. *Appl. Phys. Lett.* **1996,** *68* (22), 3150-3152.

Narayanaswamy, A.; Feiner, L. F.; Meijerink, A.; van der Zaag, P. J., The Effect of Temperature and Dot Size on the Spectral Properties of Colloidal InP/ZnS Core−Shell Quantum Dots. *ACS Nano* **2009,** *3* (9), 2539-2546.

Narayanaswamy, A.; Feiner, L. F.; van der Zaag, P. J., Temperature Dependence of the Photoluminescence of InP/ZnS Quantum Dots. *J. Phys. Chem. C* **2008,** *112* (17), 6775-6780.

Nelson, H. D.; Gamelin, D. R., Valence-Band Electronic Structures of Cu+-Doped ZnS, Alloyed Cu−In−Zn−S, and Ternary CuInS2 Nanocrystals: A Unified Description of Photoluminescence across Compositions. *J. Phys. Chem. C* **2018,** *122*, 18124–18133.

Nelson, H. D.; Hinterding, S. O. M.; Fainblat, R.; Creutz, S. E.; Li, X.; Gamelin, D. R., Mid-Gap States and Normal vs Inverted Bonding in Luminescent Cu+- and Ag+-Doped CdSe Nanocrystals. *J. Am. Chem. Soc.* **2017,** *139*, 6411–6421.

Nelson, H. D.; Li, X.; Gamelin, D. R., Computational Studies of the Electronic Structures of Copper-Doped CdSe Nanocrystals: Oxidation States, Singlet-Triplet Splittings, Jahn-Teller Distortions, and Vibronic Bandshapes. *J. Phys. Chem. C* **2016,** *120*, 5714–5723.

Pandey, A.; Brovelli, S.; Viswanatha, R.; Li, L.; Pietryga, J. M.; Klimov, V. I.; Crooker, S. A., Long-lived photoinduced magnetization in copper-doped ZnSe-CdSe core-shell nanocrystals. *Nat. Nanotech.* **2012,** *7* (12), 792-797.

Park, N.; Monahan, M.; Ritchhart, A.; Friedfeld, M. R.; Cossairt, B. M., Synthesis of In37P20(O2CR)51 Clusters and Their Conversion to InP Quantum Dots. *J. Vis. Exp.* **2019,** (147), e59425.

Perdew, J. P.; Burke, K.; Ernzerhof, M., Generalized Gradient Approximation Made Simple. *Phys. Rev. Lett.* **1996,** *77*, 3865-3868.

Pham, T. T.; Chi Tran, T. K.; Nguyen, Q. L., Temperature-dependent photoluminescence study of InP/ZnS quantum dots. *Advances in Natural Sciences: Nanoscience and Nanotechnology* **2011,** *2* (2), 025001.

Poles, E.; Selmarten, D. C.; Mićić, O. I.; Nozik, A. J., Anti-Stokes photoluminescence in colloidal semiconductor quantum dots. *Appl. Phys. Lett.* **1999,** *75* (7), 971-973.

Qu, L.; Peng, X., Control of Photoluminescence Properties of CdSe Nanocrystals in Growth. *J. Am. Chem. Soc.* **2002,** *124* (9), 2049-2055.

Qu, L.; Peng, Z. A.; Peng, X., Alternative Routes toward High Quality CdSe Nanocrystals. *Nano Lett.* **2001,** *1* (6), 333-337.

Raevskaya, A.; Rozovik, O.; Novikova, A.; Selyshchev, O.; Stroyuk, O.; Dzhagan, V.; Goryacheva, I.; Gaponik, N.; Zahn, D. R. T.; Eychmüller, A., Luminescence and photoelectrochemical properties of size-selected aqueous copper-doped Ag–In–S quantum dots. *RSC Adv.* **2018,** *8* (14), 7550-7557.

Rice, W. D.; McDaniel, H.; Klimov, V. I.; Crooker, S. A., Magneto-Optical Properties of CuInS2 Nanocrystals. *J. Phys. Chem. Lett.* **2014,** *5* (23), 4105-4109.

Rinehart, J. D.; Schimpf, A. M.; Weaver, A. L.; Cohn, A. W.; Gamelin, D. R., Photochemical Electronic Doping of Colloidal CdSe Nanocrystals. *J. Am. Chem. Soc.* **2013,** *135* (50), 18782-18785.

Roberge, A.; Stein, J. L.; Shen, Y.; Cossairt, B. M.; Greytak, A. B., Purification and In Situ Ligand Exchange of Metal-Carboxylate-Treated Fluorescent InP Quantum Dots via Gel Permeation Chromatography. *J. Phys. Chem. Lett.* **2017,** *8* (17), 4055-4060.

Ropp, R. C., *Luminescence and the Solid State*. Elsevier Science: 2013.

Rossetti, R.; Brus, L., Electron-hole recombination emission as a probe of surface chemistry in aqueous cadmium sulfide colloids. *J. Phys. Chem.* **1982,** *86* (23), 4470-4472.

Rowland, C. E.; Liu, W.; Hannah, D. C.; Chan, M. K. Y.; Talapin, D. V.; Schaller, R. D., Thermal Stability of Colloidal InP Nanocrystals: Small Inorganic Ligands Boost High-Temperature Photoluminescence. *ACS Nano* **2014,** *8* (1), 977-985.

Saha, S. K.; Guchhait, A.; Pal, A. J., Hybrid pn-junction solar cells based on layers of inorganic nanocrystals and organic semiconductors: optimization of layer thickness by considering the width of the depletion region. *Phys. Chem. Chem. Phys.* **2014,** *16* (9), 4193-4201.

Sahu, A.; Kang, M. S.; Kompch, A.; Notthoff, C.; Wills, A. W.; Deng, D.; Winterer, M.; Frisbie, C. D.; Norris, D. J., Electronic Impurity Doping in CdSe Nanocrystals. *Nano Lett.* **2012,** *12*, 2587-2594.

Sandroni, M.; Wegner, K. D.; Aldakov, D.; Reiss, P., Prospects of Chalcopyrite-Type Nanocrystals for Energy Applications. *ACS Energy Lett.* **2017,** *2*, 1076-1088.

Savchenko, S. S.; Vokhmintsev, A. S.; Weinstein, I. A., Effect of temperature on the spectral properties of InP/ZnS nanocrystals. *Journal of Physics: Conference Series* **2018,** *961*, 012003.

Schimpf, A. M.; Gunthardt, C. E.; Rinehart, J. D.; Mayer, J. M.; Gamelin, D. R., Controlling Carrier Densities in Photochemically Reduced Colloidal ZnO Nanocrystals: Size Dependence and Role of the Hole Quencher. *J. Am. Chem. Soc.* **2013,** *135* (44), 16569-16577.

Sharma, M.; Gungor, K.; Yeltik, A.; Olutas, M.; Guzelturk, B.; Kelestemur, Y.; Erdem, T.; Delikanli, S.; McBride, J. R.; Demir, H. V., Near-Unity Emitting Copper-Doped Colloidal Semiconductor Quantum Wells for Luminescent Solar Concentrators. *Adv. Mater.* **2017,** *29* (30), 1700821.

Sharma, S.; Verma, A. S.; Jindal, V. K., First principles studies of structural, electronic, optical, elastic and thermal properties of Ag-chalcopyrites (AgInX2: X=S, Se). *Phys. B: Cond. Matter* **2014,** *438*, 97-108.

Shim, M.; Wang, C. J.; Guyot-Sionnest, P., Charge-tunable optical properties in colloidal semiconductor nanocrystals. *J. Phys. Chem. B* **2001,** *105*, 2369-2373.

Shimizu, K. T.; K.Woo, W.; Fisher, B. R.; Eisler, H. J.; Bawendi, M. G., Surface-Enhanced Emission from Single Semiconductor Nanocrystals. *Phys. Rev. Lett.* **2002,** *89*, 117401.

Shionoya, S.; Koda, T.; Era, K.; Fujiwara, H., Nature of Luminescence Transitions in ZnS Crvstals. *J. Phys. Soc. Jpn.* **1964,** *19* (7), 1157-1167.

Shionoya, S.; Yen, W. M.; Yamamoto, H., *Phosphor Handbook*. CRC Press: 2006.

Shirasaki, Y.; Supran, G. J.; Bawendi, M. G.; Bulović, V., Emergence of colloidal quantum-dot light-emitting technologies. *Nat. Photonics* **2012,** *7*, 13.

Shirazi, R.; Kopylov, O.; Kovacs, A.; Kardynał, B. E., Temperature dependent recombination dynamics in InP/ZnS colloidal nanocrystals. *Appl. Phys. Lett.* **2012,** *101* (9), 091910.

Siramdas, R.; McLaurin, E. J., InP Nanocrystals with Color-Tunable Luminescence by Microwave-Assisted Ionic-Liquid Etching. *Chem. Mater.* **2017,** *29* (5), 2101-2109.

Smith, A. M.; Nie, S., Semiconductor Nanocrystals: Structure, Properties, and Band Gap Engineering. *Acc. Chem. Res.* **2010,** *43* (2), 190-200.

Son, D. H.; Hughes, S. M.; Yin, Y.; Alivisatos, A. P., Cation Exchange Reactions in Ionic Nanocrystals. *Science* **2004,** *306*, 1009-1012.

Srivastava, B. B.; Jana, S.; Pradhan, N., Doping Cu in Semiconductor Nanocrystals: Some Old and Some New Physical Insights. *J. Am. Chem. Soc.* **2011,** *133* (4), 1007-1015.

Stein, J. L.; Mader, E. A.; Cossairt, B. M., Luminescent InP Quantum Dots with Tunable Emission by Post-Synthetic Modification with Lewis Acids. *J. Phys. Chem. Lett.* **2016,** *7* (7), 1315-1320.

Stein, J. L.; Steimle, M. I.; Terban, M. W.; Petrone, A.; Billinge, S. J. L.; Li, X.; Cossairt, B. M., Cation Exchange Induced Transformation of InP Magic-Sized Clusters. *Chem. Mater.* **2017,** *29* (18), 7984-7992.

Stroyuk, O.; Raevskaya, A.; Spranger, F.; Selyshchev, O.; Dzhagan, V.; Schulze, S.; Zahn, D. R. T.; Eychmüller, A., Origin and Dynamics of Highly Efficient Broadband Photoluminescence of Aqueous Glutathione-Capped Size-Selected Ag–In–S Quantum Dots. *J. Phys. Chem. C* **2018,** *122*, 13648–13658.

Sumner, R.; Eiselt, S.; Kilburn, T. B.; Erickson, C.; Carlson, B.; Gamelin, D. R.; McDowall, S.; Patrick, D. L., Analysis of Optical Losses in High-Efficiency CuInS2-Based Nanocrystal Luminescent Solar Concentrators: Balancing Absorption vs Scattering. *J. Phys. Chem. C* **2017,** *121*, 3252–3260.

Sun, J.; Zhu, D.; Zhao, J.; Ikezawa, M.; Wang, X.; Masumoto, Y., Ultrafast Carrier Dynamics in $CuInS_2$ Quantum Dots. *Appl. Phys. Lett.* **2014,** *104*, 023118.

Suzuki, A.; Shionoya, S., Mechanism of the Green-Copper Luminescence in ZnS Crystals. I. Direct Evidence for the Pair Emission Mechanism. *J. Phys. Soc. Jpn.* **1971,** *31*, 1455-1461.

Talapin, D. V.; Gaponik, N.; Borchert, H.; Rogach, A. L.; Haase, M.; Weller, H., Etching of Colloidal InP Nanocrystals with Fluorides: Photochemical Nature of the Process Resulting in High Photoluminescence Efficiency. *J. Phys. Chem. B* **2002,** *106* (49), 12659-12663.

Talapin, D. V.; Lee, J.-S.; Kovalenko, M. V.; Shevchenko, E. V., Prospects of Colloidal Nanocrystals for Electronic and Optoelectronic Applications. *Chem. Rev.* **2010,** *110* (1), 389-458.

Talapin, D. V.; Steckel, J., Quantum dot light-emitting devices. *MRS Bulletin* **2013,** *38* (9), 685-691.

Tamang, S.; Lincheneau, C.; Hermans, Y.; Jeong, S.; Reiss, P., Chemistry of InP Nanocrystal Syntheses. *Chem. Mater.* **2016,** *28* (8), 2491-2506.

Tarantini, A.; Wegner, K. D.; Dussert, F.; Sarret, G.; Beal, D.; Mattera, L.; Lincheneau, C.; Proux, O.; Truffier-Boutry, D.; Moriscot, C.; Gallet, B.; Jouneau, P. H.; Reiss, P.; Carrière, M., Physicochemical alterations and toxicity of InP alloyed quantum dots aged in environmental conditions: A safer by design evaluation. *NanoImpact* **2019,** *14*, 100168.

Tell, B.; Shay, J. L.; Kasper, H. M., Electrical Properties, Optical Properties, and Band Structure of CuGa${\mathrm{S}}_{2}$ and CuIn${\mathrm{S}}_{2}$. *Phys. Rev. B* **1971,** *4* (8), 2463-2471.

Thomas, A.; Sandeep, K.; Somasundaran, S. M.; Thomas, K. G., How Trap States Affect Charge Carrier Dynamics of CdSe and InP Quantum Dots: Visualization through Complexation with Viologen. *ACS Energy Lett.* **2018,** *3* (10), 2368-2375.

De Trizio, L.; Manna, L., Forging Colloidal Nanostructures via Cation Exchange Reactions. *Chem. Rev.* **2016,** *116*, 10852–10887.

Tsui, E. Y.; Hartstein, K. H.; Gamelin, D. R., Selenium Redox Reactivity on Colloidal CdSe Quantum Dot Surfaces. *J. Am. Chem. Soc.* **2016,** *138*, 11105–11108.

Tsuji, I.; Kato, H.; Kudo, A., Photocatalytic Hydrogen Evolution on ZnS−CuInS2−AgInS2 Solid Solution Photocatalysts with Wide Visible Light Absorption Bands. *Chem. Mater.* **2006,** *18*, 1969–1975.

Viswanatha, R.; Brovelli, S.; Pandey, A.; Crooker, S. A.; Klimov, V. I., Copper-Doped Inverted Core/Shell Nanocrystals with "Permanent" Optically Active Holes. *Nano Lett.* **2011,** *11* (11), 4753-4758.

Vogelsang, H.; Husberg, O.; Köhler, U.; von der Osten, W.; Marchetti, A. P., Exciton self-trapping in AgCl nanocrystals. *Phys. Rev. B* **2000,** *61* (3), 1847-1852.

Wadt, W. R.; Hay, P. J., Ab initio effective core potentials for molecular calculations. Potentials for main group elements Na to Bi. *J. Chem. Phys.* **1985,** *82* (1), 284-298.

Wang, L.-W.; Li, J., First-Principles Thousand-Atom Quantum Dot Calculations. *Phys. Rev. B* **2004,** *69*, 153302.

Wegner, K. D.; Dussert, F.; Truffier-Boutry, D.; Benayad, A.; Beal, D.; Mattera, L.; Ling, W. L.; Carrière, M.; Reiss, P., Influence of the Core/Shell Structure of Indium Phosphide Based Quantum Dots on Their Photostability and Cytotoxicity. *Front. Chem.* **2019,** *7* (466).

White, M. A.; Weaver, A. L.; Beaulac, R.; Gamelin, D. R., Electrochemically Controlled Auger Quenching of Mn2+ Photoluminescence in Doped Semiconductor Nanocrystals. *ACS Nano* **2011,** *5*, 4158–4168.

Wu, P.; Yan, X.-P., Doped quantum dots for chemo/biosensing and bioimaging. *Chem. Soc. Rev.* **2013,** *42* (12), 5489-5521.

Xie, R.; Peng, X., Synthesis of Cu-Doped InP Nanocrystals (d-dots) with ZnSe Diffusion Barrier as Efficient and Color-Tunable NIR Emitters. *J. Am. Chem. Soc.* **2009,** *131* (30), 10645-10651.

Yang, C.; Faust, A.; Amit, Y.; Gdor, I.; Banin, U.; Ruhman, S., Impurity Sub-Band in Heavily Cu-Doped InAs Nanocrystal Quantum Dots Detected by Ultrafast Transient Absorption. *J. Phys. Chem. A* **2016,** *120* (19), 3088-3097.

Yang, L.; Knowles, K. E.; Gopalan, A.; Hughes, K. E.; James, M. C.; Gamelin, D. R., One-Pot Synthesis of Monodisperse Colloidal Copper-Doped CdSe Nanocrystals Mediated by Ligand–Copper Interactions. *Chem. Mater.* **2016,** *28* (20), 7375-7384.

Yen, W. M.; Shionoya, S.; Yamamoto, H., *Phosphor Handbook*. Second ed.; CRC Press: New York, 2007.

Yoon, H. C.; Oh, J. H.; Ko, M.; Yoo, H.; Do, Y. R., Synthesis and Characterization of Green Zn–Ag–In–S and Red Zn–Cu–In–S Quantum Dots for Ultrahigh Color Quality of Down-Converted White LEDs. *ACS Appl. Mater. Inter.* **2015,** *7* (13), 7342-7350.

Zhang, W.; Lou, Q.; Ji, W.; Zhao, J.; Zhong, X., Color-Tunable Highly Bright Photoluminescence of Cadmium-Free Cu-Doped Zn–In–S Nanocrystals and Electroluminescence. *Chem. Mater.* **2014,** *26* (2), 1204-1212.

Zhu, Y.-J.; Chen, F., Microwave-Assisted Preparation of Inorganic Nanostructures in Liquid Phase. *Chem. Rev.* **2014,** *114* (12), 6462-6555.